NASA CR-137888
Available to the Public

NUMERICAL STUDIES OF THREE-DIMENSIONAL BREAKDOWN IN TRAILING VORTEX WAKES

(NASA-CR-137888) NUMERICAL STUDIES OF THREE-DIMENSIONAL BREAKDOWN IN TRAILING VORTEX WAKES (Lockheed-Georgia Co., Marietta.) 100 p HC A05/MF A01 CSCL 20D G3/02
N77-10014
Unclas 09537

by

P. F. Evans
J. E. Hackett

JUNE 1976

Distribution of this report is provided in the interest of information exchange. Responsibility for the contents resides in the authors or organization that prepared it.

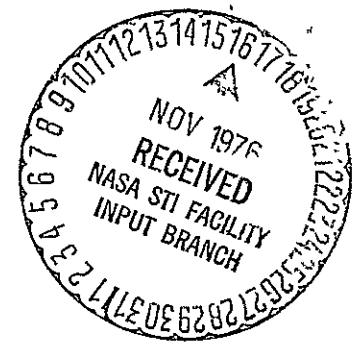

Prepared under Contract No. NAS2-8651 by
LOCKHEED-GEORGIA COMPANY
Marietta, Georgia

for Ames Research Center

NATIONAL AERONAUTICS AND SPACE ADMINISTRATION

NASA CR-137888
Available to the Public

NUMERICAL STUDIES OF THREE-DIMENSIONAL BREAKDOWN IN TRAILING VORTEX WAKES

by

P. F. Evans
J. E. Hackett

JUNE 1976

Distribution of this report is provided in the interest of information exchange. Responsibility for the contents resides in the authors or organization that prepared it.

Prepared under Contract No. NAS2-8651 by
LOCKHEED-GEORGIA COMPANY
Marietta, Georgia

for Ames Research Center

NATIONAL AERONAUTICS AND SPACE ADMINISTRATION

TABLE OF CONTENTS

FIGURE INDEX

LIST OF SYMBOLS

AR	aspect ratio
a_x	x-perturbation amplitude
a_y	y-perturbation amplitude
a	vector resultant of a_x and a_y
b	vortex span (Section 3)
b	wing span (Sections 2, 4, and 5)
C_L	lift coefficient
d	deviation of element after backward marching, see Equation (9)
ℓ	length of local vortex segment (Section 2.2)
N	downward convection velocity of a local point divided by overall mean value
R_c	local radius of curvature (Section 2.2)
s'	coordinate along the length of a vortex line (Section 2.2)
t	time (secs)
t_{CRIT}	time at which looping or convergence occurs
t_ℓ	time taken for a single vortex pair to loop
U_∞	mainstream speed
V_s	self-induced velocity (Section 2.2)
x, y, z	coordinates of perturbed element (Section 2.2)
x', y', z'	coordinates of perturbing element (Section 2.2)
β	(Equation 11) phase between maxima in a_x and a_y
β	(Section 5.6) ratio of sliding calculation frame downstream velocity to free-stream velocity
γ	ratio of tip vortex strength to flap vortex strength
Γ	resultant or total vortex strength

Γ_F	vortex strength at flap outer end
Γ_F'	$\Gamma_F/U_\infty(b/2)$
Γ_T	wing tip vortex strength
Γ_T'	$\Gamma_T/U_\infty(b/2)$
Γ_x, Γ_y, Γ_z	x-, y-, and z-components of Γ
δ	vortex core radius (Section 2.2)
η_F	flap vortex coordinate normalized on semispan
η_{MIN}	minimum span position of vortex track, normalized on semispan
η_T	tip vortex coordinate normalized on semispan
η_{CG}	center of gravity of trailing vortex system, with vortex strength as "weight"
θ_1, θ_2	angles subtended at the origin of the radius of curvature by the local point and each of the adjacent points
$\Delta\theta$	angular motion during one time step, $\Delta\tau$
λ	wavelength
ν	kinematic viscosity
σ	spiral strain index, see Equation (26)
τ	nondimensional time, equals $tU_\infty/(b/2)$ (Section 2.2)
τ_c	uncorrected time for a vortex to converge at the center plane
τ_{cc}	corrected time for vortex to converge at the center plane [Equation (32)]
τ_I	time equivalent of distance between aircraft cg and front of first calculation frame [Equation (32)]
τ_o	time equivalent of distance, within calculation frame, from its leading edge
$\Delta\tau$	nondimensional time-step
ϕ	Sum of Γ_F' and Γ_T' (i.e., total nondimensional vortex strength)

Subscripts

DUM	intermediate dummy point, see Section 2.2
f	see Equation (9)
i	see Equation (9)
L	denotes influencing point (see Section 2.2)
N	denotes influenced point (section 2.2)
o	see Equation (9)

NUMERICAL STUDIES OF THREE-DIMENSIONAL BREAKDOWN IN TRAILING VORTEX WAKES

By P. F. Evans and J. E. Hackett
Lockheed-Georgia Company

SUMMARY

Finite element, three-dimensional relaxation methods are used to calculate the development of vortex wakes behind aircraft for a considerable downstream distance. The inclusion of a self-induction term in the solution, dependent upon local curvature and vortex core radius, permits calculation of finite lifetimes for systems for which infinite life would be predicted two-dimensionally. The present report describes the associated computer program together with single-pair, twin-pair, and multiple-pair studies carried out using it. It is found, in single-pair studies, that there is a lower limit to the wavelengths at which the "Crow"-type of instability can occur. Below this limit, self-induction effects cause the plane of the disturbance waves to rotate counter to the vortex direction. Self induction in two dimensionally generated twin spiral waves causes an increase in axial length which becomes more marked with decreasing initial wavelength. The time taken for vortex convergence toward the center plane is correspondingly increased. The limited parametric twin-pair study performed suggests that time-to-converge increases with increasing flap span. Limited studies of Boeing 747 configurations show correct qualitative response to removal of the outer flap and to gear deployment, as compared with wind tunnel and flight test experience.

1. INTRODUCTION

During the past several years, strenuous efforts have been made to devise means for breaking up prematurely and permanently the trailing vortices behind large transport aircraft so as to reduce or eliminate their hazard to following aircraft. Many of the attempts aimed at modifying individual vortices have met with indifferent success or have been impractical or too costly to apply.

One of the more reliable "natural" modes of vortex pair decay is vortex looping. This form of instability was analyzed first by Crow (ref. 1), using linear methods. Shortly thereafter, his results were extended numerically by Hackett and Theisen (ref. 2), who calculated the progression from Crow's sinuous shapes toward the familiar "looped" form sometimes observed in flight (ref. 3) or in water tank experiments (refs. 2 and 4). The calculations used finite-element, time-dependent techniques applied to single vortex pairs. A limited study was made of the effect of the initial amplitude and wavelength of a "Crow"-type perturbation. Because these initial quantities must be specified, there are difficulties in specifying time-to-loop.

It is the objective of the present work to provide methods for deepening the previous single-pair studies and extending the methods to multiple-pair configurations including both wakes typical of current jumbo jets and experimental cases such as "sawtooth" loading suggested by Rossow (ref. 5) for promoting early wake disruption. Appropriate Fortran algorithms have been written and documented which achieve the above objectives. The program was delivered to NASA-Ames in April 1976 and implemented there on both the IBM 360-67 and CDC-7600 computers. Program development was carried out at the Lockheed-Georgia Company on a MAC-16 mini-computer, where CRT graphics are available and on a Univac 1106 terminal system for longer runs. The program and its documentation form Appendix A of the present report.

In any study like the present one, it is very desirable to make comparisons with experimental results. Though documented flow investigations in the near-field are quite numerous and despite the wealth of longer-time measurements at discrete downstream planes, it has proved impossible to find quantitative experiments which give adequate details of vortex looping flow. Experiments with towed models are the most suitable for this and although looping has been noted with a small model size relative to the test region cross section (ref. 2), the majority of scale models tested have had larger relative size and looping has not occurred. In some cases, wall constraints may have inhibited looping; in others the vortices have encountered a horizontal surface before looping had time to occur. Even with the looping flow properly generated, good measurements are difficult.

In carrying out numerical calculations of the vortex wake, a choice is available between a space-fixed and an aircraft-fixed reference system. During the present work, it became apparent that while vortex looping is an unsteady space-fixed event, spiral multiple-vortex development is steady in an aircraft-fixed frame of reference. Though computing considerations made space-fixed analysis mandatory for a very long wake, it was found in practice that an

aircraft-fixed analysis was essential to provide proper initial conditions for multiple vortex arrays. An extended version of the program was therefore developed for this purpose, which is compatible with the main, space-fixed algorithm.

Sufficient experience has now been obtained with the program that the proper initialization procedures, step sizes, etc. are in hand and the significance of each input variable is well appreciated. These factors are documented herein. However, since some of the quoted twin-and multiple-pair examples lie part-way up the learning curve, the corresponding results should not be regarded as definitive but rather as a qualitative guide for future application of the program.

Section 2 will outline the theoretical approach, velocity calculation methods, self-induction effects, stepping procedures, etc. used throughout the present work. Section 3 is devoted to single vortex pair events and further examines the vortex looping phenomenon. In Section 4 the distinction between looping and spiral center-plane convergence is discussed and the effects of twin pair variables are reviewed. The computational details and requirements for such calculations are also included.

In Section 5 pilot calculations are described involving multiple vortex pair wakes for actual aircraft configurations. Conclusions are given in Section 6.

2. THEORETICAL APPROACH

2.1 General Discussion

When dealing with single-pair decay, there is little option but to impose an initial perturbation either arbitrarily or via a knowledge of a specific turbulence environment for aircraft flight. For multiple pairs, however, this situation is relieved by the fact that in some cases vortex helices form naturally, starting in the near wake. In other cases, vortex strengths and positions may be such that the pattern disperses rapidly without helices forming. Figure 2.1 shows an example of each type, in end view, for twin vortex pairs. Bilanin *et al* (ref. 6) have produced classification charts showing the relative vortex strengths and relative spans associated with each type of motion.

In analyzing single-pair deformations, a space-fixed frame of reference is perfectly adequate. However, it is evident from the above that an aircraft-fixed analysis is needed for multiple pairs, at least to start the calculation. Accordingly, a variant of the original program has been written, in an aircraft-fixed frame of reference, which includes the near-field effect of the wing. The resulting program solves the steady-state problem in three dimensions by a time relaxation of an initial two-dimensional, Trefftz plane solution.

Once the initial, transient motions are complete there may remain a number of vortex pairs arranged in helices. It is not practical to continue to analyze the subsequent motion in aircraft-fixed axes, because of the prohibitive number of points involved, which must all be perturbed starting from zero time. A change is therefore made into space-fixed axes and a regular cyclic geometry is assumed. If this change is made at a distance corresponding to N miles aft of the aircraft and the subsequent time-to-looping is T seconds, the total distance to looping is given by $(N + U_\infty T)$ miles.

It must be remarked that the above transient-plus-cyclic distinction is arbitrary, since divergence may require many cycles in some cases. However, the distinction is useful and practical except possibly for borderline, near-cyclic cases.

2.2 Velocity Calculations

Given a constant-strength vortex, strength Γ, radius δ, which follows an arbitrary curved path in three dimensions from point A (x_A, y_A, z_A) to point B (x_B, y_B, z_B), we seek the three velocity components, u, v, and w, at an arbitrary point N(x, y, z) on the vortex. L(x', y', z') is a typical element which influences N.

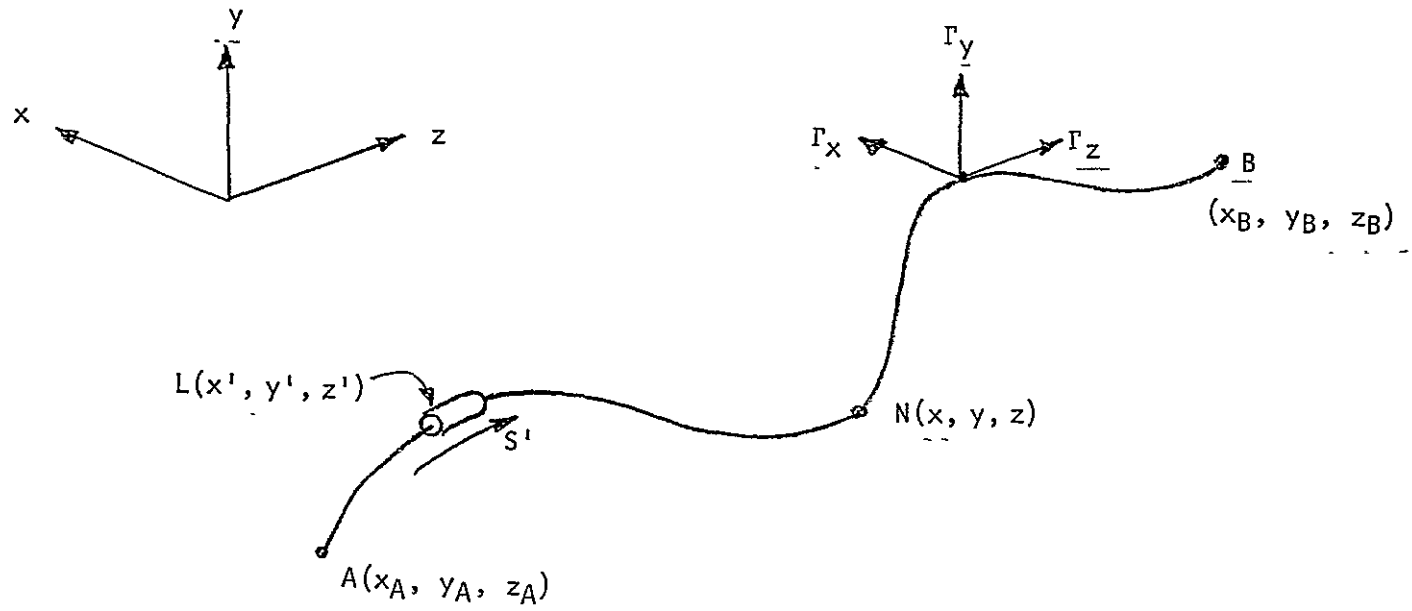

The calculation is divided into three parts: the near, intermediate, and far fields. The near field concerns the effect of an element on itself, while the far field concerns elements sufficiently remote that their detailed structure is not significant at point N. All other points are classified as intermediate.

When studying the periodic vortex cases, it is convenient to use imaging techniques such that only one side of the aircraft wake and only one-half wave (one full wave for spiral perturbations) are actually perturbed and the periodic part of the wake vortex system is represented by various reflections. In the case of aircraft-fixed analysis, there is no periodic geometry, but half-plane symmetry still applies.

Near-field. – The self-induced velocity is determined in a manner similar to that of Leonard (ref. 8). The self-induced velocity (V_s) is in a direction normal to the local plane of curvature and is given by the relation

$$V_s = \frac{\Gamma}{4\pi R_c}\left[\log_e\left\{\frac{8R_c}{\delta}\right\} - 0.558 - \frac{1}{2}\log_e\left\{\cot\frac{\theta_1}{4}\cot\frac{\theta_2}{4}\right\}\right] \tag{1}$$

where:

R_c = local radius of curvature

θ_1, θ_2 = angles between the local point and each of the adjacent points based on the origin of the radius of curvature

δ = core radius, derived from

$$\frac{d\delta^2}{dt} = 4\nu - \frac{\delta^2}{\ell}\frac{d\ell}{dt} \tag{1a}$$

ℓ = length of local segment

The terms in the time-dependent expression for core radius, δ, yield respectively the viscous growth and vortex stretching effects. Since molecular viscosity has been used in the present calculations, viscous growth is very small. Equation (1a) is evaluated in finite-difference form.

Intermediate field. — We resolve the total strength Γ into orthogonal components Γ_z, Γ_z, and Γ_z at x', y', z' so that

$$\Gamma_x^2 + \Gamma_y^2 + \Gamma_z^2 = \Gamma^2 \tag{2}$$

and

$$\Gamma = \frac{\Gamma_x}{dx'/ds'} = \frac{\Gamma_y}{dy'/ds'} = \frac{\Gamma_z}{dz'/ds'} \tag{3}$$

where

$$dx'^2 + dy'^2 + dz'^2 = ds'^2 \tag{4}$$

Reference 7 gives:

$$u = \frac{\Gamma}{4\pi} \int_A^B \left\{ \frac{dy'}{ds'} \frac{z - z'}{r} - \frac{dz'}{ds'} \frac{y - y'}{r} \right\} \frac{ds'}{r^2}$$

$$v = \frac{\Gamma}{4\pi} \int_A^B \left\{ \frac{dz'}{ds'} \frac{x - x'}{r} - \frac{dx'}{ds'} \frac{z - z'}{r} \right\} \frac{ds'}{r^2} \tag{5}$$

$$w = \frac{\Gamma}{4\pi} \int_A^B \left\{ \frac{dx'}{ds'} \frac{y - y'}{r} - \frac{dy'}{ds'} \frac{x - x'}{r} \right\} \frac{ds'}{r^2}$$

where AB is the vortex line and $r^2 = (x - x')^2 + (y - y')^2 + (z - z')^2$.

Taking the u component as typical

$$u = \int_A^B \frac{dy'}{ds'} \frac{\Gamma}{4\pi r^3} (z - z')\, ds' - \int_A^B \frac{dz'}{ds'} \frac{\Gamma}{4\pi r^3} (y - y')\, ds'$$

Now

$$\Gamma_y = \frac{dy'}{ds'} \Gamma \quad \text{and} \quad \Gamma_z = \frac{dz'}{ds'} \Gamma$$

So

$$u = \int_A^B \frac{\Gamma_y}{4\pi r^3}(z - z')\, ds' - \int_A^B \frac{\Gamma_z}{4\pi r^3}(y - y')\, ds'$$

Writing Equation (5), at a point N, as a sum over L_{TOTAL} finite elements:

$$\left.\begin{aligned} u_N &= \sum_{L=1}^{L_{TOTAL}} \frac{(\Gamma\Delta y)}{4\pi r_{NL}^3}(z_N - z_L) - \sum_{L=1}^{L_{TOTAL}} \frac{(\Gamma\Delta z)}{4\pi r_{NL}^3}(y_N - y_L) \\ v_N &= \sum_{L=1}^{L_{TOTAL}} \frac{(\Gamma\Delta z)}{4\pi r_{NL}^3}(x_N - x_L) - \sum_{L=1}^{L_{TOTAL}} \frac{(\Gamma\Delta x)}{4\pi r_{NL}^3}(z_N - z_L) \\ w_N &= \sum_{L=1}^{L_{TOTAL}} \frac{(\Gamma\Delta x)}{4\pi r_{NL}^3}(y_N - y_L) - \sum_{L=1}^{L_{TOTAL}} \frac{(\Gamma\Delta y)}{4\pi r_{NL}^3}(x_N - x_L) \end{aligned}\right\} \quad N \neq L \qquad (6)$$

where Δx, Δy, and Δz are the components of a straight, finite element which represents a segment of the vortex AB. When N = L, Equation (1) is used. In implementing Equation (6) for $N \neq L$, a "short element" concept is applied, in which the products, $\Gamma\Delta x_L$, $\Gamma\Delta y_L$, and $\Gamma\Delta z_L$ are defined as the short element strength components. Dummy points (XDUM, YDUM, ZDUM) are situated midway between the perturbed points along each vortex line. Therefore:

$$\begin{aligned} \Delta x_L &= XDUM_{L+1} - XDUM_L \\ \Delta x_L &= YDUM_{L+1} - LDUM_L \\ \Delta z_L &= ZDUM_{L+1} - ZDUM_L \end{aligned} \qquad (7)$$

By using this short element method the effects of vortex stretching in the intermediate field can be considered, without changing the total number of points, by suitable modifications to $\Gamma\Delta x_L$, $\Gamma\Delta y_L$, and $\Gamma\Delta z_L$.

Far field. – Beyond one or two complete wavelengths, each side of a perturbed point the vortex system may be extended by horizontal, straight-line elements. These are added at both ends of periodic geometries (space fixed) and at the downstream end of aircraft-fixed geometries.

2.3 Time-History Calculation

A one-step, second-order predictor-corrector computation is used in which the desired element x-displacement, for example, is defined as the midpoint of the resultant of two Euler displacement vectors, $u(t)\,dt$ and $u(t+dt)\,dt$. $u(t)$ is the induced velocity field based on the positions of the vortex element system at the time t and $u(t+dt)$ is the induced velocity based on the positions of the system at time $(t+dt)$. The general relation for displacement using predictor-corrector stepping is:

$$x'(t+dt) = \frac{1}{2}\left[x(t) + x(t+dt) + u(t+dt) \cdot dt\right] \tag{8}$$

where

$$x(t+dt) = x(t) + u(t) \cdot dt \text{ (Euler value at } (t+dt))$$

$$x(t) = \text{value at } t$$

$$x'(t+dt) = \text{predictor-corrector value at } t+dt$$

The other two components are treated similarly.

In two-dimensional calculations the accuracy of the time-integration may be checked fairly readily by determining the vortex center of gravity, moments, and the Kirkoff-Routh path function (see ref. 5). Such checks are generally not available for three-dimensional motions. In principle, checks should be made that conservation laws are obeyed, but the necessary volume integrations are more difficult and more numerically hazardous than the original calculation. The only check found feasible so far is to employ a reversed-marching technique to find the degree of accuracy to which the system returns to its original state. At the end of a series of time steps, the sign of the time increment is reversed and the program marches back to the initial time. The deviation for each vortex element is then defined as:

$$d_i = \left[(x_{i_f} - x_{i_o})^2 + (y_{i_f} - y_{i_o})^2 + (z_{i_f} - z_{i_o})^2\right]^{\frac{1}{2}} \tag{9}$$

where f denotes position after backward marching, and o denotes initial position. The arithmetic

$$\left(= \frac{1}{N} \sum_{i=1}^{N} d_i\right) \tag{10}$$

and geometric

$$\left(= (d_1\, d_2 \text{ --- } d_N)^{1/N}\right)$$

means are then determined. Some typical results are illustrated in the following table:

TABLE I. — ACCURACY OF TIME-STEPPING METHODS
(SINGLE PAIR, 51 STEPS)

Calculation Method	Arith. Mean	Geom. Mean
Predictor-Corrector	.00319	.00271
Euler	.801	.696

The predictor-correlator method, which takes little more than twice the running time of the simple Euler stepping method, provides a 250-fold accuracy gain in this particular example. In practice, a part of such benefits is used to reduce computer run time.

2.4 Time-to-Loop

The formation of long loops along the track of an originally parallel trailing vortex pair is a well-known occurrence. The development from the initial sinuous perturbation (ref. 1) towards the near-ring shapes may be calculated (ref. 2) by finite element methods. The next stage, the formation of loops, is not well understood. In real flows, the point of nearest approach, across the plane of symmetry, starts to convect downwards; but almost immediately there is a "click" and the vortices break, change partners, and then link across the center-plane to form loops. This event is a very fundamental one since it also typifies the cascading process by which large eddies break down to smaller ones in turbulent flows. Nevertheless, there is little detailed knowledge of the mechanism, and no criterion exists which defines when the "click" occurs.

Fortunately, it is sufficiently accurate for present purposes to define the start of looping as the time at which the point of closest approach is convected downward at ten times the mean downdrift velocity for the whole wake. This defines the start of looping sufficiently sharply for use in long-time solutions. (See Figure 2.2.)

3. SINGLE-PAIR LOOPING

3.1 Significant Parameters

Reference 2 gives examples which extend numerically the linearized analysis by Crow (ref. 1). As indicated above, these space-fixed calculations have been improved, both numerically and by the addition of the element self-induction term of Equation (1). As a result, the tendency to a fine-grain waviness instability on each individual loop has been reduced very considerably. The use of the higher precision CDC-7600 computer for many of the runs reported here gave additional numerical improvements and permitted longer time histories to be calculated. Figures 3.1(a), (b), and (c) show, respectively, plan views of the initial condition, a later geometry using results from a reference 2 type of calculation and the corresponding result from the present program.

For a given vortex spacing (b), the time to loop (t_ℓ), as defined in Section 2.4, is a function of the vortex strength (Γ); the amplitudes (a_x, a_y), phase (β), and wavelength (λb) of the initial perturbation and the vortex core radius (δ). The relationships take the nondimensional form:

$$\frac{\Gamma t_\ell}{b^2} = f\left\{\lambda, \frac{a_x}{b}, \frac{a_y}{b}, \beta, \frac{\delta}{b}\right\} \tag{11}$$

3.2 Effect of Perturbation Amplitude

In Section 3, the initial perturbations a_x and a_y usually will be equal and in phase, giving the classical 45°-inclined plane wave shown in Figure 3.1(a). In Figure 3.2, it is evident that there is an approximately inverse relationship between time-to-loop and initial amplitude. The constant of proportionality is, of course, dependent upon vortex core radius and wavelength. As perturbation amplitude increases, the drift velocity of the point-of-close-approach will increase. Eventually, this will reach ten times the mean (straight vortex) drift velocity as used to define the onset of looping. This produces the intercept with the horizontal axis. In potential flow, this would correspond approximately to the condition when the distance of closest approach was 10% of the mean vortex spacing.

Limited checks have also been made of the effect of using spiral and planar initial conditions. Labelled points in Figure 3.2 show that the use of a spiral initial condition increases the time-to-loop by nearly 40%. This is important because multiple vortex pairs develop spiral modes. Clearly, the "Crow" mode is more efficient at driving the system towards looping. It is interesting to note that, if the x- and y-perturbations are applied separately, the x-perturbation on its own is very inefficient in this regard. However, applying solely y-perturbation increases time-to-loop by only 20% over the combined perturbation.

These results suggest that the present methods could be used to determine optimum configurations for deliberately induced initial perturbations in real flows.

3.3 Effect of Vortex Core Radius

Figure 3.3 shows the results of three calculations made for the same total time. The first uses current numerics, but omits the self-induction effect on each element. Figures 3.3(b) and (c) show corresponding results for medium and large-sized cores. As might be expected, increase in core size has a damping effect on the overall motion. It is also interesting to note that the omission of curvature effects produces a result intermediate to the other two; i.e. an effective core radius has been implied. This is a somewhat similar situation to the use of a cut-off radius by Crow (ref. 1). In the present case, the effective radius is determined (if self-terms are neglected) by the number of elements per wave.

Figure 3.4 returns to the full equations and shows a gradual increase in time-to-loop with vortex core radius. It should be noted that the right hand part of this curve becomes less valid because the small radius assumptions inherent in Equation (1) are violated.

A number of investigators have suggested means for diffusing individual vortices to reduce their hazard to following aircraft. The present result suggests that such diffusion may actually increase the time to ultimate decay, by delaying looping. It is therefore important to be certain that such attempts to accelerate diffusion have a sufficient effect.

3.4 Effect of Perturbation Wavelength

Though time-to-loop decreased with decrease in wavelength, as previously (ref. 2), an unexpected upturn in the curve occurred at short wavelengths in the present calculations (see Figure 3.5).

To better understand the mechanisms, let us first examine in more detail the progression towards "conventional" looping. Figure 3.6 shows, at zero time, an end view of the right-hand vortex, inclined outward at 45 degrees. The individual points are calculation points on a half-wave. As time progresses the whole array drifts downward, largely maintaining its 45-degree inclination. At the two longest times shown, the lower points are moving downward and inward at an increasing rate: a nascent looping stage has been reached.

Figure 3.7 has essentially the same conditions as previously, but a shorter wavelength. Initially, the innermost vortices move inward as before but at a faster rate, as would be expected from previous experience concerning wavelength effects. However, the 45-degree inclination is not retained as before. A clockwise rotation, opposing the direction of the vortex, develops.

In consequence, the distance-of-closest approach starts to increase markedly and looping is forestalled.

The suggested mechanism for the above motion is illustrated in Figure 3.8(a). At any wavelength, there is a tendency for the crests of each sine wave to self-convect like part of a vortex ring. The corresponding motion is outward and downward at the top of the wave, inward and upward at the bottom, and zero at the inflection points. This motion increases as the wavelength is reduced. Counterbalancing this effect is the velocity gradient due to the opposite vortex, which is approximately constant. Thus, the outward rotation due to self-induction, which is dependent upon the ratio of amplitude to wavelength, is offset against the velocity gradient effect, which depends only upon amplitude. An illustrative velocity vector diagram is shown in Figure 3.8(b).

Boundaries have been found, in an amplitude - wavelength domain, which define the lower limit for looping. Figure 3.9 shows the results of a number of numerical calculations, for two core radii. As might be expected from cored-ring convection properties, the larger vortex core radii cases are less likely to self-rotate.

To each point on the boundaries shown in Figure 3.9, there corresponds a (different) time-to-loop. These are minima, as was noted in Figure 3.5. Figure 3.10 illustrates the nature of time-to-loop contours in the same coordinates as the previous figure.

4. TWIN PAIR CONVERGENCE

4.1 The Generation and Disruption of Spiral Waves

It was noted previously that single spiral waves were noticeably more stable than plane waves of the "Crow" type. In this section we shall examine the properties of spiral waves with emphasis on the mechanisms and flow geometries which lead to vortex destruction. Though the same calculation procedures and divergence criteria may be used for each, there is a very important distinction between the instability of a spiral wave and that of a plane wave of the "Crow"-type. Figure 4.1 illustrates this distinction from the viewpoint of an observer fixed in space. When a vortex trail with plane waves reaches a sufficient age, this observer sees "necking" start to occur, followed by the aforementioned "click" when looping occurs. Thereafter, the looping point remains fixed in space. In contrast, the spiral wave is fed continuously towards the center plane. Prior to the critical time, the fixed-observer sees a convergence event moving towards him in the direction of aircraft motion. The "time-to-converge" corresponds to its passage directly in front of him. In contrast to the previous case, the event is steady as seen from an aircraft frame of reference. These considerations in no way preclude space-fixed events due to atmospheric disturbance or other modes of instability. However, to underline the distinction, the distruction of spiral waves by meeting at the center plane will be referred to as "convergence" and "looping" will be reserved for the space-fixed event.

Definition of variables. The spiral wavelength for a twin-pair trail is determined by aircraft forward speed, as well as vortex details and it must be included in the normalization scheme. Thus, if primed quantities are dimensionless and the kinematic variables are as shown in Figure 4.2, we define

$$\Gamma_F' = \frac{\Gamma_F}{U_\infty\, b/2} \qquad \Gamma_T' = \frac{\Gamma_T}{U_\infty\, b/2} \tag{12}$$

with a total

$$\phi = \Gamma_F' + \Gamma_T' \tag{13}$$

For convenience, we write

$$\gamma = \frac{\Gamma_T}{\Gamma_F} = \frac{\Gamma_T'}{\Gamma_F'} \tag{14}$$

The following relationships are noted:

$$\Gamma_F' = \frac{\phi}{1+\gamma} \qquad \Gamma_T' = \frac{\gamma\phi}{1+\gamma}$$

$$\eta_F + \gamma\eta_T = (1+\gamma)\eta_{CG} \tag{15}$$

$$C_L/AR = \phi\eta_{CG} \tag{16}$$

We normalize time t (secs), after aircraft passage, via

$$\tau = \frac{t\, U_\infty}{b/2} \tag{17}$$

For multiple vortex arrays and because of the possibility of c.g. variations under viscous, three-dimensional conditions, we measure wavelength of spiral motions, etc., in aircraft spans, as λb. It may be shown that the time per revolution of Γ_F and Γ_T about their c.g., in two dimensions, is given by

$$\tau/\text{rev.} = 4\pi^2 \frac{(1+\gamma)^2}{\phi} (\eta_T - \eta_{CG})^2 \tag{18}$$

or in aircraft variables

$$\tau/\text{rev.} = 4\pi^2 \frac{AR}{C_L} \frac{(\eta_F + \gamma\eta_T)}{(1+\gamma)} (\eta_T - \eta_F)^2 \tag{19}$$

and we note also that the wavelength,

$$\lambda = \frac{1}{2}\ \tau/\text{rev.} \tag{20}$$

Conditions for convergence. Figures 4.3 and 4.4 show the effects, on the calculated development towards convergence, of varying the relative span positions and strengths of the vortices. The vortex wavelength, after three-dimensional relaxation, is a function of these variables and both end view and time-to-loop follow from this. Vortex radius also becomes a significant variable.

With a wing tip vortex somewhat weaker than the flap vortex, Figure 4.4 indicates that small flap spans lead to early convergence of the tip vortex. As the flap span increases, the spiral amplitude is reduced, and the trajectories approach the center plane less closely. Consequently, convergence is delayed. A simple geometric analysis shows that when the flap vortex is the stronger, the tip vortex will intersect the center plane after 180-degrees or less of travel provided that

$$\eta_F \le \frac{1-\gamma}{2}, \qquad (\gamma \le 1). \tag{21}$$

Equation (21) is a particular case of a geometric expression for minimum centerplane clearance by the tip vortex, i.e.

$$\eta_{MIN} = \frac{2}{1+\gamma} (\eta_F + \gamma) - 1, \qquad (\gamma \le 1). \tag{22}$$

Figure 4.4 illustrates the consequences of Equation (22). With flap-span constant, a case with γ less than one [Figure 4.4(a)] clearly converges much more quickly than with equal strength [Figure 4.4(b)]. We note here that since the two spirals are of equal amplitude, they each have an equal chance of converging.

Once $\gamma > 1$, the flap vortex (now weaker) forms the outermost spiral and consequently η_{MIN} clearly cannot be less than η_F. This explains the range of validity of Equation (22).

The velocity condition for convergence. Equations (21) and (22), being based solely upon geometric considerations, do not reflect the velocity condition used to define convergence in the present calculations. The effect is to move the critical point outward from the center plane by an amount

$$\Delta\eta = \frac{\gamma(\eta_F + \gamma)}{N(\gamma + 1)^2} \tag{23}$$

which is added to Equation (22) to give

$$\eta_{MIN} = \frac{1}{1+\gamma}(\eta_F + \gamma)\left\{2 + \frac{\gamma}{N(\gamma+1)}\right\} - 1 \qquad \gamma \leq 1 \tag{24}$$

Since $\gamma \leq 1$ and an N-value of 10.0 is used, the effect of the added term is evidently small. A corresponding analysis modifies Equation (21) to the form

$$\eta_F = \frac{(\gamma-1)^2 N}{(2(\gamma+1)N - \gamma)} - \gamma \qquad (\gamma \leq 1) \tag{25}$$

This reduces to Equation (21) for $N \to \infty$ or $\gamma \to 0$. Again, the differences are small within the range of validity. The differences between results derived from (24) and (25) and those from the simpler expressions are not sufficient to justify the added complexity in most applications.

The spiral strain index, σ. Equations (21) and (25) describe the conditions under which the flap vortex drives the tip vortex into, or near to the the center plane after half a revolution or less of travel. The tip vortex, being the weaker, forms the outermost spiral, which converges. However, it is evident from Figures 4.3 and 4.4 that, for cases with several revolutions prior to convergence, it is also possible for the inner, more intense, spiral to converge first. Figure 4.5 shows a further example of each type.

Figure 4.6 is a parametric map with flap span as ordinate and relative vortex strength as abscissa. Each plotted point depicts one computer run in a parametric study which will be described in Section 4.2. Triangles and circles represent, respectively, flap and tip vortex convergence as the first event. As might be expected, tip vortex convergence occurs in the vicinity of the lower-left boundary [Eqns. (21) and (25)], but then flap vortex convergence becomes more likely as η_F is increased. There is also a change on passing through $\gamma = 1.0$ (i.e. flap and tip strengths equal). To understand the structure of these domains, we shall examine the distortion mechanism which leads ultimately to convergence.

On passing through its innermost position, each vortex receives an extra downward impulse induced by the opposite-hand vortex at a distance $2\eta_{MIN}$ away. This causes an outward-spiraling tendency which, continued long enough, leads to convergence at the center plane. We may quantify this tendency in terms

of the nondimensional velocity increment causing the effect. Thus, we define spiral-strain indices:

$$\sigma_F = \frac{\Gamma_F'}{\eta_{MINF}}$$

$$\text{and} \qquad \sigma_T = \frac{\Gamma_T'}{\eta_{MINT}} \tag{26}$$

We now hypothesize that the vortex which has the larger σ value will converge first. Thus, for the tip vortex to converge first requires that

$$\sigma_T > \sigma_F$$

Using Equation (22) and noting that $\eta_{MINF} = \eta_F$, this yields

$$\frac{\Gamma_F'\gamma(1+\gamma)}{2\eta_{F_{CRIT}} - (1-\gamma)} > \frac{\Gamma_F'}{\eta_{F_{CRIT}}} \tag{27}$$

for the tip vortex to converge first.

A borderline case may be found by using an equality in Equation (27) which readily yields

$$\eta_{F_{CRIT}} = \frac{1}{\gamma+2} \tag{28}$$

This line partitions the data in Figure 4-5 quite successfully though not perfectly because of the simplifying assumptions. However, resolution of the flap- or tip-convergent regions requires some care.

Provided that $\eta_{F_{CRIT}}$ and Γ_F' are both positive, Equation (27) may be written

$$\frac{N}{D} = \frac{\eta_{F_{CRIT}}\gamma(1+\gamma)}{2\eta_{F_{CRIT}} - (1-\gamma)} > 1$$

We may clear this further, by multiplying by D, only if

$$2\eta_{F_{CRIT}} - (1-\gamma) > 1$$

i.e. if $\gamma > 1 - 2\eta_{F_{CRIT}}$.

This defines a region in Figure 4.5 above the line marked "Eqn. (21)." Thus,

$$\eta_{F_{CRIT}}\,\gamma(1+\gamma) > (2\eta_{F_{CRIT}} - (1-\gamma)), \qquad \gamma > (1-2\eta_{F_{CRIT}})$$

giving

$$\eta_{F_{CRIT}}\,(\gamma^2+\gamma-2) > (\gamma-1), \qquad \gamma > (1-2\eta_{F_{CRIT}}) \tag{29}$$

Since both sides change sign at $\gamma = 1$, the cases $\gamma \lesssim 1$ must be considered separately. This yields, eventually

$$\eta_{F_{CRIT}} > \frac{1}{\gamma+2}, \qquad \gamma > 1$$

and (30)

$$\eta_{F_{CRIT}} < \frac{1}{\gamma+2}, \qquad (1-2\eta_{F_{CRIT}}) < \gamma < 1$$

for the tip vortex to converge first. This agrees with most of the test cases in Figure 4.6. More elaborate treatments are obviously possible, using Equation (25), for example, or taking spiral diameter into account. However, the simplicity of Equation (30) is attractive.

4.2 Twin-Pair, Parametric Study

By suitable choices of flap span and loading, it is possible to reduce the vortex hazard for any specific aircraft at a given weight and speed. Recent studies (ref. 11) have demonstrated the hazard reduction benefits of reduced flap span, for example. In order to provide a basis for quantifying the trades between flap span and setting angle, convergence times have been calculated over a wide range of η_F and Γ_T/Γ_F. Boundaries for rapid convergence have been published previously (ref. 6), but no attempt has been made to calculate the time taken for cases within such limits. This is only possible if three-dimensional, self-induction effects are included.

Figure 4.7a shows contours of the dimensionless time-to-converge [see Equation (17)]. For computational consistency a constant wavelength $\lambda = 5.375$, was employed for the whole figure, the implicit assumption being that λ is a weak parameter. However, subsequent studies (see Section 4.3) have shown this to be untrue. Consequently, the loading parameter (C_L/AR) cannot be merged with nondimensional time τ, as was originally hoped. It follows that a map like Figure 4.7a should be prepared for each of a series of constant values of C_L/AR. In the present case the relevant C_L/AR value for any specific point may be found from Figure 4.7b using the fact that $\lambda \approx 5.375$ in the previous figure. Figure 4.8 presents the results of a limited study (for $C_L/AR = 0.25$) using proper wavelengths for each run. An increase in time-to-converge with increasing flap span is indicated. In view of the significance of other parameters (notably vortex radius), there is a very real question whether it is preferable to treat even twin pair cases on an individual, rather than a parametric basis.

When convergent vortices reach the center plane, they merge and dissipate. However, it is possible and even probable, in still air, that the surviving vortex will still represent a hazard. Figure 4.9 shows that, for short convergence times near the lower hatched boundary, the surviving vortex is undesirably strong. At any given flap span (>.333b) it is evident that the surviving vortex strength is maximized if flap- and tip-vortex strengths are equal. It is possible to adopt a systems approach to define a minimum hazard condition and then determine optimum flap spans and vortex strengths for a given flight condition with both the surviving vortex strength (Figure 4.9) and time-to-converge (Figure 4.7a) taken into account. However, Figure 4.7a should be revised to include values of spiral wavelength consistent with the relevant C_L/AR condition before such studies are undertaken.

4.3 Three-Dimensional Effects

As indicated above, changes in spiral wavelengths were found to have a significant effect on time-to-converge. Figure 4.10, which was calculated on the same space-fixed basis as the previous study, shows an increase in time-to-converge as wavelength is increased. When two-dimensional calculations were attempted, to provide a limiting case, convergence was not obtained even well beyond τ values corresponding to the six-mile limit generally applied. This indicates agreement between the present numerical result and Bilanin's (ref. 6) analytical result which predicts infinite time for two-dimensional cases outside the lower boundary.

The detailed reasons for wavelength dependence are not understood. However, it is noted that the self-convection effect on an element is similar in nature in a spiral to that found previously for plane waves; there is a tendency to slow down the gross rotation rate. Another distinction concerns "axial pumping." A tightly-wound spiral vortex has transverse vorticity components, which correspond to "ring" vorticity. In the core of the spiral, these vorticity components induce a velocity away from the generating wing and a proportion is felt by the spiral itself, tending to lengthen it. It follows that any vortex spiral geometry generated on the basis of quasi-two-dimensional assumptions will have too short a wavelength. Figure 4.11 quantifies this effect. Vortex spirals were first calculated two-dimensionally, then relaxed three-dimensionally in a wing-fixed frame of reference. In view of the λ-dependence of time-to-converge (Figure 4.10), it is clearly desirable to determine a 3-D relaxed wavelength, rather than one derived simply from two-dimensional considerations, before embarking on detailed or definitive studies.

4.4 Notes on Computing

Initialization. We saw in the preceding section that a spiral wavelength assigned on the basis of two-dimensional considerations [Eqns. (19) and (20)] will not be in equilibrium axially. It has also been necessary to assign unit

value to the tip vortex span, in the interest of reducing the number of variables. To circumvent such difficulties, it is now clear that any space-fixed calculation involving more than one vortex pair should at least start with a corresponding aircraft-fixed calculation which determines vortex spans and wavelengths, which are in self-equilibrium and which are consistent with the span loading. The two-dimensions-plus-time type of calculation provides a suitable starting geometry for three-dimensional relaxation of an appropriate (i.e. more than one-full wavelength) length of wake.

Since it is unfeasible to relax the equivalent of several miles of wake simultaneously, in aircraft-fixed axes, a transition to a single-wave, space-fixed calculation is made. A suitable whole wavelength is selected* which is downstream of the direct influence of the wing; this is assigned time value $\tau = 0$ in the space-fixed calculation. Figure 4.12 shows how subsequent time steps march down the wake. There are, thus, three computational components to the distance of any particular point from the wing. These are: x_1, the distance from the wing to the leading edge of the frame $\tau = 0$; τ, which defines the distance travelled by the leading edge of the frame; and finally x_o, the axial distance within the frame τ, measured from its leading edge.

The trajectory of a particular point. Since the point which converges is of predominant interest in the present study, we shall use this as an example. At the start of the calculation, it cannot be known which point will converge. Consequently, all points on every frame must be output. Once the convergent point has been identified, however, its complete trajectory may be determined, frame-by-frame, back to the point x_o on the initial frame. The examples in Figure 4.5 were plotted in this way. τ_o, which corresponds to the position on the original frame, is given by

$$\tau_o = \frac{2N - 1}{NTOT} \; 2\lambda \tag{31}$$

where N is the vortex element number and NTOT is the number of elements per wave. The total time-to-converge is thus given by

$$\tau_{cc} = \tau_1 + \tau_o + \tau_c \tag{32}$$

where τ_1 equals x_1/U_∞ and τ_c, as before, is the time step (space fixed) at which convergence occurred. Any other specific point may be treated in the same way.

Conjugate runs. In twin-pair parametric studies, advantage may be taken of the fact that, after the first half wavelength, the flap and tip vortices interchange. If these are now renamed and suitable changes are made to the length scales, a new point on the parametric may may be obtained. If a tilde is used to signify the conjugate run, we may write

$$\tilde{\gamma} = 1/\gamma \tag{33}$$

---

*For multiple-pair cases, see Section 5.

and

$$\frac{\tilde{\eta}_F}{\tilde{\eta}_T} = \frac{2\eta_{CG} - \eta_T}{2\eta_{CG} - \eta_F} \tag{34}$$

The assumption implicit above, that true spiral form is retained for the first half wave, has been confirmed in practice. However, attempts to carry out a similar procedure further down the wake have shown that true conjugates are not obtained; distortion of the spiral has become too significant.

Size of time-step. The angle, $\Delta\theta$, through which the joining line between two vortices rotates during one time step, $\Delta\tau$, is given approximately by:

$$\Delta\theta = \frac{(\Gamma_1' + \Gamma_2')}{2\pi(\eta_T - \eta_F)^2} \Delta\tau \text{ radians} \tag{35}$$

For consistent accuracy, it is fairly obvious that the value of the stepping index, $\Delta\theta$, must be maintained at an appropriately small level for all cases. It is also evident that as η_F or loading becomes large, a large number of small time steps will be required. Typical step sizes, $\Delta\tau$, in the previous study have ranged from 1/3 to 2.0, depending upon flap span, at a (C_L/AR) value of 0.1714. It is generally found that the longer running cases (larger η_F) also require the smaller values of time-step. This affects computation time severely.

Figure 4.13 shows the effect of step size on time-to-converge for four flap and tip vortex geometries. Quite good accuracy is obtained provided the stepping index is maintained at 8-degrees or below. Thereafter, the larger η_F cases degrade fairly rapidly. This occurs not only because longer times result at larger η_F but also because errors are larger at any given step size. Figure 4.14, which shows the relative distance between two vortices after 50 time units, demonstrates this. In the absence of center-plane images, an ideal stepping system would maintain constant spacing indefinitely. Figure 4.14 shows that deviations from this trend increase with η_F.

5. MULTIPLE-PAIR CALCULATIONS

5.1 Introduction

For each vortex pair in a multi-component system, there are at least three independent variables, even if a horizontal, unswept trailing edge is assumed. These are: vortex strength, span position, and core radius. Effective viscosity is a possible fourth candidate. For N multiple vortices there are thus 3N or 4N minus one variables. (Length scale may be embedded in the core Reynolds number.) For a twin vortex system, a two variable map like Figure 4.7 must be repeated at least over a parametric range of C_L/AR, for example, even for constant core properties.

It is evident that it is not profitable to attempt to extend generalized results beyond twin-pair cases. A number of realistic, multiple-pair cases have therefore been selected, as examples for the present section, involving up to seven vortex pairs. These cases, defined in Figure 5.1, will be described further in later sections.

An additional motivation for treating cases individually concerns the calculation itself. For example, if a 4-pair rather than a two-pair case is considered, point density must be increased along each vortex, by a factor of two, giving four times as many points and a factor of 16 on the number of velocity calculations required. Yet a further factor of two is needed to properly relate the time step-size to vortex spacing*, yielding an overall computation increase of 32-times, or 2^5. Computer run time considerations are much more critical than core storage requirements, which vary only as the square of the number of vortex pairs.

For these reasons, and because of the relative cost-per calculation, three-pair runs and up were carried out on Lockheed-Georgia computers only as necessary for program checkout, i.e. one or two time steps. The multiple pair runs reported in this section were made on the NASA-Ames CDC 7600 computer during a three-week period which included program checkout. Part of the development of the aircraft-fixed algorithms was also carried out at this time. This was sufficient to complete a number of test cases and to establish preferred methods and guidelines. Owing to the "one-shot" nature of the runs it was not possible, however, to produce completed calculations which may be regarded as totally definitive. The Ames results, plus subsequent studies, indicate that the program does have the required capability, however.

**This is mandatory for aircraft-fixed calculations, but some relief is possible in space-fixed cases.*

5.2 General Approach

The decay of a complex, multi-vortex wake involves successive reductions in the number of vortices, either via convergence at the center plane (see Section 4) or by merging of two vortices into one (see ref. 10). Figure 5.2 shows how the length of the wake may be partitioned on this basis. In the present context, the terms "near-," "middle-," or "far-wake" relate only to the number of vortices present and have no specific counterparts in miles.

Starting at the downstream end, we see that the "far" wake contains just one vortex pair. Since this has the potential for very long life under calm conditions, it is important to design the initial wake configuration in such a way that this remaining pair is a weak one. (We saw in Section 4 that, with suitable starting conditions, earlier convergence of stronger pairs is possible).

The "middle" wake involves a twin pair. This may be dealt with either using parametric plots or on a specific basis depending upon whether the geometry is near-spiral or has suffered noticeable distortion in the near wake*. In the latter case, space-fixed calculation methods may be used, as described in Section 4.

It is the "near" wake which is of principal concern in this section. Considering briefly the simplest, three-vortex case, it is noted that an embedded twin-pair wavelength will no longer characterize the motion. In most cases, this will prevent effective use of a space-fixed analysis, because the wavelength over which the motion *is* cyclic (assuming no convergences) is impractically long. It follows that an aircraft-fixed analysis must be used.

The dependence of computer run time upon the fifth power of the number of vortices (see Section 5.1) makes it highly desirable to eliminate from the calculation those vortices which converge early and to merge those which spiral together in close proximity. Figure 5.3 shows examples of both types. This particular case concerns a "sawtooth" loading configuration designed by Rossow (ref. 5). The reduction from seven to four vortex pairs is clearly most desirable, computationally.

The results shown in Figure 5.3 were obtained using an aircraft-fixed two-dimensional calculation. A corresponding three-dimensional relaxation was attempted but proved unstable. Since complicated 3-D relaxation cases are likely to require individual treatment to overcome stability problems and are liable to be very expensive to run, it may be acceptable to rely on a simpler method for the early wake provided that the convergence or merging events are strongly indicated. If this is so, the predictive accuracy of the overall calculation will probably be acceptable.

**If specific core details are to be used, the parametric approach is likely to be precluded.*

In summary, the overall approach includes the following steps, given vortex dispositions along the trailing edge and their strengths:

(1a) Use 2-D, reference 9, or (preferably, if stable) 3-D relaxation methods to identify and treat each vortex merging and convergence to the center plane. This will usually reduce the wake to no more than three or four vortex pairs.

(1b) Continue to treat the remaining wake using aircraft-fixed methods until two pairs remain.

(2) If the remaining twin pair is largely undistorted and individual core details are not available, a parametric map may be consulted. A recommendation for the preparation of such plots is included later in this report.

(3) Once one member of the twin pair has either converged on the center plane or merged with its mate, the ensuing single pair wake cannot be calculated by present methods because it is straight and undisturbed in still air. If it is possible to postulate a periodic disturbance, the methods of Section 3 may be used.

5.3 Three-Dimensional Relaxation of the Near Wake

Before starting a three-dimensional relaxation, it is desirable to determine a reasonably close approximation to the final result. This reduces computer time and may prevent instability problems in some cases. Either a two-dimensional or a quasi-two-dimensional (ref. 9) initial run may be used. Figure 5.4 shows an example of each type, together with a fully-relaxed, three dimensional run for the same case. Both of the two-dimensional methods display wake geometries very similar to the fully-relaxed, three-dimensional method. The fully-relaxed run does not extend as far downstream as the two-dimensional runs due to computer limitations.

The three-dimensional relaxation process is well behaved for all the three-pair wakes reviewed. Disturbances originating near the trailing edge propagate away at approximately mainstream speed (see Figure 5.5) leaving a stable vortex system whose transverse velocities are of order 10^{-5} or 10^{-6} – the limit of computer resolution. The vertical arrows in Figure 5.5 depict the downstream end of the converged region.

Attempts were made to converge 4-, 5-, 6-, and 7-pair cases in the same manner as above, with decreasing degrees of success. However, all of these cases employed a swept trailing edge starting line which caused elements on adjacent vortices to be staggered relative to each other. It is believed that this destabilized the relaxation calculation.

5.4 Three-Pair Cases

Certain three-pair wakes may be described as near-cyclic [see Figure 5.6(a)], while in others [Figure 5.6(b)] the third vortex causes irregularities in the shorter wavelength which gives the overall motion a more transient nature. In such cases, there is, therefore, no prospect for using a space-fixed analysis which uses reflection techniques based on the shortest wavelength.

In near-cyclic cases [Figure 5.6(a)], an attempt was made to simplify the problem by assuming that beyond the initial relaxation region, the third vortex remains straight.* A space-fixed calculation at the shorter wavelength was then carried out with the full streamwise image system, as used previously for twin pairs. As for the corresponding aircraft-fixed case, the innermost vortices travelled together as they were convected downward and outward by the main flap vortex. However, a rapid spiraling then occurred which is uncharacteristic of the aircraft-fixed result. The straight-vortex approximation was therefore unsuccessful.

Recognizing the inherent aircraft-fixed nature of the expected phenomena, the above data were scanned as if by an observer moving at aircraft speed. This produced improvements in some cases, but cyclic instabilities which occurred at frame passage frequency prevented useful results from being obtained. However, deeper investigation suggested a hybrid aircraft-fixed/space-fixed calculation technique which appears promising. This will be described in Section 5.6.

5.5 "Jumbo-Jet" and "Sawtooth" Cases

The Boeing 747 runs outlined in Figure 5.1 were selected in the light of recent wind tunnel and flight wake hazard test experience at NASA concerning the effect of removing the outer flap and using the inner flap alone to restructure the vortex wake, and concerning the effect of landing gear deployment on such results. In the present calculations the representation of the gear is via its estimated effect upon span load: this omits all viscous wake considerations. Nonetheless, the gear-related span-load changes are found to have a significant impact upon the vortex wake structure. Pre-runs, to identify convergence, merging, etc. (see Section 5.2), permitted simplifications to the distributions shown in the upper part of Figure 5.1 such that three-pair loading configurations could be used as depicted in the lower part of that figure. Three-dimensional relaxation of these three-pair configurations to a steady state then produced the wake structures shown in Figure 5.7.

The upper two cases of Figure 5.7 correspond to early flight tests which were carried out, gear-up, for full flaps and for inboard flaps only. Wider vortex dispersion is evident in the latter case, which should be beneficial. Lowering the gear reduced the strength of the (anti-lift) inboard flap vortex in both cases. With outer flaps present, lowering the gear caused a much less regular periodic near-wake solution. The reduction in inboard vortex

*Though not fixed.

strength, due to the gear, also greatly reduced the tendency of the flap and tip vortices to spread apart. A more hazardous wake is therefore implied with the gear down. This corresponds to flight test observations.

The results of Figure 5.7, and other "jumbo"-jet runs not reported here because of step-size problems, have not been extended to determine time-to-converge. Two-dimensional extensions of the B747 runs have been made which indicate that convergence is occurring in the cases shown, but such runs can give no further information because curvature terms, which lead to convergence, are lacking.

It is urged that the "jumbo"-jet demonstration runs started during the present study, are completed and compared with corresponding flight and wind tunnel test results. The use of the sliding-frame calculation method (see below) should make such studies more economical than was envisaged previously.

5.6 The Sliding-Frame, Aircraft-Fixed Calculation Method

In previous sections of this report, space-fixed and aircraft-fixed calculations have been regarded as quite separate approaches for solving the far vortex wake. However, a review of results, particularly the moving observer, space-fixed study of Section 5.4, has suggested a hybrid method which is best regarded from an aircraft-fixed point of view.

In Figure 5.5, the history of an aircraft-fixed three-dimensional relaxation is dominated by a disturbance wave which propagates downstream at approximately mainstream speed and leaves behind the desired steady solution. Let us define the wave propagation speed as β times aircraft speed. We may choose a time, in the aircraft-fixed calculation, at which direct wing influence is no longer felt at the position of the disturbance front: "TIME = 20" is suitable (Figure 5.5). A calculation frame, stretching, say from Station 16 to Station 28, is now drawn around the disturbance front. If this frame is slid along the wake at β times mainstream speed, the disturbance front in Figure 5.5 remains centered and converged wake is always contained in the left half of the frame. If suitable precautions are taken with conditions at the ends of the frame, particularly upstream, this provides an attractive and economical basis for a wake solution. In fact, if $\beta = 1$, the method reduces to a space-fixed calculation. The corresponding ($\beta = 1$) program changes are trivial.

Treatment of the downstream end of the frame presents little difficulty: a two-dimensional type of initial solution will clearly suffice, as for the aircraft fixed case. At the upstream end care must be taken both to ensure that a sufficient length of converged wake is included and to provide sufficiently realistic upstream conditions that the converged wake within the box is not contaminated. Such questions could be resolved by comparison with existing cases run with the current aircraft-fixed algorithms.

Since the program changes involved are minor, and test examples exist, the above modifications and checkout appear to be highly worthwhile.

6. CONCLUSIONS AND RECOMMENDATIONS

A computer program has been developed which uses finite-element three-dimensional relaxation methods to calculate the development of vortex wakes behind aircraft for a considerable downstream distance. The program is now operational at NASA-Ames. The inclusion of a self-induction term in the solution, dependent upon local curvature and vortex core radius, permits calculation of finite lifetimes for systems for which infinite life would be predicted two dimensionally. The present report describes the program together with single-pair, twin-pair, and multiple-pair studies carried out using it. Though "jumbo" aircraft wake examples are included, these have not been carried far enough for other than qualitative conclusions to be drawn.

The wake studies have lead to the following conclusions:

Single-Pair Wakes

(1) There is a lower limit to the wavelengths at which the "Crow"-type instability can occur. Below this limit, self-induction effects cause the plane of the disturbance waves to rotate counter to the vortex direction.

(2) Disturbance waves in a horizontal plane are several times more stable than the classic, 45-degree "Crow" case. Vertical and spiral waves are slightly more stable.

Twin-Pair Wakes

(3) There is an important distinction between single-and twin-pair vortex convergence at the center plane. The first is usually a space-fixed event, but the latter moves at aircraft speed.

(4) The self-induction term causes the time taken for vortices to converge at the center plane to be a strong function of wavelength (see Figure 4.10). Either vortex can converge first (Figure 4.6).

(5) In the limited twin-pair studies performed for constant C_L/AR, time-to-converge increases with increasing flap span.

(6) Choosing equal strengths for flap (for $\eta_F > .333$) and tip vortices maximizes the strength of the vortex which survives after one has converged at the center plane (see Figure 4.9).

Multiple-Pair Wakes

(7) Though space-fixed axial-imaging techniques can be used for single- and twin-pair wakes, they are not applicable directly to multiple pairs.

Calculations must at least start in an aircraft-fixed coordinate system. Thereafter, a "sliding-frame" method is suggested which has potential for applying three-dimensional relaxation methods economically to the far wake. The method is very similar to a space-fixed calculation but is controlled differently (see Section 5.6).

(8) Pilot studies of Boeing 747 configurations show correct qualitative response to removal of the outer flap and to gear deployment, as compared with wind tunnel and flight test experience (see Figure 5.7).

Recommendations

(1) More detailed studies should be undertaken of the separate effects of vortex core radius and relaxed wavelength on the time to attain center-plane convergence in twin-pair cases. This should provide useful design guidance for low-hazard wakes.

(2) Further time-to-converge, twin-pair parametric studies (see Section 4.2) should be carried out, holding C_L/AR constant for each of several maps like Figure 4.7a and 4.8.

(3) The "sliding frame" calcultion method should be implemented and used to complete the present jumbo-jet studies.

(4) More comprehensive studies should be made concerning wakes designed for early disruption, e.g. the "sawtooth" design. This requires more detailed aircraft fixed runs for near wake, including an improved rationale for vortex merging. If significant vortices then remain, the "sliding frame" method should be applied.

7. REFERENCES

1. Crow, S. C.: Stability Theory for a Pair of Trailing Vortices. *AIAA Journal*, vol. 8, no. 12, December 1970, pp. 2172-2179.

2. Hackett, J. E.; and Theisen, J. G.: Vortex Wake Development and Aircraft Dynamics. *Aircraft Wake Turbulence and Its Detection*. Edited by J. Olsen, A. Goldberg, and M. Rogers, Plenum Press, 1971.

3. Chevalier, H.: Flight Test Studies of the Formation and Dissipation of Trailing Vortices. *J. Aircraft*, vol. 10, no. 1, January 1973, pp. 14-18.

4. Widnall, S. E.; Bliss, D. B.: and Zalay, A.: Theoretical and Experimental Study of the Stability of a Vortex Pair. *Aircraft Wake Turbulence and Its Detection*, edited by J. Olsen, A. Goldberg, and M. Rogers, Plenum Press, 1971.

5. Rossow, V. J.: Theoretical Study of Lift-Generated Vortex Wakes Designed to Avoid Roll-Up. *AIAA Journal*, vol. 13, no. 4, April 1975, pp. 476-484.

6. Bilanin, A. J.; Donaldson, C. duP., and Snedeker, R. S.: An Analytical and Experimental Investigation of the Wakes Behind Flapped and Unflapped Wings. AFFDL-TR-74-90, May 1974.

7. Lamb, Sir Horace: *Hydrodynamics*. Sixth ed. Dover Publications, 1945.

8. Leonard, A.: Numerical Simulation of Interacting, Three-Dimensional Vortex Filaments. Proc. of the Fourth International Conference on Numerical Methods in Fluid Dynamics, Spring-Verlag, 1974.

9. Hackett, J. E.; and Evans, M. R.: Vortex Wakes Behind High-Lift Wings. *J. Aircraft*, vol. 8, no. 5, May 1971, pp. 334-340.

10. Rossow, V. J.: Convective Merging of Vortex Cores in Lift-Generated Wakes. AIAA Paper No. 76-415.

11. Proceedings, NASA Symposium on Wake Vortex Minimization, Washington, February 25-26, 1976.

APPENDIX

VORTEX LOOPING COMPUTER PROGRAM OPERATION

PRECEDING PAGE BLANK NOT FILMED

1. GENERAL PROGRAM OPERATION

A computer program has been developed to apply the previous methods to multiple vortex pair instabilities. The program has been implemented on the U1106 computer and the MAC-16 mini-computer at Lockheed-Georgia and the IBM 360-67 and the CDC-7600 computers at NASA-Ames.

The program has the capability to analyze up to seven vortex pairs and up to ninety points per wavelength in the cyclic, space-fixed option and ninety points per vortex in the aircraft-fixed option. In the space-fixed option each point is perturbed at each time step and a new geometry is calculated for the next time step. Since the frame of reference is fixed in space, no velocity is imparted to the system except that induced on each point by the system. The calculations are continued until the vortex system becomes unstable.

The aircraft-fixed option is more complex. An initial two-dimensional time dependent, space-fixed calculation is performed. Time is then converted to downstream distance to set up the initial geometry for a three-dimensional time relaxation. In the aircraft-fixed frame of reference the free stream velocity must be added to the induced velocities. The free stream velocity causes the points to move downstream. To keep the frame of reference fixed with the aircraft, the points must be reordered at each time step. Each point, N, at time, t, becomes the point, N+1, at time, $t+\Delta t$. The points on the wing are fixed with time, and the trailing edge point is used twice at $t+\Delta t$; once fixed on the wing and once shed downstream. The last downstream point is removed at each time step. The calculation continues until equilibrium is reached. This normally requires that the number of time steps equal the number of points per vortex considered.

2. INPUT

The general input parameters to the vortex looping program are:

Spatial coordinates (x, y, z)
Vortex strength (Γ)
Semi-wavelength ($\lambda/2$)
Wave amplitude (a)
Core radius (δ)

A description of the input parameters is given in Table A-1. All variables used in the vortex looping program are normalized on wing semispan (b/2) and free stream velocity (U_∞). If the subscript, s, denotes normalized value used in the program and the subscript, o, denotes dimensional values, then:

TABLE A-1. INPUT PARAMETERS

IPRT	Frequency of printout
NCASE	Number of cases to be run (1 in current version)
ITAPE	Graphics or plotter option (1 if desired)
IU	Output unit for graphics or plotter
IW	Output unit for printout
IWR	Printout option (1 if desired)
IPRTA	Frequency of output for graphics or plotter
IBACK	Backward march option (1 if desired)
J	Case number
DELTM(J)	Time increment
RNCM(J)	Reference Reynolds number
IPM(J)	Number of wavelengths considered
IZLM(J)	Number of points.per wavelength — must be even if IOP2M(J)=0. For aircraft-fixed or 2-D options IZLM(J)=1.
NPM(J)	Number of vortex pairs
MTIMM(J)	Number of time steps
ICASM(J)	Graphics case number (not used in current version)
IOPTM(J)	Input option 0 Sinusoidal input 1 Point-by-point input -1 Spiral input
IOP2M(J)	Full/half wave option 0 Half wave considered 1 Full wave considered
TIMEM(J)	Initial time
DELTB(J)	Time increment (= distance increment) for initial 2-D aircraft fixed calculation. DELTB(J) must equal DELTM(J).
CBAR(J)	Wing mean aerodynamic chord.
MPTS(J)	Number of time steps for initial aircraft fixed calculation. If MPTS(J)=0, then space fixed option is used.
TITLE(II,J)	Title

TABLE A-1. INPUT PARAMETERS (Concluded)

I	Vortex pair number. For aircraft fixed calculations, vortices must be input from inboard to outboard.
NPAM(I,J)	Vortex reference number
CIRCM(I,J)	Vortex strength
WVLM(I,J)	Wavelength/2.0. Must be the same for all vortices.
AMPXM(I,J)	Amplitude of sinusoidal/spiral disturbance in x-direction
AMPYM(I,J)	Amplitude of sinusoidal/sprial disturbance in y-direction
RCORM(I,J)	Core radius
SSM(I,J)	Initial spanwise location of vortex
HINM(I,J)	Initial vertical location of vortex
PHASM(I,J)	Phase shift of disturbance. Must be the same for all vortices.
N	Point number for point-by-point input
XIN(N,I,J)	X location of N
YIN(N,I,J)	Y location of N
ZIN(N,I,J)	Z location of N
RCOMI(N,I,J)	Core radius of N

$$x_{i_s} = x_{i_o}/(b/2)$$

$$\Gamma_s = \Gamma_o/(U_\infty b/2)$$

$$v_{i_s} = v_{i_o}/(U_\infty)$$

$$t_s = t_o(U_\infty/b/2)$$

$$\lambda_s = \lambda_o/(b/2)$$

$$a_s = a_o/(b/2)$$

$$\delta_s = \delta_o/(b/2)$$

The input format is summarized in Table A-2. Note that x is the spanwise coordinate, y is the vertical coordinate, and z is the downstream coordinate.

3. MAIN PROGRAM/SUBROUTINE FUNCTIONS

The principal functions performed by the main program and each subroutine are:

SUBROUTINE		FUNCTIONS
Main Program	1.	Case data input.
	2.	Initial geometry for one side of each vortex pair determined using sinusoidal or spiral distribution or point-by-point input.
	3.	Other parameters used in calculations determined (X_iDUM, $CX_i = \Gamma\Delta x_i$, etc.).
	4.	Displacements and new geometry for each time step calculated.
	5.	Geometry at each time step output.
PCOR	1.	Induced velocities summed.
	2.	Element compression applied.

TABLE A-2. INPUT FORMAT

Card	Format	Input Parameters
1	9I4	IPRT, NCASE, ITAPE, IU, IW, IWR, IPRTA, IBACK
2	2F10.0,7I4	DELTM(J), RNCM(J), IPM(J), IZLM(J), NPM(J) MTIMM(J), ICASM(J), IOPTM(J), IOP2M(J)
3	3F10.0,I4	TIMEM(J), DELTB(J), CBAR(J), MPTS(J) *(If aircraft fixed calculations are not to be done, then MPTS(J) = 0.)*
4	20A4	TITLE(II,J)
If IOPTM(J)=0		
5	I4,8F9.0	NPAM(I,J), CIRCM(I,J), WVLM(I,J), AMPXM(I,J), AMPYM(I,J), RCORM(I,J), SSM(I,J), PHASM(I,J), HINM(I,J)
		(Repeat card 5 for each vortex pair.)
If IOPTM(J)=1		
5	I4,8F9.0	NPAM(I,J), CIRCM(I,J), WVLM(I,J)
6	4F10.0	XIN(N,I,J), YIN(N,I,J), ZIN(N,I,J), RCOMI(N,I,J) *(Repeat card 6 for each point (N = 1, INPI) on a single vortex pair (one side only).)* *(Note: Calculations are performed on the points N = 2, INPI-1.)* *(Repeat cards 5 and 6 for each vortex pair.)*
		(Repeat cards 2 through 6 for each case.)

FAAVEL	1. Induced velocities from each point determined.
	2. Imaging techniques used to determine the effects of up and downstream points and the vortices shed from the other wing.
CURV	1. Local radius of curvature calculated.
	2. Core radius at time, t, calculated.
	3. Self-induced velocity calculated.
STAT	1. Final geometry at end of backward march compared to initial geometry.

4. PROGRAM LISTING

A listing of the vortex looping program as used on the U1106 computer follows.

```
      C      PROGRAM MAIN(INPUT,OUTPUT,TAPE5=INPUT,TAPE6=OUTPUT,TAPE8,TAPE1)
      C        MAIN PROG
            DIMENSION NPAM(7,1 ),CIRCM(7,1 ),WVLM(7,1 ),AMPXM(7,1 ),
           1 AMPYM(7,1 ),RCORM(7,1 ),SSM(7,1 ),PHASM(7,1 ),ICASM(1 ),
           2 MTIMM(1 ),DELTM(1 ),RNCM(1 ),IPM(1 ),IZLM(1 ),NPM(1 )
           3 ,XIN(92,7,1 ),YIN(92,7,1 ),ZIN(92,7,1 ),RCOMI(92,7,1 )
           4 ,IOPTM(1),IOP2M(1),HINM(7,1),TIMEM(1),TITLE(20,1),TTL(20)
           5 ,DELTB(1),MPTS(1),CBAR(1)
            DIMENSION XP(92,7),YP(92,7),ZP(92,7),NPA(7),WVL(7),AMPX(7),AMPY(7)
           1 ,RCORE(7),SS(7),SEMIW(7),PH(7),PHAS(7),HIN(7)
            COMMON X(92,7),Y(92,7),Z(92,7),U(92,7),V(92,7),W(92,7),
           1 XDUM(93,7),YDUM(93,7),ZDUM(93,7),CX(92,7),CY(92,7),CZ(92,7),
           2 CIRC(7),ALMBDA(7),X0(92,7),Y0(92,7),Z0(92,7),DELRM(92,7)
           3 ,RCOM(92,7)
            DATA PI/3.1415926/,QPI/.7853982/,QPI2/1.5707963/,ZERO/0.0/,PI2/6.2
           $831852/
         90 CONTINUE
            IR=5
            I2D=0
      C       INPUT
            READ(IR,106)IPRT,NCASE,ITAPE,IU,IW,IWR,IPRTA,IBACK
            IF(IPRT.LT.0) GO TO 998
            DO 54 J=1,NCASE
            READ(IR,107)DELTM(J),RNCM(J),IPM(J),IZLM(J),NPM(J),MTIMM(J),
           1 ICASM(J),IOPTM(J),IOP2M(J)
            READ(IR,120)TIMEM(J),DELTB(J),CBAR(J),MPTS(J)
            READ(IR,302)(TITLE(II,J),II=1,20)
            NPRE=NPM(J)
            IF(IZLM(J).LE.1) I2D=1
            DO 54 I=1,NPRE
            IOPTT=IOPTM(J)
            IF(IOPTT.LE.0) GO TO 56
            READ(IR,103)NPAM(I,J),CIRCM(I,J),WVLM(I,J)
            INPI=IZLM(J)/2+2
            IF(IOP2M(J).GE.1) INPI=IZLM(J)+2
            IF(I2D.GE.1) INPI=1
            DO 57 K=1,INPI
         57 READ(IR,117)XIN(K,I,J),YIN(K,I,J),ZIN(K,I,J),RCOMI(K,I,J)
            GO TO 54
         56 READ(IR,103)NPAM(I,J),CIRCM(I,J),WVLM(I,J),AMPXM(I,J),
           1 AMPYM(I,J),RCORM(I,J),SSM(I,J),PHASM(I,J),HINM(I,J)
         54 CONTINUE
            DO 5 J=1,NCASE
      C       INITIAL COND. FOR EACH CASE
            DO 88 I=1,20
         88 TTL(I)=TITLE(I,J)
            DELTZ=0.0
            I2D=0
            MTIME=MTIMM(J)
            IAC=0
            JAC=0
            IF(MPTS(J).GE.1) IAC=1
            IF(IAC.GE.1) JAC=1
            IF(IAC.GE.1) MTIME=MPTS(J)
            XMAC=CBAR(J)
            ICASE=ICASM(J)
            DELT=DELTM(J)
            IF(IAC.GE.1) DELT=DELTB(J)
```

ORIGINAL PAGE IS
OF POOR QUALITY

```
      RNC=RNCM(J)
      IP=IPM(J)
    6 IZLINK=IZLM(J)
      IF(IZLINK.LE.1) I2D=1
      NPAIR=NPM(J)
      IOPT=IOPTM(J)
      IOP2=IOP2M(J)
      DO 55 I=1,NPAIR
      NPA(I)=NPAM(I,J)
      IF(IOPT.LE.0) GO TO 58
      INP=IZLINK/2+2
      IF(IOP2.GE.1) INP=IZLINK+2
      IF(I2D.GE.1) INP=1
      DO 97 K=1,INP
      X(K,I)=XIN(K,I,J)
      Y(K,I)=YIN(K,I,J)
      Z(K,I)=ZIN(K,I,J)
      RCOM(K,I)=RCOMI(K,I,J)
      XO(K,I)=XIN(K,I,J)
      YO(K,I)=YIN(K,I,J)
   97 ZO(K,I)=ZIN(K,I,J)
   58 CONTINUE
      WVL(I)=WVLM(I,J)
      IF(IOPT.GT.0) GO TO 55
      AMPX(I)=AMPXM(I,J)
      AMPY(I)=AMPYM(I,J)
      RCORE(I)=RCORM(I,J)
      SS(I)=SSM(I,J)
      PHAS(I)=PHASM(I,J)
      HIN(I)=HINM(I,J)
   55 CIRC(I)=CIRCM(I,J)
      RNC=RNC*10000.
      IMARCH=0
      IF(IWR.LE.0)GO TO 61
      WRITE(IW,303)
      WRITE(IW,302)TTL
      WRITE(IW,108)
      IF(DELT)999,999,60
   60 WRITE(IW,109)DELT,RNC,IP,IZLINK,NPAIR
      IF(IAC.LE.0) GO TO 26
      WRITE(IW,305)XMAC
   26 IF(IOPT.LE.0) GO TO 67
      WRITE(IW,118)
      GO TO 68
   67 WRITE(IW,114)
   68 CONTINUE
      DO 52 I=1,NPAIR
      IF(IOPT.LE.0) GO TO 59
      WRITE(IW,104)I,CIRC(I)
      GO TO 52
   59 WRITE(IW,104)I,CIRC(I),WVL(I),AMPX(I),AMPY(I),RCORE(I)
     1  ,SS(I),PHAS(I)
   52 CONTINUE
   61 RIZL=IZLINK
      ITE=0
      IST=0
C      INITIAL VORTEX GEOMETRY
      DO 66 I=1,NPAIR
      IF(IOP2)70,70,71
```

ORIGINAL PAGE IS
OF POOR QUALITY

```
      71 IHALF=IZLINK
         GO TO 72
      70 IHALF=IZLINK/2
      72 IF(IHALF-90) 10,10,11
      11 WRITE(IW,110) IZLINK
         GO TO 999
      10 IHALFP=IHALF+2
         IF(I2D.GE.1) IHALFP=1
         IHPP=IHALFP+1
         IH1=IHALF+1
         IBR=(2+IH1)/2
         IF(I2D.GE.1) GO TO 82
         IF(IOPT.LE.0) GO TO 63
         DO 64 N=2,IHALFP
         NM=N-1
         XDUM(N,I)=0.50*(X(N,I)+X(NM,I))
         YDUM(N,I)=0.50*(Y(N,I)+Y(NM,I))
      64 ZDUM(N,I)=0.50*(Z(N,I)+Z(NM,I))
         DO 65 N=2,IH1
         NP=N+1
         CX(N,I)=CIRC(I)*(XDUM(N,I)-XDUM(NP,I))
         CY(N,I)=CIRC(I)*(YDUM(N,I)-YDUM(NP,I))
      65 CZ(N,I)=CIRC(I)*(ZDUM(N,I)-ZDUM(NP,I))
         CX(1,I)=-CX(2,I)
         CY(1,I)=-CY(2,I)
         CZ(1,I)=CZ(2,I)
         CX(IHALFP,I)=-CX(IH1,I)
         CY(IHALFP,I)=-CY(IH1,I)
         CZ(IHALFP,I)=CZ(IH1,I)
         ALMBDA(I)=2.0*(ZDUM(IHALFP,I)-ZDUM(2,I))
         IF(IOP2.GE.1) ALMBDA(I)=ALMBDA(I)/2.0
         GO TO 66
      63 AMP=AMPY(I)
         ALMBDA(I)=2.0*WVL(I)
         PH(I)=PHAS(I)*ALMBDA(I)
         ZLINK=ALMBDA(I)/RIZL
         HZLINK=ZLINK/2.0
         SEMIW(I)=SS(I)
         ZDUM(1,I)=-ALMBDA(I)/2.0+PH(I)-ZLINK
         IF(IOPT.LT.0) GO TO 18
         YDUM(1,I)=HIN(I)+AMP*COS(PI2*ZDUM(1,I)/ALMBDA(I))
         GO TO 19
      18 YDUM(1,I)=HIN(I)+AMP*SIN(PI2*ZDUM(1,I)/ALMBDA(I))
      19 XDUM(1,I)=SEMIW(I)+AMPX(I)*COS(PI2*ZDUM(1,I)/ALMBDA(I))
         DO 12 N=2,IHPP
         NM=N-1
         ZDUM(N,I)=ZDUM(NM,I)+ZLINK
         IF(IOPT.LT.0) GO TO 27
         YDUM(N,I)=HIN(I)+AMP*COS(PI2*ZDUM(N,I)/ALMBDA(I))
         GO TO 28
      27 YDUM(N,I)=HIN(I)+AMP*SIN(PI2*ZDUM(N,I)/ALMBDA(I))
      28 XDUM(N,I)=SEMIW(I)+AMPX(I)*COS(PI2*ZDUM(N,I)/ALMBDA(I))
         Z(NM,I)=0.50*(ZDUM(NM,I)+ZDUM(N,I))
         IF(IOPT.LT.0) GO TO 29
         Y(NM,I)=HIN(I)+AMP*COS(PI2*Z(NM,I)/ALMBDA(I))
         GO TO 36
      29 Y(NM,I)=HIN(I)+AMP*SIN(PI2*Z(NM,I)/ALMBDA(I))
      36 X(NM,I)=SEMIW(I)+AMPX(I)*COS(PI2*Z(NM,I)/ALMBDA(I))
         X0(NM,I)=X(NM,I)
```

```
177             YO(NM,I)=Y(NM,I)
178             ZO(NM,I)=Z(NM,I)
179             CX(NM,I)=CIRC(I)*(XDUM(NM,I)-XDUM(N,I))
180             CY(NM,I)=CIRC(I)*(YDUM(NM,I)-YDUM(N,I))
181          12 CZ(NM,I)=CIRC(I)*(ZDUM(NM,I)-ZDUM(N,I))
182             GO TO 66
183          82 CX(1,I)=0.
184             CY(1,I)=0.
185             CZ(1,I)=-CIRC(I)
186             ALMBDA(I)=2.0*WVL(I)
187          66 CONTINUE
188             IF(I2D.GE.1) GO TO 87
189             IF(IOP2.GE.1) DELTZ=(Z(IH1,1)+Z(2,1))/2.0
190             DELTZO=DELTZ
191          87 CONTINUE
192             WRITE(IW,111)
193             IPTI=0
194             IPTA=0
195             TIME=TIMEM(J)
196             DO 25 I=1,NPAIR
197             DO 25 N=1,IHALFP
198             XP(N,I)=X(N,I)
199             YP(N,I)=Y(N,I)
200             ZP(N,I)=Z(N,I)
201             IF(IOPT.GT.0) GO TO 25
202             RCOM(N,I)=RCORE(I)
203          25 DELRM(N,I)=0.0
204             XBAR=0.0
205             YBAR=0.0
206             DELTYB=0.0
207          23 CONTINUE
208             IF(IAC.LE.0) GO TO 2
209             FAC=0.75*XMAC/2.0
210             FAC1=FAC
211             DO 80 I=1,NPAIR
212             KK=1
213             RCOMI(1,I,J)=RCOM(1,I)
214             YIN(1,I,J)=YO(1,I)
215             ZIN(1,I,J)=ZO(1,I)-2.0*FAC1
216             IF(I.EQ.1) GO TO 81
217             XIN(1,I,J)=XO(1,I-1)
218             GO TO 80
219          81 XIN(1,I,J)=0.0
220          80 WRITE(IW,112)KK,XIN(1,I,J),YIN(1,I,J),ZIN(1,I,J)
221             DO 3 I=1,NPAIR
222             DO 3 K=2,3
223             RCOMI(K,I,J)=RCOM(1,I)
224             XIN(K,I,J)=XO(I,I)
225             YIN(K,I,J)=YO(1,I)
226             ZIN(K,I,J)=ZO(1,I)-FAC-FAC1
227             WRITE(IW,112)K,XIN(K,I,J),YIN(K,I,J),ZIN(K,I,J)
228           3 FAC=-FAC
229           2 CONTINUE
230             DO 50 IT=1,MTIME
231       C     OUTPUT OF WAVE GEOMETRY
232             IF(IAC.GE.1) K=IT+3
233             IPCO=0
234             IF(IMARCH.GE.1)GO TO 30
235             IF(IWR.LE.0)GO TO 20
```

ORIGINAL PAGE IS
OF POOR QUALITY

```
      IF(IPTI.GE.IPRT)IPTI=0
      XBAR0=XBAR
      YBAR0=YBAR
      GXT=0.0
      GYT=0.0
      GT=0.0
      DO 79 I=1,NPAIR
      DO 79 NN=2,IH1
      N=NN
      IF(I2D.GE.1) N=NN-1
      GXT=GXT+CZ(N,I)*X(N,I)
      GYT=GYT+CZ(N,I)*Y(N,I)
   79 GT=GT+CZ(N,I)
      XBAR=GXT/GT
      YBAR=GYT/GT
      VDR=(YBAR-YBAR0)/DELT
      DELTYB=DELTYB+VDR*DELT
      IF(IAC.GE.1) GO TO 7
      WRITE(IW,113)TIME
    7 IF(IPTI.GE.1) GO TO 20
      IF(IAC.GE.1) GO TO 8
      WRITE(IW,304)XBAR,YBAR,VDR,DELTYB
    8 CONTINUE
      DO 78 I=1,NPAIR
      DO 78 N=1,IHALFP
      U(N,I)=(X(N,I)-XP(N,I))/DELT
      V(N,I)=(Y(N,I)-YP(N,I))/DELT
   78 W(N,I)=(Z(N,I)-ZP(N,I))/DELT
      DO 51 I=1,NPAIR
      IF(I2D.GE.1) ZDUM(1,I)=0.
      IF(IAC.GE.1) GO TO 9
      WRITE(IW,105)I,DELTZ
    9 CONTINUE
      DO 51 NN=1,IHALF
      N=NN+1
      IF(I2D.GE.1) N=NN
      IF(IAC.LE.0) GO TO 13
      IF(IT.LE.1) GO TO 51
      KP=K-1
      WRITE(IW,112)KP,XIN(KP,I,J),YIN(KP,I,J),ZIN(KP,I,J),
     1 U(N,I),V(N,I),W(N,I)
      GO TO 51
   13 WRITE(IW,112)NN,X(N,I),Y(N,I),Z(N,I),U(N,I),V(N,I),W(N,I)
   51 CONTINUE
   20 IPTI=IPTI+1
      IF(ITAPE.LE.0)GO TO 30
      IF(I2D.GE.1) GO TO 30
      IF(ITE.GE.1)GO TO 17
      DO 41 I=1,NPAIR
      DO 41 NN=1,IHALF
      N=NN+1
      IXN=X(N,I)
      IYN=Y(N,I)
      IZN=Z(N,I)
      IF(IABS(IXN).GE.100 ) GO TO 42
      IF(IABS(IYN).GE.100 ) GO TO 42
      IF(IABS(IZN).GE.100 ) GO TO 42
      GO TO 41
   42 ITE=1
```

```
295           WRITE(IW,115)
296           GO TO 17
297        41 CONTINUE
298           IF(IPTA.GE.IPRTA)IPTA=0
299           IF(IPTA.GE.1)GO TO 17
300           IF(IT.GT.1) GO TO 86
301           IF(TIME.GT.0.01) GO TO 17
302        86 CONTINUE
303           DO 15 I=1,NPAIR
304           DO 15 NN=1,IHALF
305           N=NN+1
306           YTAP=Y(N,I)-DELTYB
307           IF(JAC.GE.1) YTAP=Y(N,I)
308           ZTAP=Z(N,I)-DELTZ0
309        15 WRITE(IU,300)X(N,I),YTAP,ZTAP
310        17 IPTA=IPTA+1
311        30 IF(IT.GE.MTIME) GO TO 50
312           DO 43 I=1,NPAIR
313           DO 43 NN=1,IHALF
314           N=NN+1
315           IF(I2D.GE.1) N=NN
316           IF(ABS(X(N,I))-1000000.)44,45,45
317        44 IF(ABS(Y(N,I))-1000000.)46,45,45
318        46 IF(ABS(Z(N,I))-1000000.)43,45,45
319        45 IST=1
320           WRITE(IW,116)
321           GO TO 48
322        43 CONTINUE
323     C     CALCULATION OF INDUCED VELOCITIES
324           DO 40 I=1,NPAIR
325           DO 40 NN=2,IH1
326           NC=NN
327           N=NN
328           IF(I2D.GE.1) N=NN-1
329           CALL PCOR(N,I,IPCO,IP,IBR,NPAIR,IH1,IHALFP,DELT,IW,IST,IOP2,
330          1 JAC,XMAC)
331           IF(IST.GE.1) GO TO 48
332           IF(I2D.GE.1) GO TO 83
333           IF(JAC.GE.1) W(N,I)=W(N,I)+1.0
334           IF(JAC.LE.0) GO TO 69
335           IF(N.LE.3) GO TO 83
336        69 CONTINUE
337           CALL CURV(NC,DELT,IHALF,IPCO,IT,RNC,I,UC,VC,WC,IW,IST)
338           IF(IST.GE.1) GO TO 48
339           GO TO 84
340        83 UC=0.
341           VC=0.
342           WC=0.
343        84 U(N,I)=U(N,I)+UC
344           V(N,I)=V(N,I)+VC
345           W(N,I)=W(N,I)+WC
346        40 CONTINUE
347     C     MOD. OF INDUCED VEL. SO THAT VEL ALONG VORTEX = 0
348           IF(JAC.LE.0) GO TO 96
349           IF(IAC.GE.1) GO TO 96
350           DO 1 I=1,NPAIR
351           DO 1 N=1,IH1
352           IF(N.LE.2) GO TO 93
353           RX=XDUM(N+1,I)-XDUM(N,I)
```

ORIGINAL PAGE IS
OF POOR QUALITY

```
354             RY=YDUM(N+1,I)-YDUM(N,I)
355             RZ=ZDUM(N+1,I)-ZDUM(N,I)
356             RPSQ=RY*RY+RZ*RZ
357             RP=SQRT(RPSQ)
358             RSQ=RPSQ+RX*RX
359             R=SQRT(RSQ)
360             AL31=RX/R
361             AL32=RY/R
362             AL33=RZ/R
363             AL21=0.0
364             AL22=RZ/RP
365             AL23=-RY/RP
366             SIGN=RZ/ABS(RZ)
367             AL11=SIGN*RP/R
368             AL12=-SIGN*(RX*RY)/(R*RP)
369             AL13=-SIGN*(RX*RZ)/(R*RP)
370             UP=AL11*U(N,I)+AL12*V(N,I)+AL13*W(N,I)
371             VP=AL21*U(N,I)+AL22*V(N,I)+AL23*W(N,I)
372             WP=AL31*U(N,I)+AL32*V(N,I)+AL33*W(N,I)
373             WPP=WP
374             U(N,I)=AL11*UP+AL21*VP+AL31*WPP
375             V(N,I)=AL12*UP+AL22*VP+AL32*WPP
376             W(N,I)=AL13*UP+AL23*VP+AL33*WPP
377             IF(N.GE.3) GO TO 1
378          93 U(N,I)=0.0
379             V(N,I)=0.0
380             W(N,I)=0.0
381           1 CONTINUE
382          96 CONTINUE
383             DO 53 I=1,NPAIR
384             IF(I2D.GE.1) GO TO 75
385             IF(IOP2)73,73,74
386          73 U(1,I)=U(2,I)
387             V(1,I)=V(2,I)
388             W(1,I)=-W(2,I)
389             U(IHALFP,I)=U(IH1,I)
390             V(IHALFP,I)=V(IH1,I)
391             W(IHALFP,I)=-W(IH1,I)
392             GO TO 75
393          74 IF(JAC.GE.1) GO TO 95
394             U(1,I)=U(IH1,I)
395             V(1,I)=V(IH1,I)
396             W(1,I)=W(IH1,I)
397             U(IHALFP,I)=U(2,I)
398             V(IHALFP,I)=V(2,I)
399             W(IHALFP,I)=W(2,I)
400             GO TO 75
401          95 U(IHALFP,I)=2.0*U(IH1,I)-U(IH1-1,I)
402             V(IHALFP,I)=2.0*V(IH1,I)-V(IH1-1,I)
403             W(IHALFP,I)=2.0*W(IH1,I)-W(IH1-1,I)
404          75 CONTINUE
405             IF(I.EQ.1) IPCO=IPCO+1
406          C  CALCULATION OF VORTEX GEOMETRY
407             IF(IPCO-1)32,32,33
408          32 DO 31 N=1,IHALFP
409             XP(N,I)=X(N,I)
410             YP(N,I)=Y(N,I)
411             ZP(N,I)=Z(N,I)
412             X(N,I)=XP(N,I)+U(N,I)*DELT
```

```
413           Y(N,I)=YP(N,I)+V(N,I)*DELT
414        31 Z(N,I)=ZP(N,I)+W(N,I)*DELT
415           GO TO 35
416        33 DO 34 N=1,IHALFP
417           X(N,I)=0.5*(XP(N,I)+X(N,I)+U(N,I)*DELT)
418           Y(N,I)=0.5*(YP(N,I)+Y(N,I)+V(N,I)*DELT)
419        34 Z(N,I)=0.5*(ZP(N,I)+Z(N,I)+W(N,I)*DELT)
420           IF(JAC.LE.0) GO TO 4
421           IF(IAC.GE.1) GO TO 38
422           DO 14 N=1,IHALFP
423           NDE=IHALFP-N+1
424           IF(IMARCH.GE.1) NDE=N
425           IF(NDE.LE.2) GO TO 4
426           IDP=1
427           IF(IMARCH.GE.1) IDP=-1
428           X(NDE+IDP,I)=X(NDE,I)
429           Y(NDE+IDP,I)=Y(NDE,I)
430        14 Z(NDE+IDP,I)=Z(NDE,I)
431         4 CONTINUE
432           IF(JAC.LE.0) GO TO 38
433           DO 39 N=1,3
434           X(N,I)=XP(N,I)
435           Y(N,I)=YP(N,I)
436        39 Z(N,I)=ZP(N,I)
437           IF(IMARCH.LE.0) GO TO 38
438           X(IHALFP,I)=XP(IHALFP,I)
439           Y(IHALFP,I)=YP(IHALFP,I)
440           Z(IHALFP,I)=ZP(IHALFP,I)
441        38 CONTINUE
442           IF(IAC.LE.0) GO TO 35
443           IF(IMARCH.GE.1) GO TO 35
444           XIN(K,I,J)=X(1,I)
445           YIN(K,I,J)=Y(1,I)
446           ZIN(K,I,J)=ZIN(K-1,I,J)+DELT
447           RCOMI(K,I,J)=RCOM(1,I)
448        35 CONTINUE
449           IF(I2D.GE.1) GO TO 53
450           DELTZ=(Z(IH1,I)+Z(2,I))/2.0
451           IF(IOP2.LT.1) DELTZ=0.0
452           IF(JAC.LE.0) Z(1,I)=Z(1,I)-DELTZ
453           DO 47 N=2,IHALFP
454           NM=N-1
455           IF(JAC.LE.0) Z(N,I)=Z(N,I)-DELTZ
456           XDUM(N,I)=0.50*(X(N,I)+X(NM,I))
457           YDUM(N,I)=0.50*(Y(N,I)+Y(NM,I))
458        47 ZDUM(N,I)=0.50*(Z(N,I)+Z(NM,I))
459           DO 49 N=2,IH1
460           NP=N+1
461           CX(N,I)=CIRC(I)*(XDUM(N,I)-XDUM(NP,I))
462           CY(N,I)=CIRC(I)*(YDUM(N,I)-YDUM(NP,I))
463        49 CZ(N,I)=CIRC(I)*(ZDUM(N,I)-ZDUM(NP,I))
464        53 CONTINUE
465           IF(IPCO.LE.1)GO TO 30
466           TIME=TIME+DELT
467        50 CONTINUE
468           IF(IAC.GE.1) GO TO 92
469           DO 85 I=1,NPAIR
470           DO 85 N=1,IHALFP
471        85 WRITE(IW,119)I,N,X(N,I),Y(N,I),Z(N,I),RCOM(N,I)
```

ORIGINAL PAGE IS
OF POOR QUALITY

```
472          92 CONTINUE
473          48 CONTINUE
474          99 IF(IWR.LE.0) GO TO 98
475             WRITE(IW,301)
476          98 IF(IBACK.LE.0)GO TO 21
477             IF(IST.GE.1) GO TO 21
478             IF(IMARCH.LE.0)GO TO 22
479             WRITE(IW,113)TIME
480             WRITE(IW,202)
481             DO 24 I=1,NPAIR
482             XAM=0.0
483             XGM=1.0
484             WRITE(IW,203)I
485             DO 24 N=2,IH1
486          24 CALL STAT(N,I,IH1,XAM,XGM,IW)
487             GO TO 21
488          22 IMARCH=1
489             DELT=-DELT
490             IPTI=IPTI-1
491             GO TO 23
492          21 IF(IAC.LE.0) GO TO 5
493             IAC=0
494             IZLM(J)=MTIME
495             I2D=0
496             MTIME=MTIMM(J)
497             DELT=DELTM(J)
498             GO TO 6
499           5 CONTINUE
500         999 GO TO 90
501         101 FORMAT(20A4)
502         102 FORMAT(2I3)
503         103 FORMAT(I4,8F9.0)
504         104 FORMAT(I3,7E11.4)
505         105 FORMAT(1X,7HIPAIR =,I4,3X,7HDELTZ =,E11.4)
506         106 FORMAT(9I4)
507         107 FORMAT(2F10.0,7I4)
508         108 FORMAT(/,10X,4HDELT,11X,5HRNREF,9X,2HIP,3X,3HIZL,2X,5HNPAIR)
509         109 FORMAT(3X,2(2X,E14.6),3(2X,I4))
510         110 FORMAT(5(/),82H***DIAGNOSTIC***---IZLINK MUST BE LESS THAN OR EQU
511            $AL TO 40. THE INPUT VALUE WAS (,I4,1H))
512         111 FORMAT(3(/),5X,1HN,4X,4HX(N),8X,4HY(N),8X,4HZ(N),8X,
513           14HU(N),8X,4HV(N),8X,4HW(N))
514         112 FORMAT(1X,I4,6(1X,E11.4))
515         113 FORMAT(3X,6HTIME =,F9.3)
516         114 FORMAT(/,2X,1HI,2X,4HCIRC,8X,3HWVL,7X,4HAMPX,7X,4HAMPY,
517           1 7X,5HRCORE,5X,10HSPAN. LOC.,1X,10HDEL. PHASE)
518         115 FORMAT(30H NUMBER TOO LARGE FOR MAG TAPE)
519         116 FORMAT(31H NUMBER TOO LARGE FOR CONT CALC)
520         117 FORMAT(4F10.0)
521         118 FORMAT(/,2X,5HIPAIR,5X,4HCIRC)
522         119 FORMAT(2I4,4E13.6)
523         120 FORMAT(3F10.0,I4)
524         202 FORMAT(2X,1HN,5X,2HXF,9X,2HYF,9X,2HZF,9X,2HDX,9X,2HDY,9X,2HDZ,9X,
525            12HDR)
526         203 FORMAT(1X,7HNPAIR =,I4)
527         300 FORMAT(3F10.4)
528         301 FORMAT(1H1)
529         302 FORMAT(20A4)
530         303 FORMAT(1H1)
```

```
      304 FORMAT(2X,,44HXCG=,E11.4,6H  YCG=,E11.4,9H  VDRIFT=,E11.4,
     17H  DYCG=,E11.4)
      305 FORMAT(2X,5HXMAC=,F10.4)
      998 CONTINUE
          STOP
          END
```

ORIGINAL PAGE IS
OF POOR QUALITY

```
C      PREDICTOR - CORRECTOR TIME-STEPPING
      SUBROUTINE PCOR(N,I,IPCO,IP,IBR,NPAIR,IH1,IHALFP,DELT,IW,IST,IO,
     1 JAC,XMAC)
      DIMENSION XBAR(7),YBAR(7),ZBMI(7),ZBPL(7),ZBMI2(7),ZBPL2(7)
      COMMON X(92,7),Y(92,7),Z(92,7),U(92,7),V(92,7),W(92,7),
     1 XDUM(93,7),YDUM(93,7),ZDUM(93,7),CX(92,7),CY(92,7),CZ(92,7),
     2 CIRC(7),ALMBDA(7),X0(92,7),Y0(92,7),Z0(92,7),DELRM(92,7)
     3 ,RCOM(92,7)
      DATA PI4/12.566370/
      XIP=IP
      IF(IHALFP.LE.1) GO TO 12
      DO 5 L=1,NPAIR
      IF(IO.GE.1) GO TO 6
      XBAR(L)=(XDUM(2,L)+XDUM(IHALFP,L))/2.0
      YBAR(L)=(YDUM(2,L)+YDUM(IHALFP,L))/2.0
      ZBMI(L)=-XIP*ALMBDA(L)/2.0
      ZBPL(L)=(XIP-1.0)*ALMBDA(L)/2.0
      GO TO 5
    6 XBAR(L)=(XDUM(2,L)+XDUM(IBR+1,L))/2.0
      YBAR(L)=(YDUM(2,L)+YDUM(IBR+1,L))/2.0
      IF(JAC.LE.0) GO TO 13
      XBAR(L)=XDUM(IHALFP,L)
      YBAR(L)=YDUM(IHALFP,L)
   13 ZBMI(L)=-(XIP-1.0)*ALMBDA(L)
      ZBPL(L)=(XIP-1.5)*ALMBDA(L)
      ZBMI2(L)=-(XIP-1.5)*ALMBDA(L)
      ZBPL2(L)=(XIP-1.0)*ALMBDA(L)
      IF(JAC.LE.0) GO TO 5
      ZBMI2(L)=Z(2,L)-0.375*XMAC
      ZBPL2(L)=ZDUM(IHALFP,L)
    5 CONTINUE
   12 CONTINUE
      USL=0.
      VSL=0.
      WSL=0.
      DO 11 J=1,NPAIR
      DO 10 LL=2,IH1
      L=LL
      IF(IHALFP.LE.1) L=LL-1
      CALL FAAVEL(N,I,J,L,IP,UL,VL,WL,IBR,IHALFP,IW,IST,IO)
      USL=USL+UL
      VSL=VSL+VL
   10 WSL=WSL+WL
      IF(IHALFP.LE.1) GO TO 11
      IF(IO.LE.0) GO TO 1
      IF(JAC.GE.1) GO TO 14
      IF(N.LE.IBR) GO TO 1
   14 ZPL=ZBPL2(J)
      ZMI=ZBMI2(J)
      GO TO 2
    1 ZPL=ZBPL(J)
      ZMI=ZBMI(J)
    2 DXB=XBAR(J)-X(N,I)
      DYB=YBAR(J)-Y(N,I)
      HSQ=DXB*DXB+DYB*DYB
      H=SQRT(HSQ)
      DXB1=-XBAR(J)-X(N,I)
      DYB1=DYB
```

```
59              HSQ1=DXB1*DXB1+DYB1*DYB1
60              H1=SQRT(HSQ1)
61              DZP=ZPL-Z(N,I)
62              DZM=ZMI-Z(N,I)
63              IF(HSQ-.0001)3,4,4
64            3 VEL=0.0
65              GO TO 7
66            4 COSP=DZP/SQRT(DZP*DZP+HSQ)
67              COSM=DZM/SQRT(DZM*DZM+HSQ)
68              IF(JAC.GE.1) COSM=-1.0
69              VEL=-CIRC(J)*(2.0+(COSM-COSP))/(PI4*H)
70            7 IF(HSQ1-.0001)8,9,9
71            8 VEL1=0.0
72              GO TO 15
73            9 COSP1=DZP/SQRT(DZP*DZP+HSQ1)
74              COSM1=DZM/SQRT(DZM*DZM+HSQ1)
75              IF(JAC.GE.1) COSM1=-1.0
76              VEL1=CIRC(J)*(2.0+(COSM1-COSP1))/(PI4*H1)
77           15 IF(HSQ-.0001)16,17,17
78           16 COSA=1.0
79              SINA=1.0
80              GO TO 18
81           17 COSA=DXB/H
82              SINA=DYB/H
83           18 IF(HSQ1-.0001)19,20,20
84           19 COSA1=1.0
85              SINA1=1.0
86              GO TO 21
87           20 COSA1=DXB1/H1
88              SINA1=DYB1/H1
89           21 USL=USL-VEL*SINA-VEL1*SINA1
90              VSL=VSL+VEL*COSA+VEL1*COSA1
91           11 CONTINUE
92              U(N,I)=USL
93              V(N,I)=VSL
94              W(N,I)=WSL
95              RETURN
96              END
```

ORIGINAL PAGE IS
OF POOR QUALITY

```
      C       INDUCED VELOCITY SUBROUTINE
            SUBROUTINE FAAVEL(N,I1,I2,I,MMAX,US,VS,WS,IBR,IHALFP,IW,IST,IOP2)
            COMMON X(92,7),Y(92,7),Z(92,7),U(92,7),V(92,7),W(92,7),
           1 XDUM(93,7),YDUM(93,7),ZDUM(93,7),DCX(92,7),DCY(92,7),DCZ(92,7),
           2 CIRC(7),ALMBDA(7),X0(92,7),Y0(92,7),Z0(92,7),DELRM(92,7)
           3 ,RCOM(92,7)
            DATA PI/3.1415926/,PI4/12.566370/
            ZM1=Z(I,I2)
            ZN1=Z(N,I1)
            SIGN2=1.0
            IAB=0
            ICD=0
            US=0.0
            VS=0.0
            WS=0.0
      C           M=1,MMAX LOOP PICKS UP SUCCESSIVE HALF-WAVES.
      C       EFFECTS OF BASIC VORTICIES PLUS REFLECTIONS IN THE
      C       OTHER THREE QUADRANTS
            CX=DCX(I,I2)
            CY=DCY(I,I2)
            CZ=DCZ(I,I2)
            XRAT1=X(I,I2)-X(N,I1)
            YRAT1=Y(I,I2)-Y(N,I1)
            XRAT2=-X(I,I2)-X(N,I1)
            YRAT2=-Y(I,I2)-Y(N,I1)
            XR1S=XRAT1*XRAT1
            YR1S=YRAT1*YRAT1
            XR2S=XRAT2*XRAT2
            YR2S=YRAT2*YRAT2
            DO 990 M=1,MMAX
            IM=MMAX-M
            UE=0.0
            VE=0.0
            WE=0.0
            IF(MMAX.EQ.1)GO TO 50
            IF((1-M)*IM) 40,10,20
         10 IF(IM) 50,1,50
         20 WRITE(IW,200)
            GO TO 999
          1 IF(IOP2)6,6,7
          6 ICD=1
            GO TO 40
          7 IF(N.GT.IBR) GO TO 8
            ICD=1
            IF(I.LE.IBR) GO TO 32
            GO TO 40
          8 IAB=1
            IF(I.GT.IBR) GO TO 32
         40 IF(IOP2.GE.1)GO TO 36
            CX=-CX
            CY=-CY
         36 SIGN2=-SIGN2
            SIGN1=-(M/2)
            Z(I,I2)=SIGN1*ALMBDA(I2)+SIGN2*ZM1
            IF(IOP2.GE.1) Z(I,I2)=-(M-1)*ALMBDA(I2)+ZM1
         50 ZRAT1=Z(I,I2)-ZN1
            IF(IHALFP.LE.1) ZRAT1=0.
            ZR1S=ZRAT1*ZRAT1
```

```
      IF(IAB.GE.1) GO TO 2
      RSQA=XR1S+YR1S+ZR1S
      IF(IOP2.LE.0) GO TO 37
    2 ZRAT2=Z(I,I2)+(2*M-2)*ALMBDA(I2)-ZN1
      IF(IHALFP.LE.1) ZRAT2=0.
      GO TO 38
   37 ZRAT2=-Z(I,I2)-ZN1
   38 ZR2S=ZRAT2*ZRAT2
      IF(IAB.GE.1) GO TO 3
      RSQB=XR2S+YR1S+ZR1S
      IF(IHALFP.LE.1) GO TO 43
      IF(ICD.GE.1) GO TO 5
    3 RSQC=XR2S+YR1S+ZR2S
      RSQD=XR1S+YR1S+ZR2S
   43 IF(IAB.GE.1) GO TO 4
    5 IF(RSQA-.0001)11,12,12
   11 RECIPA=0.0
      GO TO 13
   12 RECIPA=1.0/(PI4*RSQA*SQRT(RSQA))
      IF(IHALFP.LE.1) RECIPA=1.0/(2.0*PI*RSQA)
   13 IF(RSQB-.0001)14,15,15
   14 RECIPB=0.0
      GO TO 16
   15 RECIPB=1.0/(PI4*RSQB*SQRT(RSQB))
      IF(IHALFP.LE.1) RECIPB=1.0/(2.0*PI*RSQB)
   16 IF(ICD.GE.1) GO TO 22
      IF(IHALFP.LE.1) GO TO 17
    4 IF(RSQC-.0001)17,18,18
   17 RECIPC=0.0
      GO TO 19
   18 RECIPC=1.0/(PI4*RSQC*SQRT(RSQC))
   19 IF(IHALFP.LE.1) GO TO 23
      IF(RSQD-.0001)23,21,21
   23 RECIPD=0.0
      GO TO 22
   21 RECIPD=1.0/(PI4*RSQD*SQRT(RSQD))
   22 IF(IAB.GE.1) GO TO 30
      UE=RECIPA*(CZ*YRAT1-CY*ZRAT1)
      VE=RECIPA*(CX*ZRAT1-CZ*XRAT1)
      WE=RECIPA*(CY*XRAT1-CX*YRAT1)
      UE=UE+RECIPB*(CY*ZRAT1-CZ*YRAT1)
      VE=VE+RECIPB*(CX*ZRAT1+CZ*XRAT2)
      WE=WE+RECIPB*(-CY*XRAT2-CX*YRAT1)
      IF(ICD.GE.1) GO TO 32
      IF(IOP2.GE.1) GO TO 30
      UE=UE+RECIPC*(-CZ*YRAT1-CY*ZRAT2)
      VE=VE+RECIPC*(-CX*ZRAT2+CZ*XRAT2)
      WE=WE+RECIPC*(CY*XRAT2+CX*YRAT1)
      UE=UE+RECIPD*(CZ*YRAT1+CY*ZRAT2)
      VE=VE+RECIPD*(-CX*ZRAT2-CZ*XRAT1)
      WE=WE+RECIPD*(-CY*XRAT1+CX*YRAT1)
      GO TO 32
   30 IF(M.EQ.1) GO TO 32
      UE=UE+RECIPC*(-CZ*YRAT1+CY*ZRAT2)
      VE=VE+RECIPC*(+CX*ZRAT2+CZ*XRAT2)
      WE=WE+RECIPC*(-CY*XRAT2-CX*YRAT1)
      UE=UE+RECIPD*(CZ*YRAT1-CY*ZRAT2)
      VE=VE+RECIPD*(+CX*ZRAT2-CZ*XRAT1)
      WE=WE+RECIPD*(+CY*XRAT1-CX*YRAT1)
```

ORIGINAL PAGE IS
OF POOR QUALITY

```
118          32 US=US-UE
119             VS=VS-VE
120         990 WS=WS-WE
121             Z(I,I2)=ZM1
122             Z(N,I1)=ZN1
123         999 RETURN
124         200 FORMAT(5(/),71H***DIAGNOSTIC***---=-THE NUMBER OF PERIODS (IP) CANN
125            $OT BE GREATER THAN 5)
126             END
```

```
      C       CURVATURE EFFECTS SUBROUTINE
              SUBROUTINE CURV(N,DELT,IHALF,IPCO,IT,RNC,I,UC,VC,WC,IW,IST)
              COMMON X(92,7),Y(92,7),Z(92,7),U(92,7),V(92,7),W(92,7),
             1 XDUM(93,7),YDUM(93,7),ZDUM(93,7),CX(92,7),CY(92,7),CZ(92,7),
             2 CIRC(7),ALMBDA(7),X0(92,7),Y0(92,7),Z0(92,7),DELRM(92,7)
             3 ,RCOM(92,7)
              DATA PI/3.1415926/
              ITHET=0
      C       RADIUS OF CURVATURE CALCULATION
              ASQ=(X(N+1,I)-X(N-1,I))**2+(Y(N+1,I)-Y(N-1,I))**2+
             1 (Z(N+1,I)-Z(N-1,I))**2
              A=SQRT(ASQ)
              BSQ=(X(N+1,I)-X(N,I))**2+(Y(N+1,I)-Y(N,I))**2+(Z(N+1,I)-Z(N,I))**2
              B=SQRT(BSQ)
              CSQ=(X(N,I)-X(N-1,I))**2+(Y(N,I)-Y(N-1,I))**2+(Z(N,I)-Z(N-1,I))**2
              C=SQRT(CSQ)
              DELR=B+C
              CCX=(Y(N,I)-Y(N-1,I))*(Z(N+1,I)-Z(N,I))-(Z(N,I)-Z(N-1,I))*
             1(Y(N+1,I)-Y(N,I))
              CCY=(Z(N,I)-Z(N-1,I))*(X(N+1,I)-X(N,I))-(X(N,I)-X(N-1,I))*
             1(Z(N+1,I)-Z(N,I))
              CCZ=(X(N,I)-X(N-1,I))*(Y(N+1,I)-Y(N,I))-(Y(N,I)-Y(N-1,I))*
             1(X(N+1,I)-X(N,I))
              CCSQ=CCX*CCX+CCY*CCY+CCZ*CCZ
              IF(CCSQ)41,5,5
            5 IF((CCSQ/(CSQ*BSQ))-.0001)6,6,7
            6 IF(ASQ-(BSQ+CSQ))32,32,33
           32 COSA=0.707
              COSB=0.707
              COSC=0.0
              GO TO 22
           33 COSA=1.0
              COSB=1.0
              COSC=1.0
              GO TO 23
            7 CC=SQRT(CCSQ)
              COSA=CCX/CC
              COSB=CCY/CC
              COSC=CCZ/CC
              IF(C)13,42,13
           13 IF(B)11,42,11
           11 SINAL=CC/(C*B)
              IF(ASQ-(BSQ*CSQ))3,4,4
            3 QALPHA=1.0
              GO TO 8
            4 QALPHA=2.0
            8 IF(SINAL-.001)9,2,2
            9 IF(QALPHA-1.5)22,22,23
            2 RC=A/(2.0*SINAL)
              GO TO 26
           22 RC=(B+C)/2.0
              TH14=PI/2.0
              TH24=TH14
              ITHET=1
              GO TO 12
           23 VELC=0.0
              RCO=SQRT(RCOM(N,I)**2+4.0*DELT/RNC)
              ITHET=2
```

```
      GO TO 12
C     CORE RADIUS AND SELF INDUCED VELOCITY CALCULATION
   26 IF(B-2.0*RC)28,43,43
   28 IF(C-2.0*RC)27,43,43
   27 TH14=0.25*ATAN(B/(SQRT(4.0*RC*RC-B*B)))
      TH24=0.25*ATAN(C/(SQRT(4.0*RC*RC-C*C)))
   12 IF(IT.GT.1)GO TO 34
      IF(IPCO.EQ.0)DELRM(N,I)=DELR
   34 IF(ITHET.EQ.2) GO TO 10
   16 D2=RCOM(N,I)**2*(DELR-DELRM(N,I))/DELR
      DRCO2=4.0*DELT/RNC-D2
      RCO2=RCOM(N,I)**2+DRCO2
      IF(RCO2)44,44,29
   29 RCO=SQRT(RCO2)
      IF(RC)45,45,30
   30 DV1=ALOG(8.0*RC/RCO)-0.558
      IF(ITHET)18,18,19
   19 DV2=0.0
      GO TO 20
   18 DV2=0.5*ALOG((COS(TH14)/SIN(TH14))*(COS(TH24)/SIN(TH24)))
   20 VELC=CIRC(I)*(DV1-DV2)/(4.0*PI*RC)
   10 UC=VELC*COSA
      VC=VELC*COSB
      WC=VELC*COSC
      IF(IPCO.GE.1)GO TO 1
      DELRM(N,I)=DELR
      RCOM(N,I)=RCO
      GO TO 1
   41 WRITE(IW,100)
      GO TO 46
   42 WRITE(IW,101)
      GO TO 46
   43 WRITE(IW,102)
      GO TO 46
   44 WRITE(IW,103)
      GO TO 46
   45 WRITE(IW,104)
   46 IST=1
    1 CONTINUE
      RETURN
  100 FORMAT(15H ABS(CXB).LT.0.)
  101 FORMAT(23H ADJ. POINTS COINCIDENT)
  102 FORMAT(24H RAD. OF CURV. TOO SMALL)
  103 FORMAT(12H RCORE.LE.0.)
  104 FORMAT(19H RAD. OF CURV.LE.0.)
      END
```

```
      C      COMPARISON OF GEOMETRY AFTER BKWD. MARCH WITH INIT. GEOMETRY
            SUBROUTINE STAT(N,I,IH1,XAM,XGM,IW)
            COMMON X(92,7),Y(92,7),Z(92,7),U(92,7),V(92,7),W(92,7),
           1 XDUM(93,7),YDUM(93,7),ZDUM(93,7),CX(92,7),CY(92,7),CZ(92,7),
           2 CIRC(7),ALMBDA(7),X0(92,7),Y0(92,7),Z0(92,7),DELRM(92,7)
           3 ,RCOM(92,7)
            DX=X(N,I)-X0(N,I)
            DY=Y(N,I)-Y0(N,I)
            DZ=Z(N,I)-Z0(N,I)
            DR=SQRT(DX*DX+DY*DY+DZ*DZ)
            XNP=N
            XAM=XAM+DR
            XGM=XGM*DR
            NP=N-1
            WRITE(6,200)NP,X(N,I),Y(N,I),Z(N,I),DX,DY,DZ,DR
            IF(N.LT.IH1) GO TO 25
            XAME=XAM/XNP
            XGME=(XGM)**(1./XNP)
            WRITE(6,201)XAME,XGME
         25 CONTINUE
            RETURN
        200 FORMAT(I3,7E11.4)
        201 FORMAT(2X,16HARITH MEAN DEV =,E11.4,2X,15HGEOM MEAN DEV =,E11.4)
            END
```

ORIGINAL PAGE IS
OF POOR QUALITY

FIGURES

PRECEDING PAGE BLANK NOT FILMED

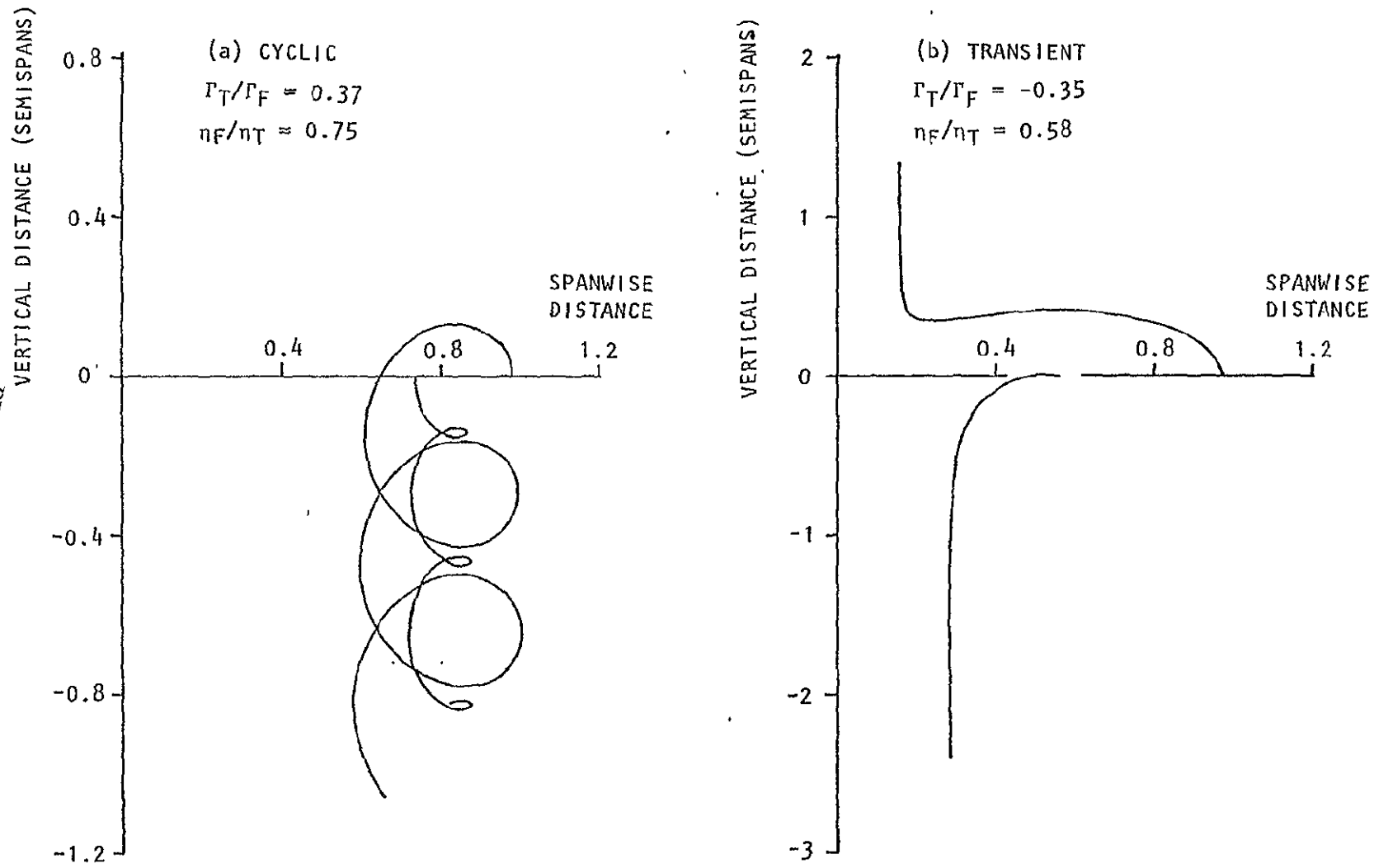

NOTE: DISTANCES NORMALIZED ON WING SEMI-SPAN

Figure 2.1 Two-Dimensional Twin Vortex Pair Trajectories

PRECEDING PAGE BLANK NOT FILMED

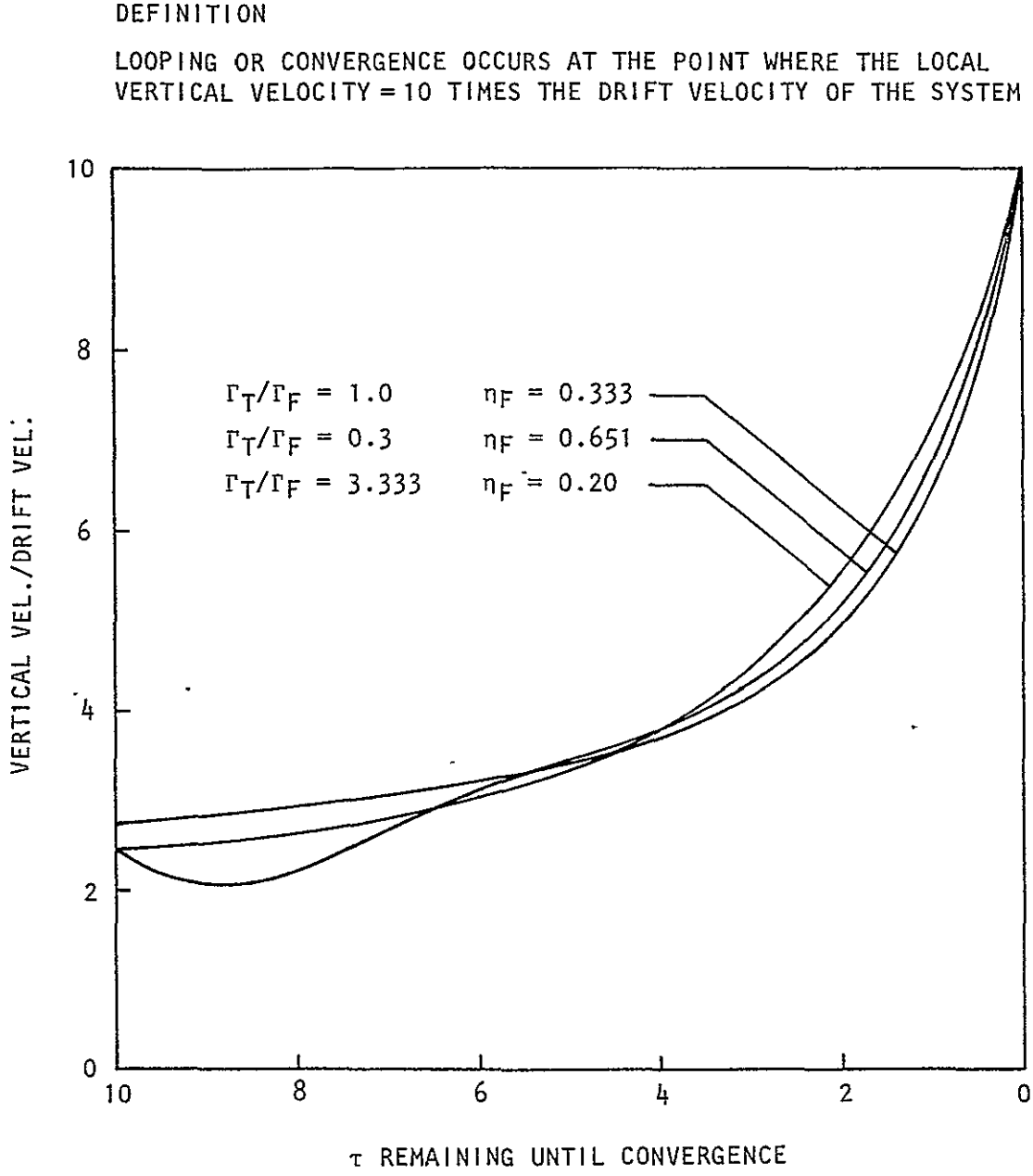

Figure 2.2 Definition of the Onset of Convergence

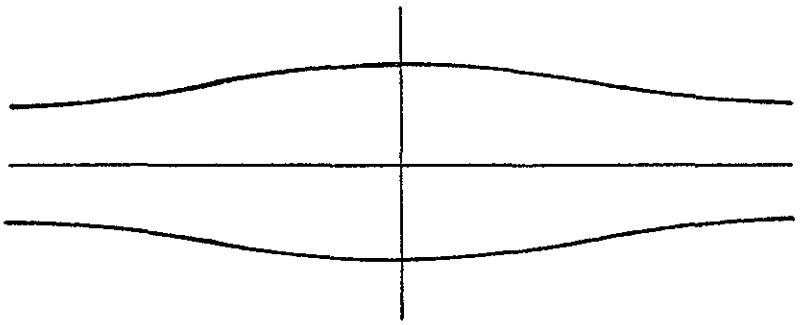

(a) INITIAL CONDITIONS

$\Gamma = 0.127\ U_\infty\ b$

$\lambda = 5.0\ b$

$a_x = a_y = 0.125\ b$

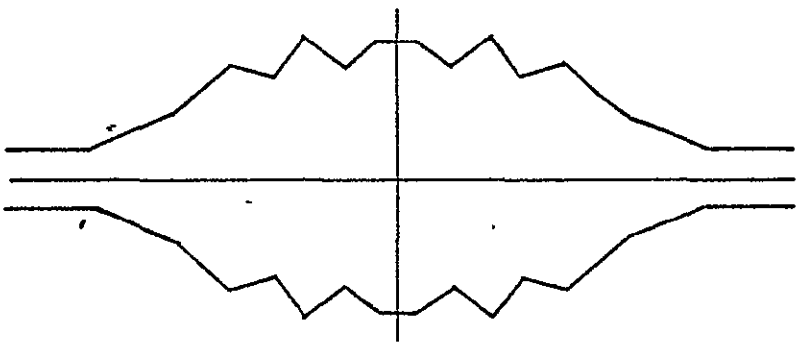

(b) CALCULATION FROM REF. 2
10 POINTS/HALF WAVE
CORE UNSPECIFIED
TIME = $5.33\ b^2/\Gamma$

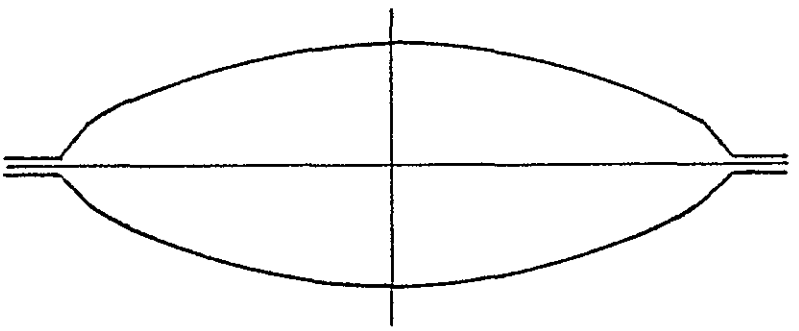

(c) PRESENT CALCULATION
10 POINTS/HALF WAVE
CORE RADIUS = .098 b
TIME = $5.33\ b^2/\Gamma$

Figure 3.1 Previous and Present Calculations of the Distortion of a Vortex Pair

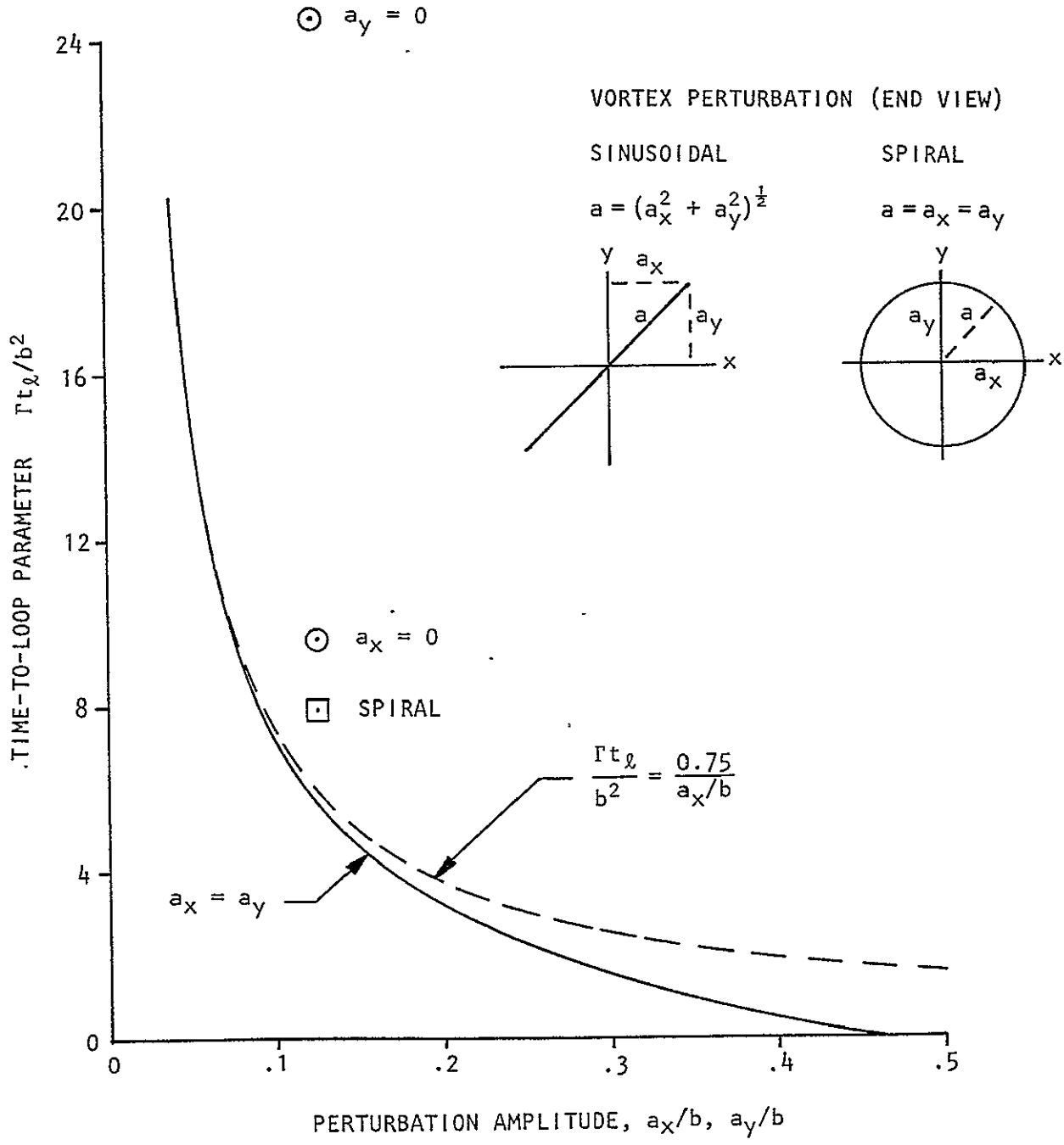

Figure 3.2 Dependence of Time-to-Loop upon Initial Perturbation Amplitude, $\lambda = 5.0$, $\delta/b = .098$

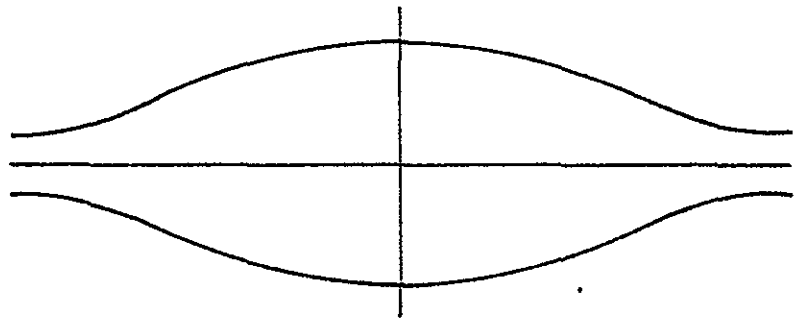

(a) NO CURVATURE EFFECTS
$\Gamma = 0.127\ U\ b$
$\lambda = 5.0\ b$
$a_x = a_y = 0.125\ b$
CORE UNSPECIFIED
TIME = $5.33\ b^2/\Gamma$

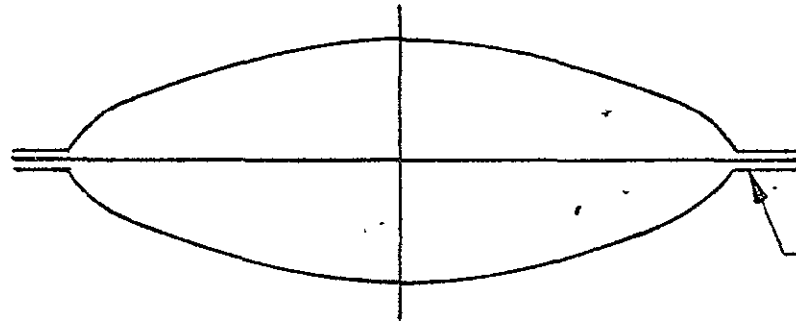

(b) CORE RADIUS = .098 b
TIME = $5.33\ b^2/\Gamma$

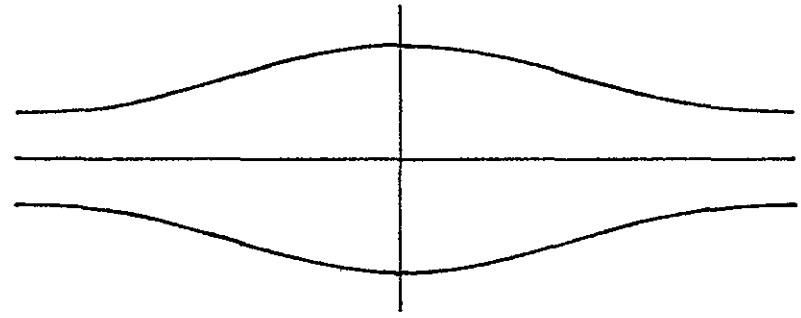

(c) CORE RADIUS = .382 b
TIME = $5.33\ b^2/\Gamma$

Figure 3.3 Effect of Vortex Core Radius on the Distortion of a Vortex Pair

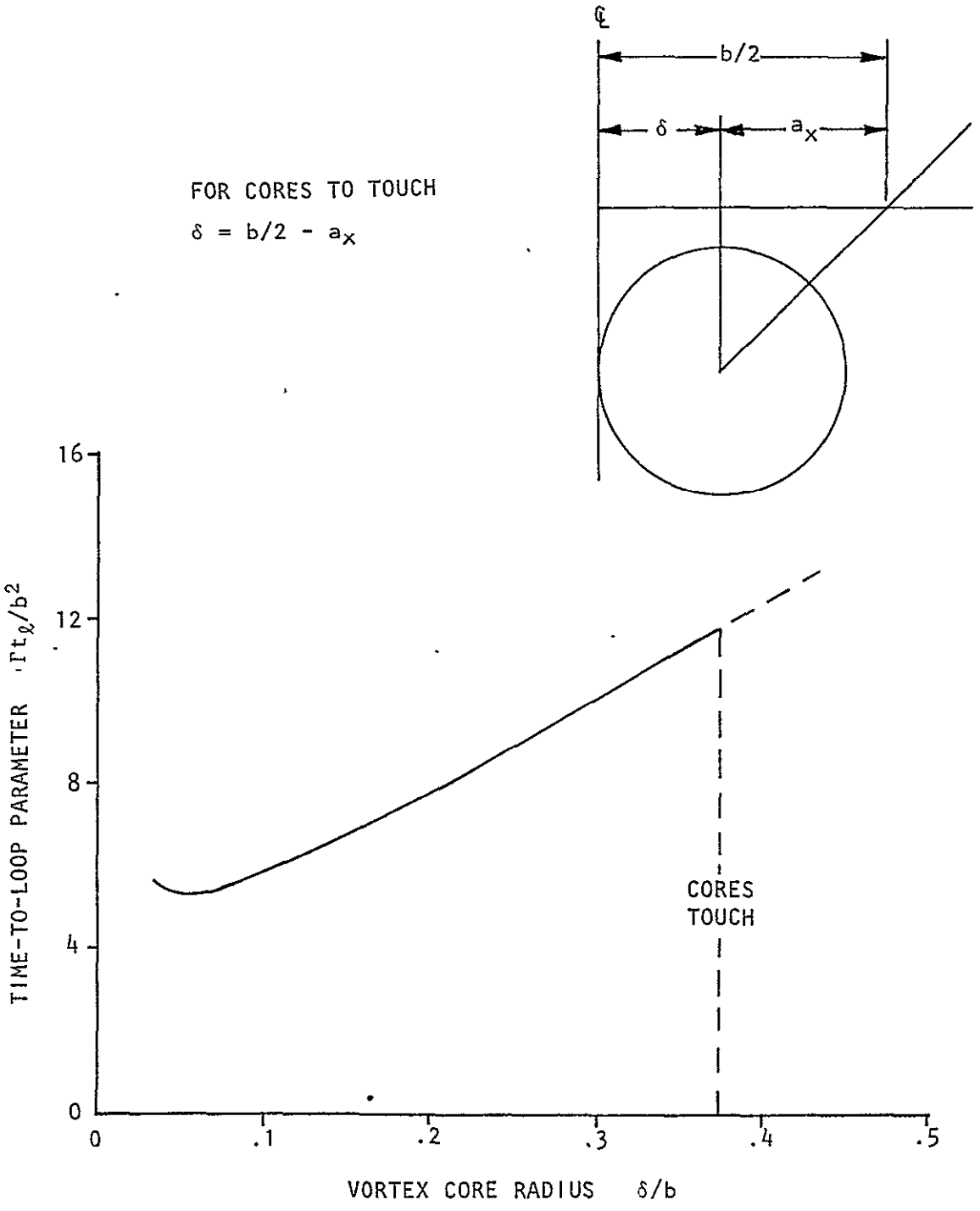

Figure 3.4 Dependence of Time-to-Loop Upon Vortex Core Radius, $a_x/b = a_y/b = 0.125$, $\lambda = 5.0$

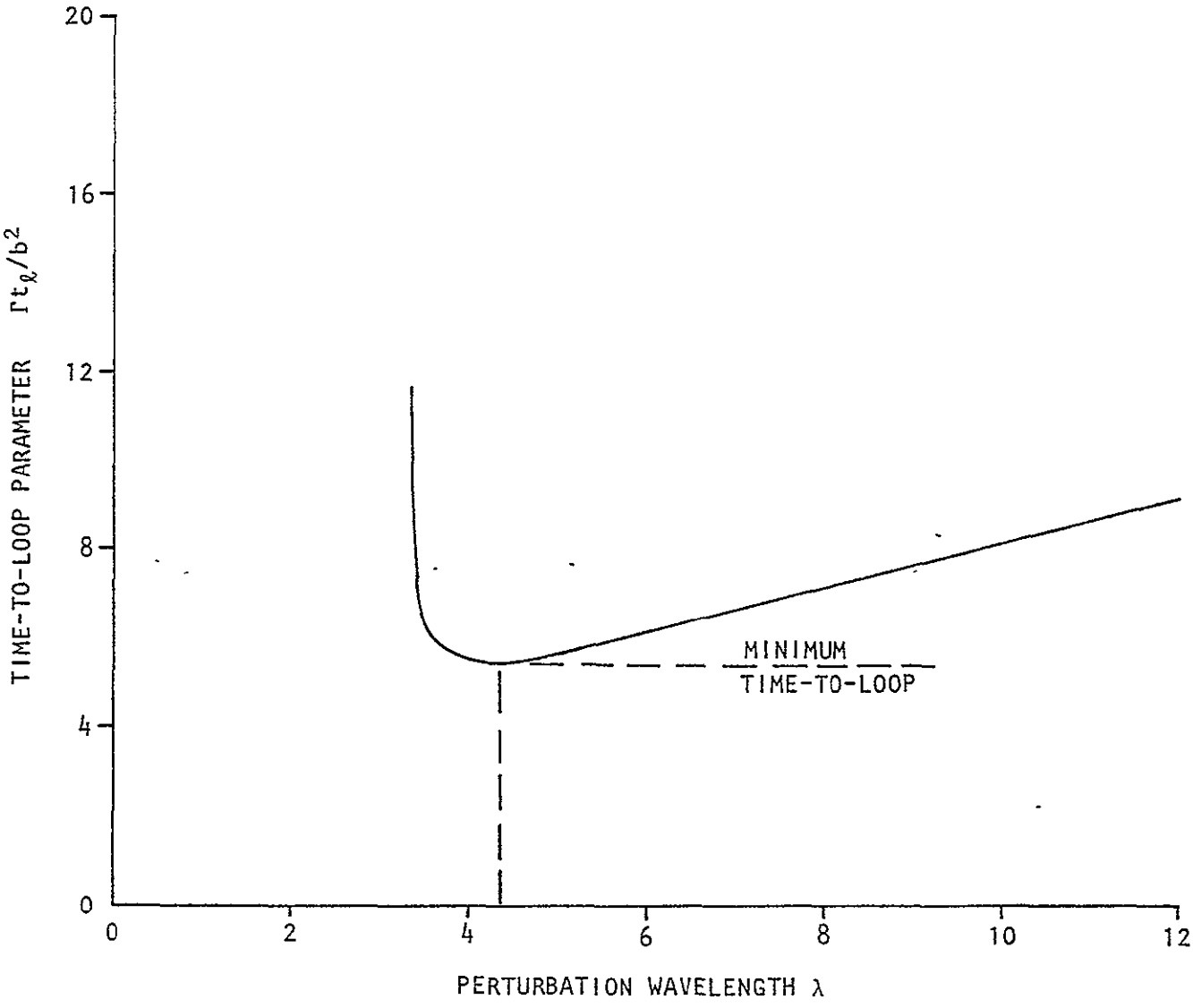

Figure 3.5 Dependence of Time-to-Loop Upon Perturbation Wavelength, $a_x/b = a_y/b = .125$, $\delta/b = .098$

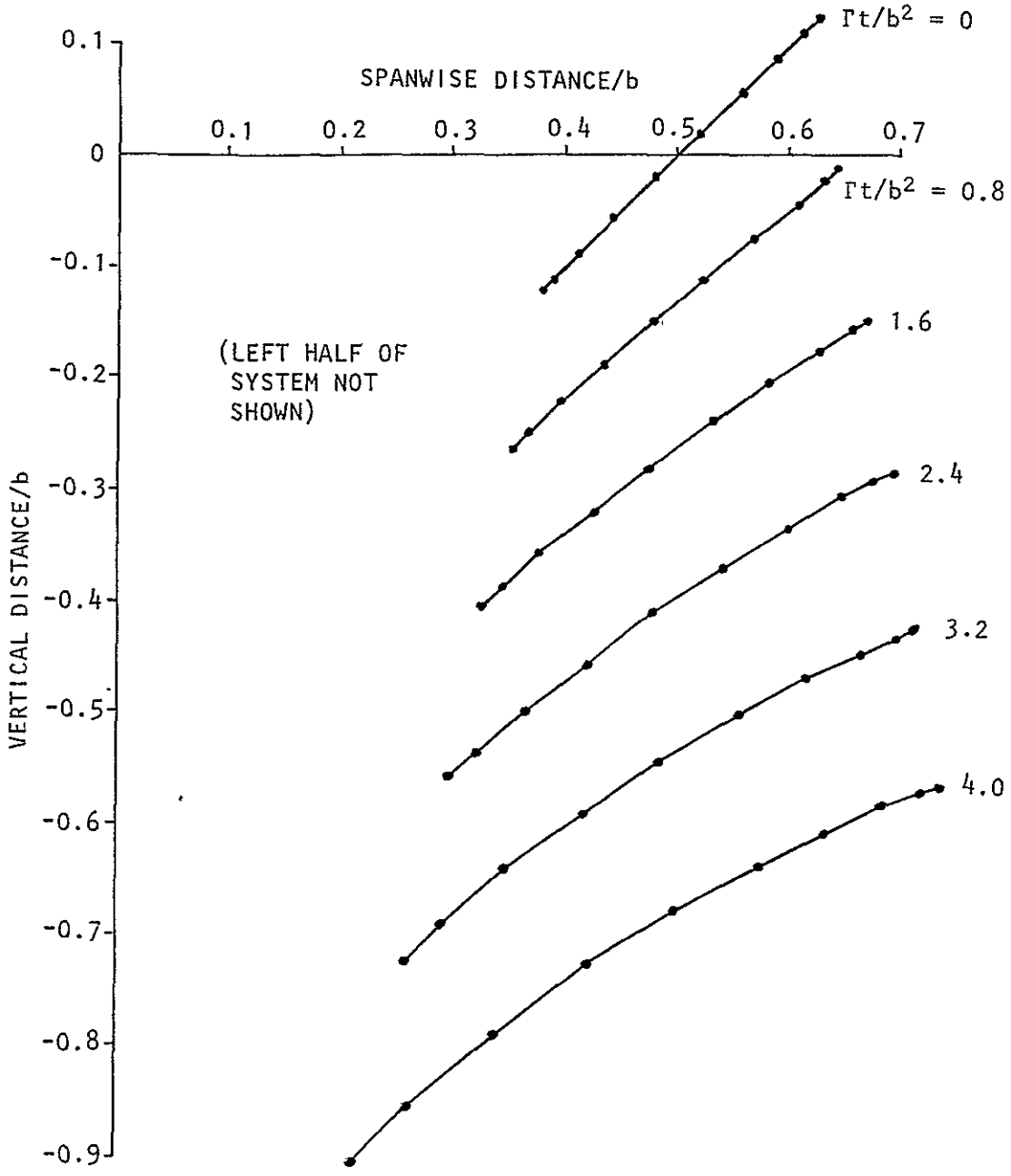

Figure 3.6 End-View of Vortex-Pair Distortion Toward Looping, $\lambda = 5.0$, $\delta/b = 0.098$

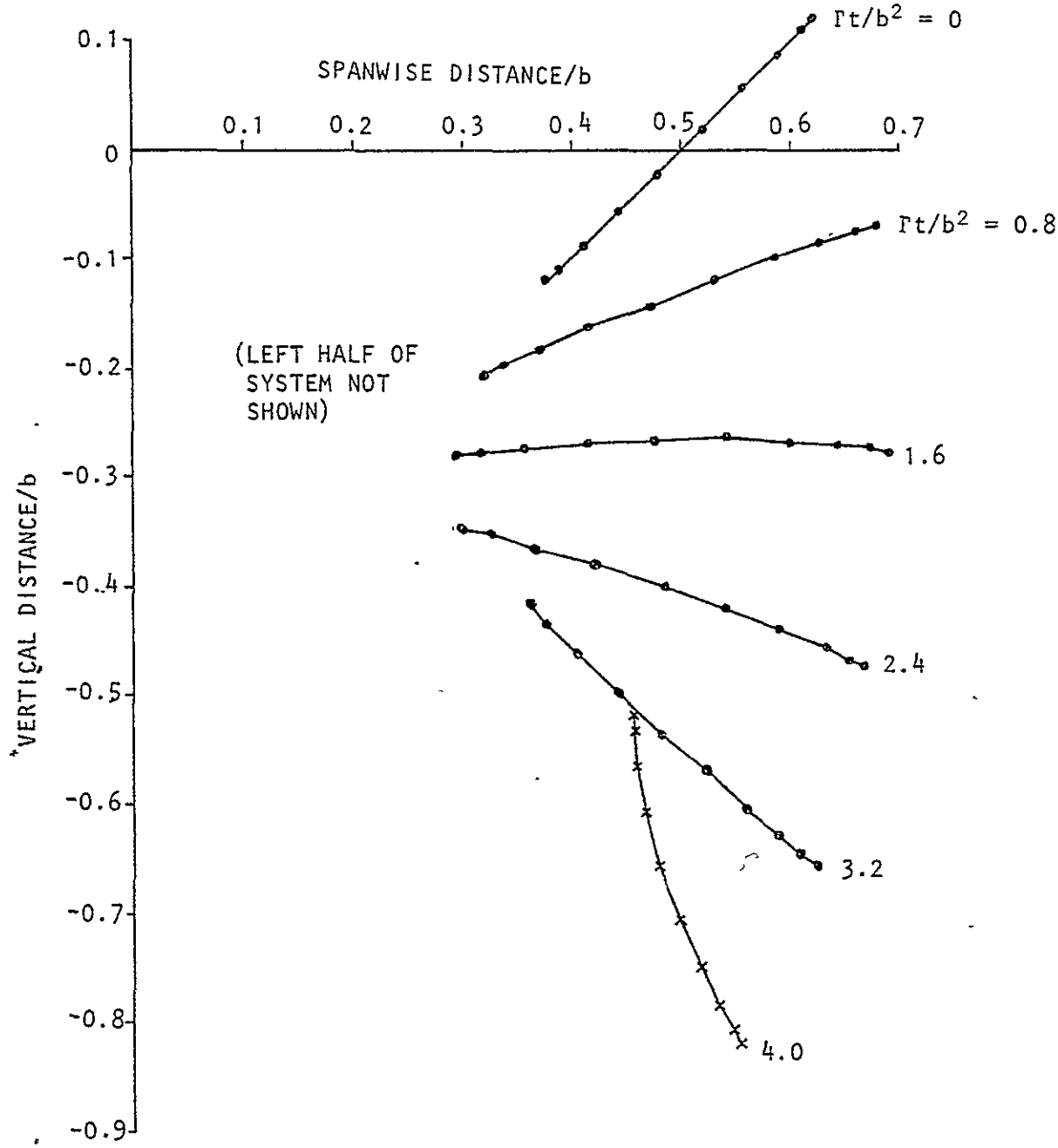

Figure 3.7 End View of Vortex Pair Distortion at Sub-Looping Wavelength, $\lambda = 2.5$, $\delta/b = .048$

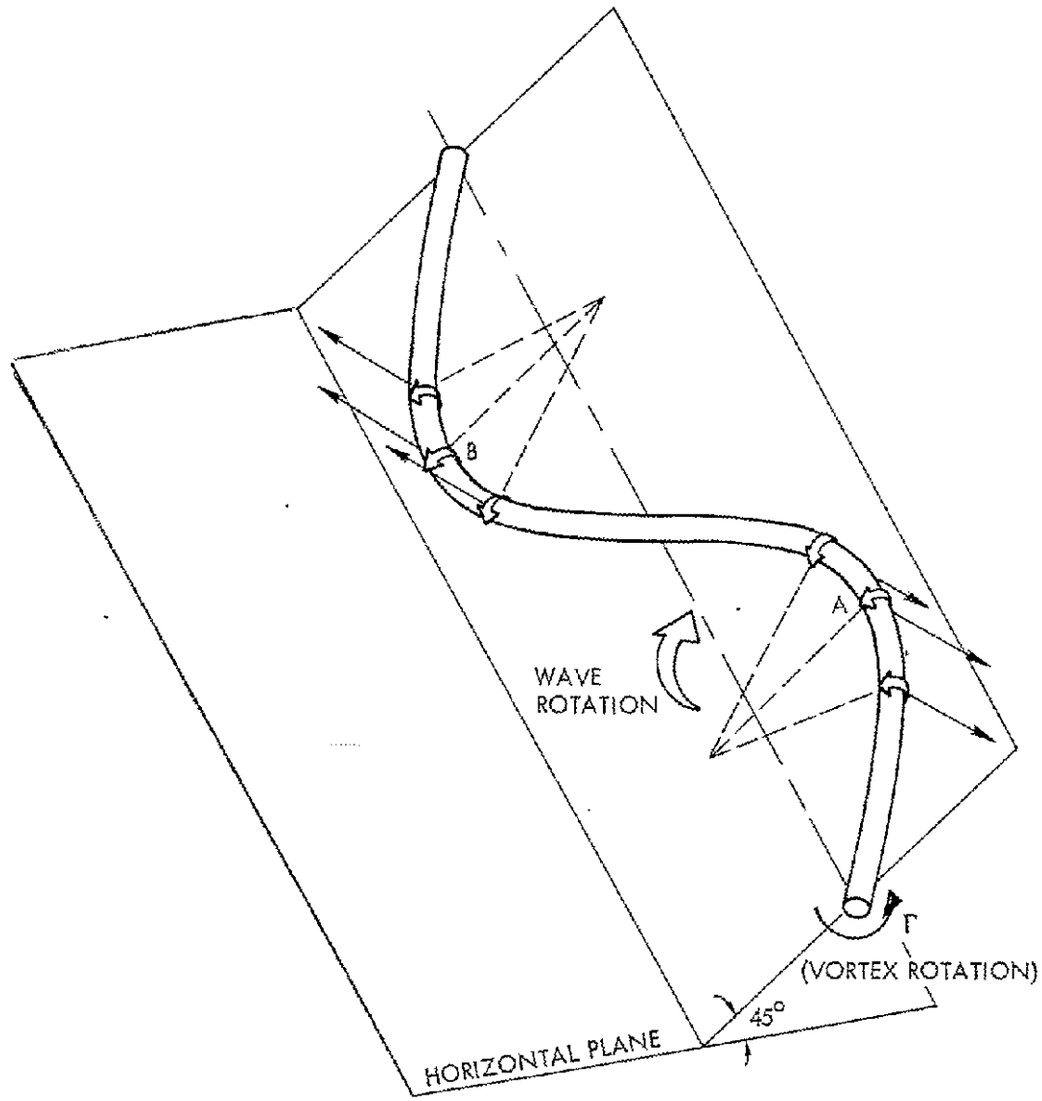

Figure 3.8(a) Mechanism for Opposing-Sense Vortex and Wave Rotations - Geometry

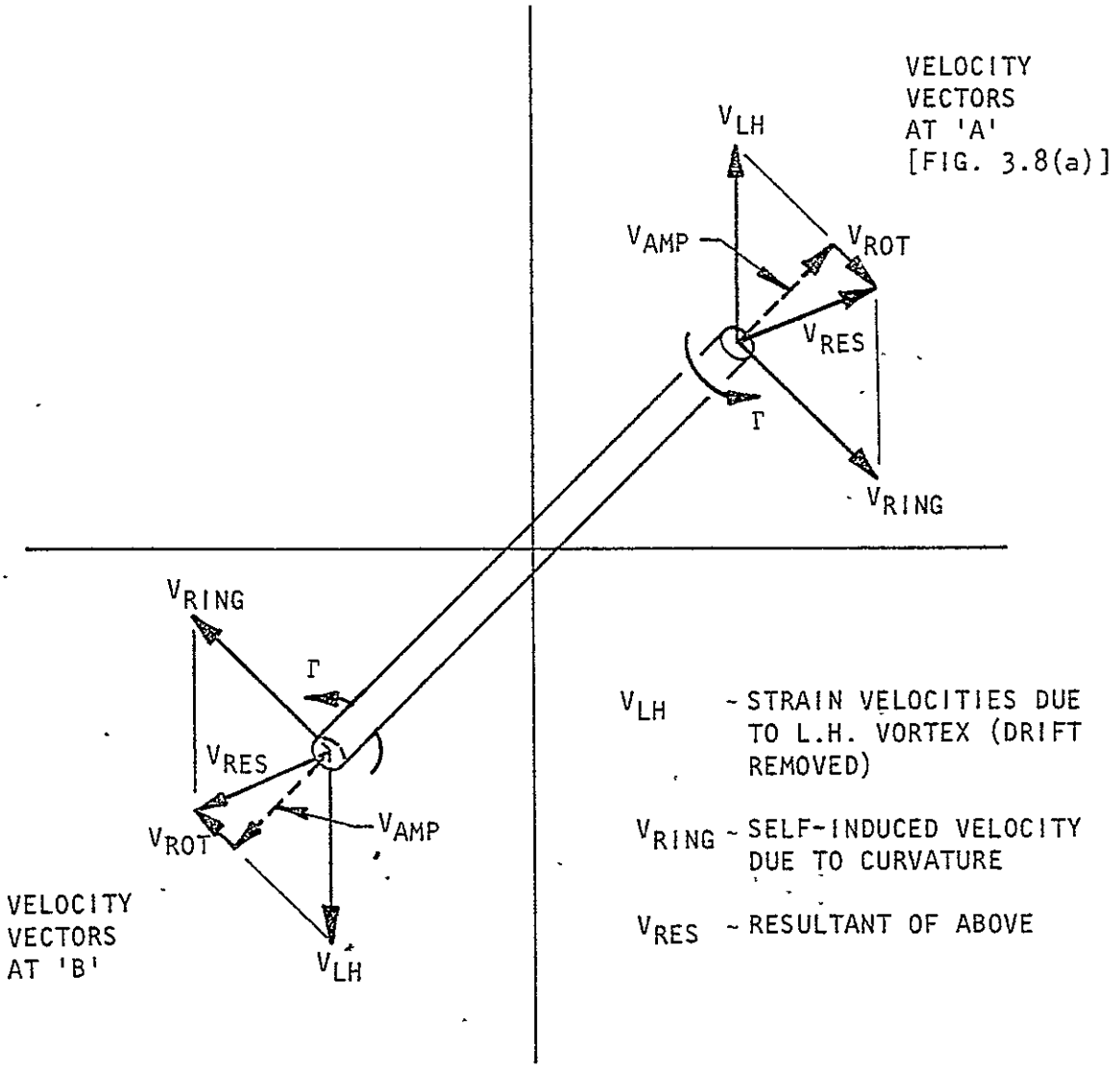

V_{AMP} - VELOCITY TENDING TO AMPLIFY WAVE

V_{ROT} - VELOCITY TENDING TO ROTATE WAVE 'BACKWARDS'

Figure 3.8(b) Mechanism for Opposing-Sense Vortex and Wave Rotations - Velocities

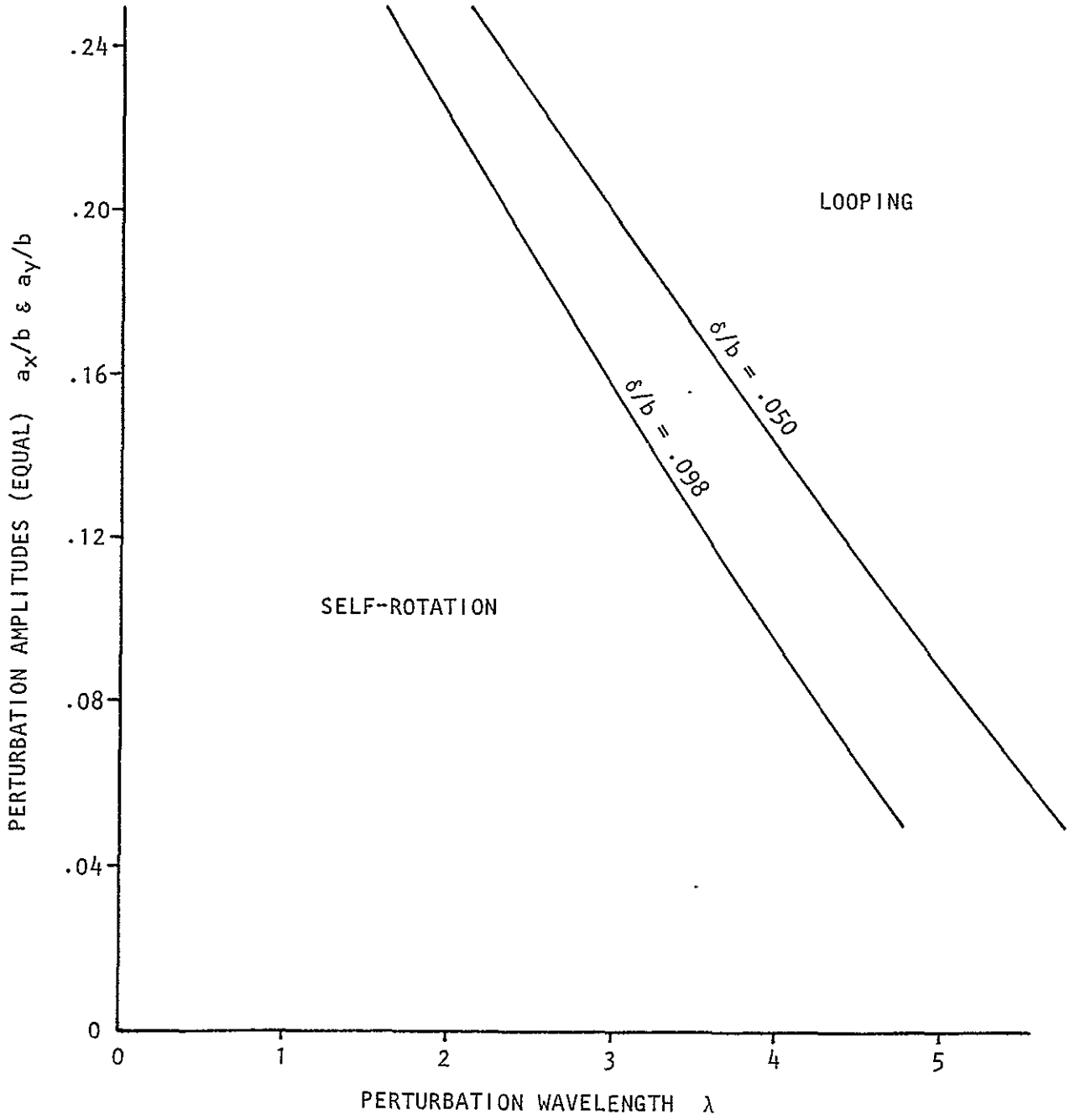

Figure 3.9 Lower Limit Wavelengths for Vortex Looping to Occur

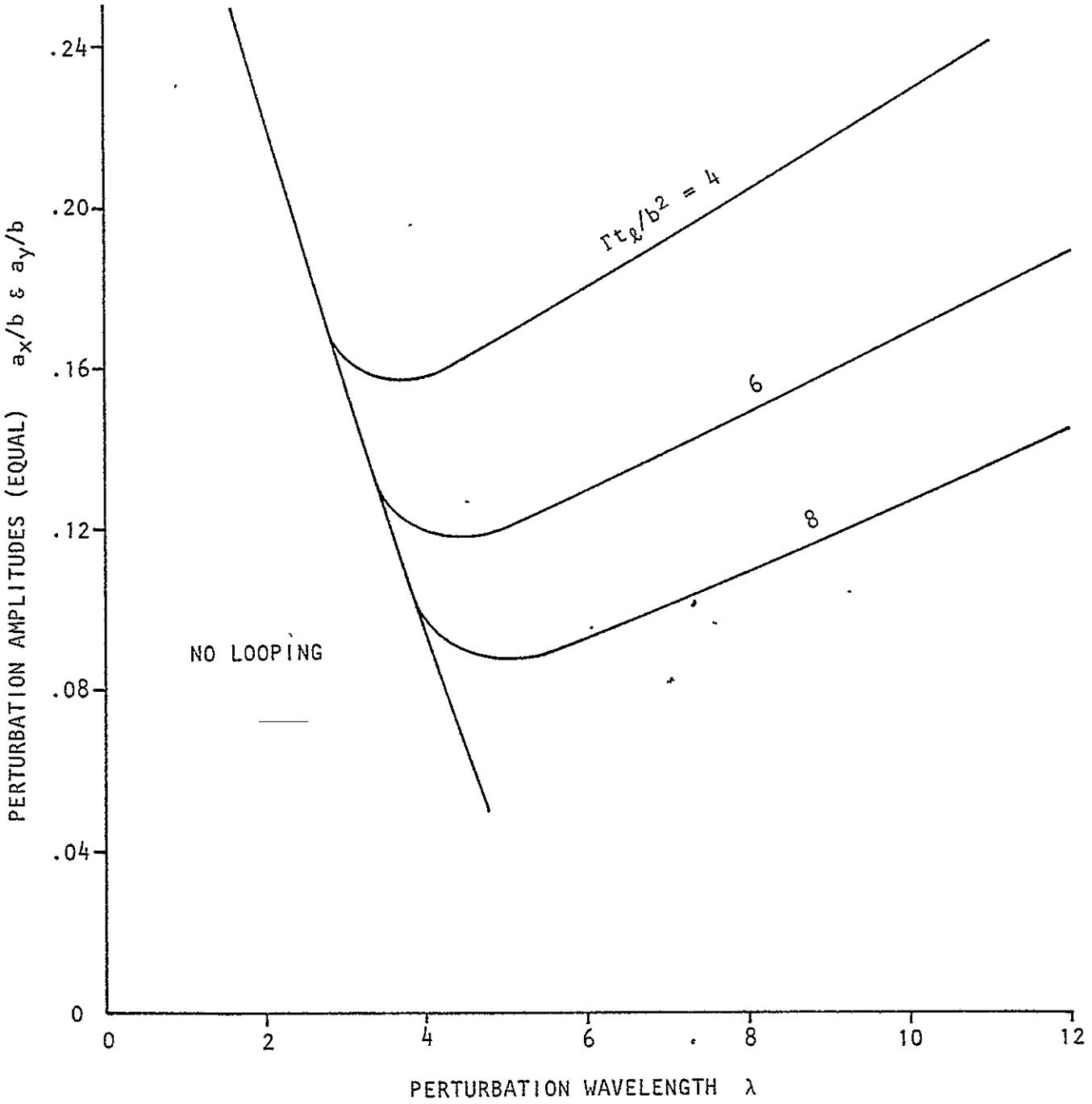

Figure 3.10 Time-to-Loop as a Function of Perturbation Wavelength and Initial Amplitude, $\delta/b = .098$

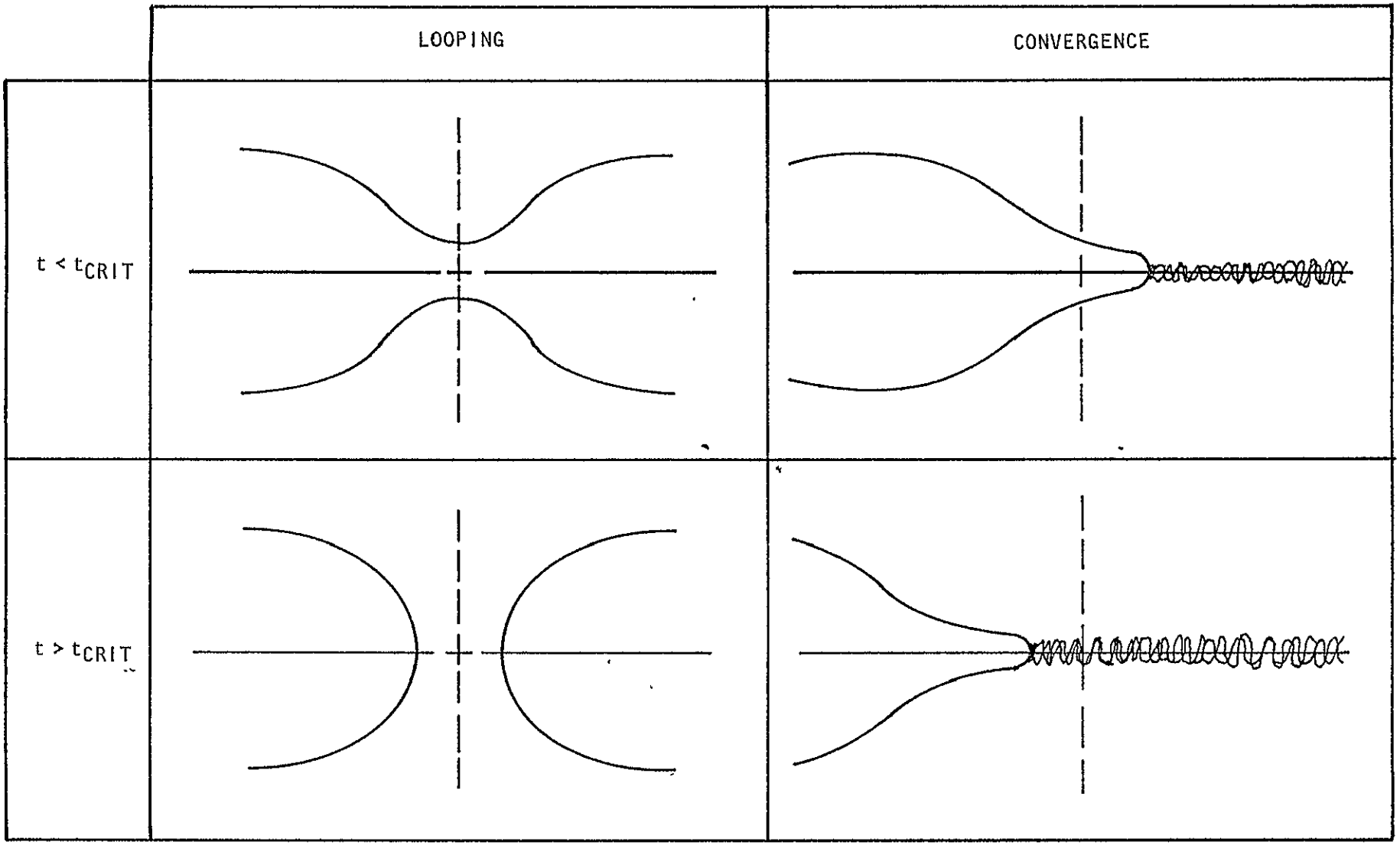

Figure 4.1 The Distinction Between Vortex "Looping" and "Convergence"

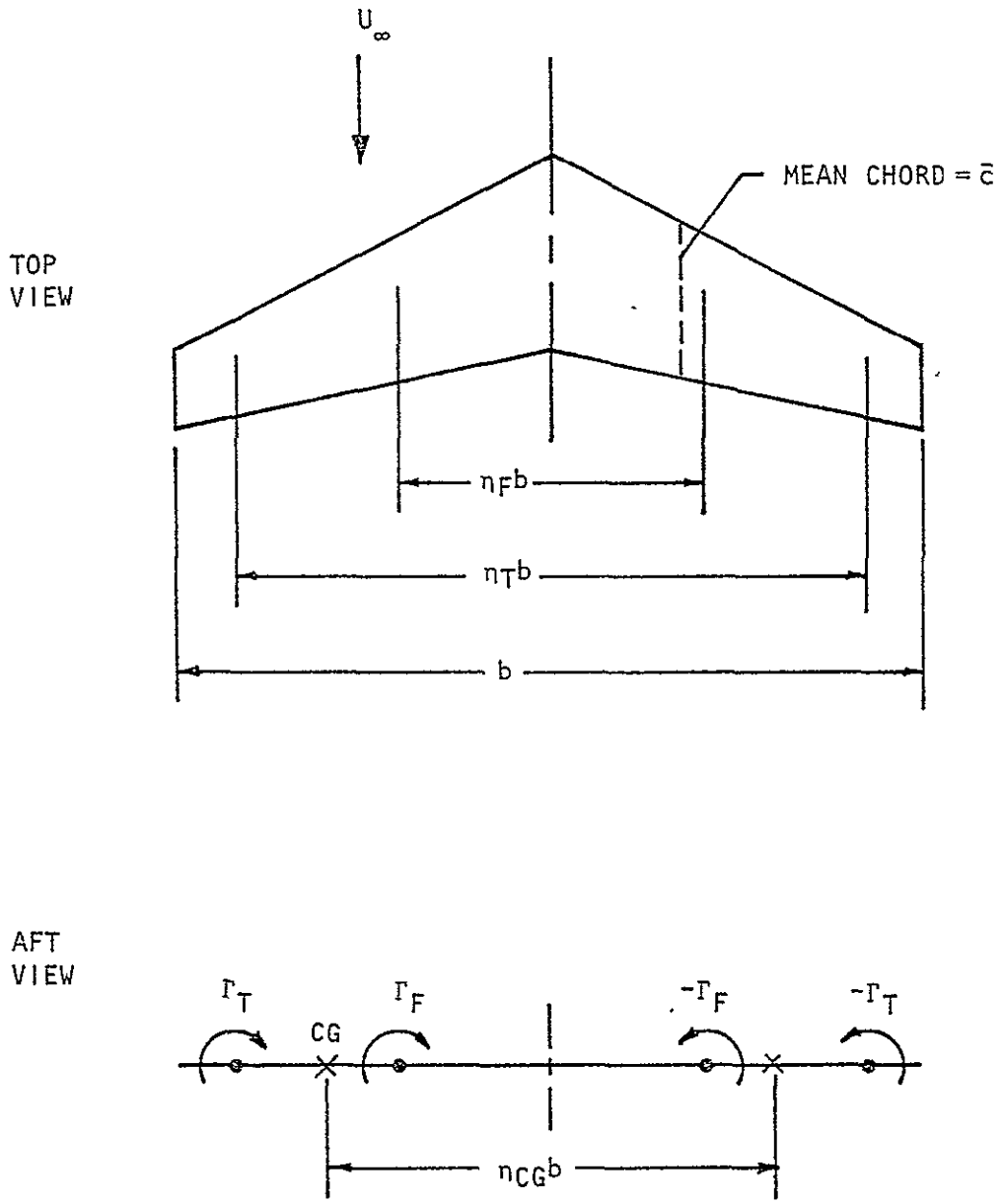

WHERE

$$\eta_{CG}(\Gamma_F + \Gamma_T) = \eta_F \Gamma_F + \eta_T \Gamma_T$$

Figure 4.2 Kinematic Variables for Twin Pair Studies

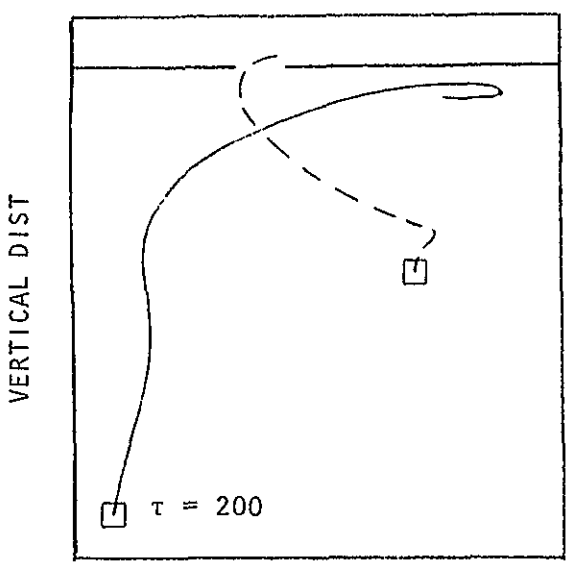

(a) $\eta_F = 0.2$

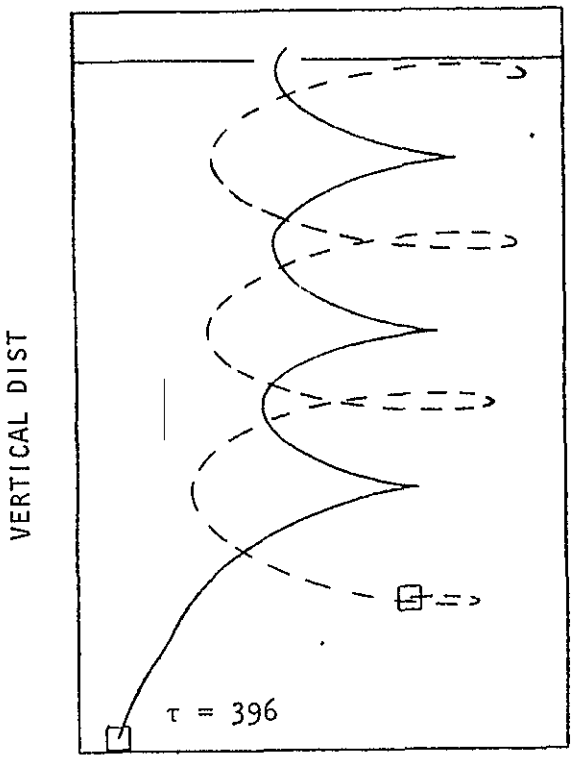

(b) $\eta_F = 0.333$

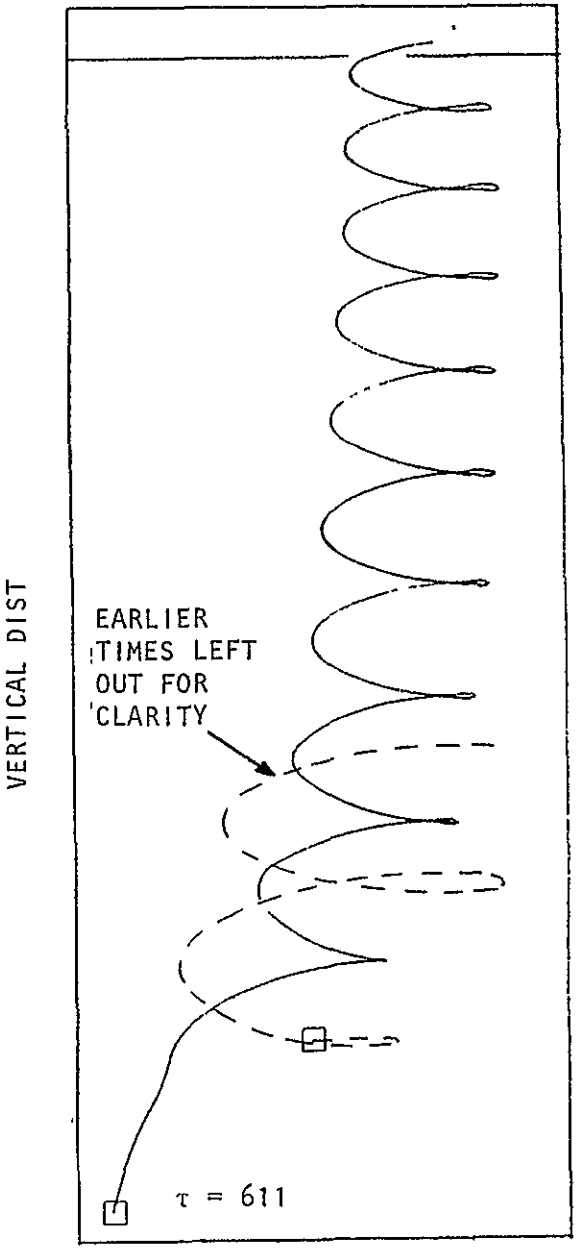

(c) $\eta_F = 0.556$

NOTE: VERTICAL SCALE COMPRESSED BY A FACTOR OF 5.

Figure 4.3 Cross-Sectional Trace for the Convergence Point on Twin Vortex Systems, as a Function of η_F ($\Gamma_T/\Gamma_F = 0.60$, $\eta_T = 1.0$)

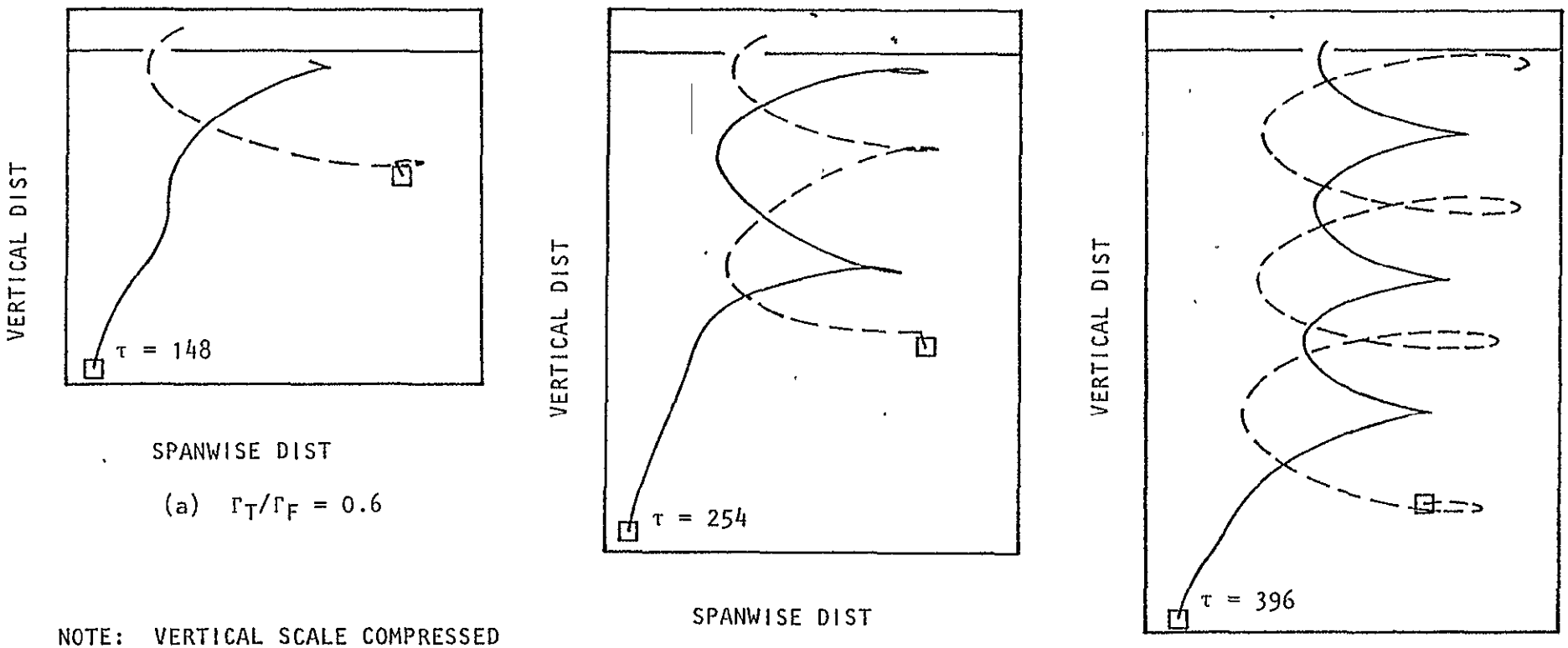

Figure 4.4 Cross-sectional Trace for the Convergence Point on Twin Vortex Systems as a Function of Γ_T/Γ_F (n_F = 0.333, n_T = 1.0)

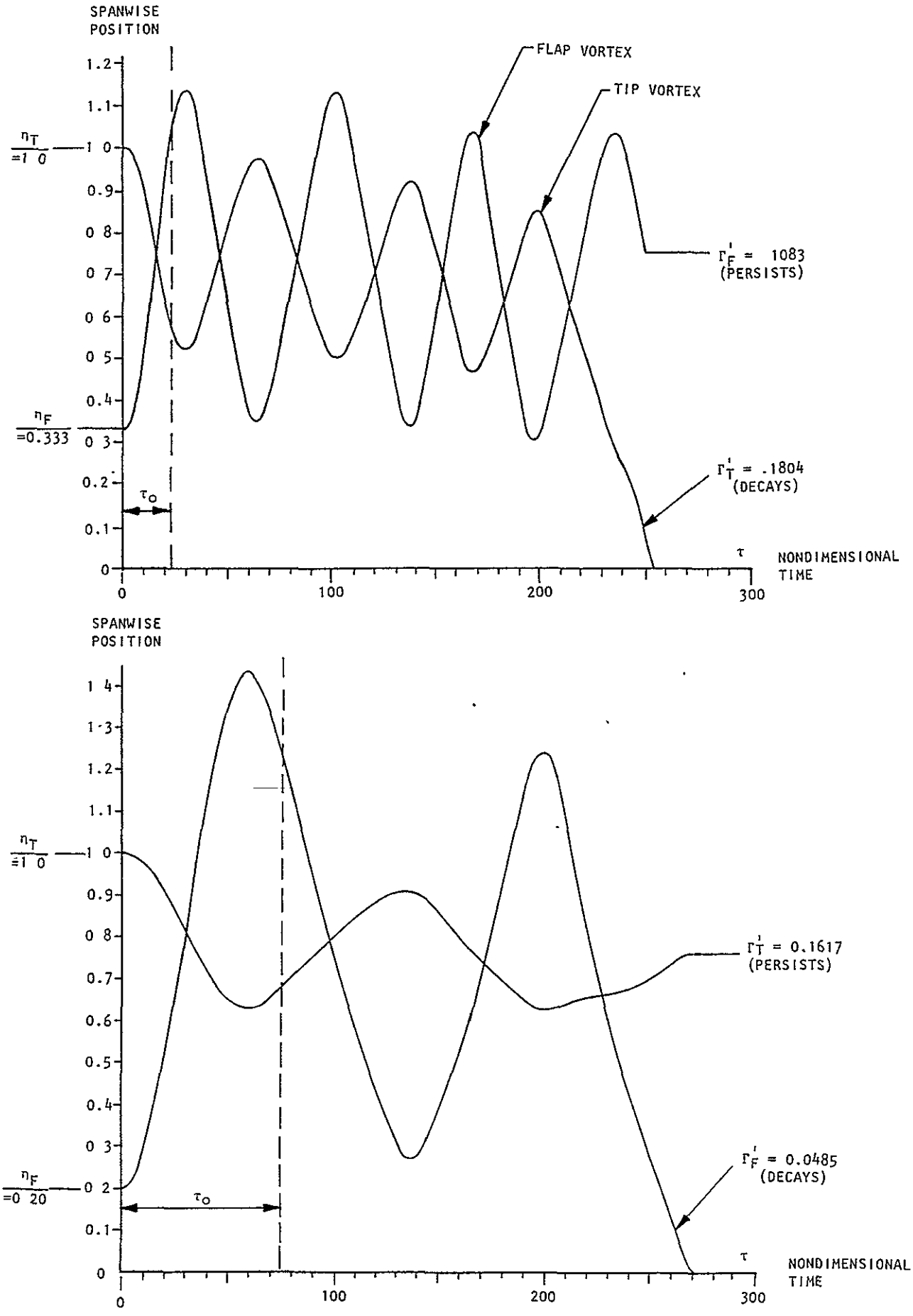

Figure 4.5 Examples of Tip- and Flap-Vortex Convergence

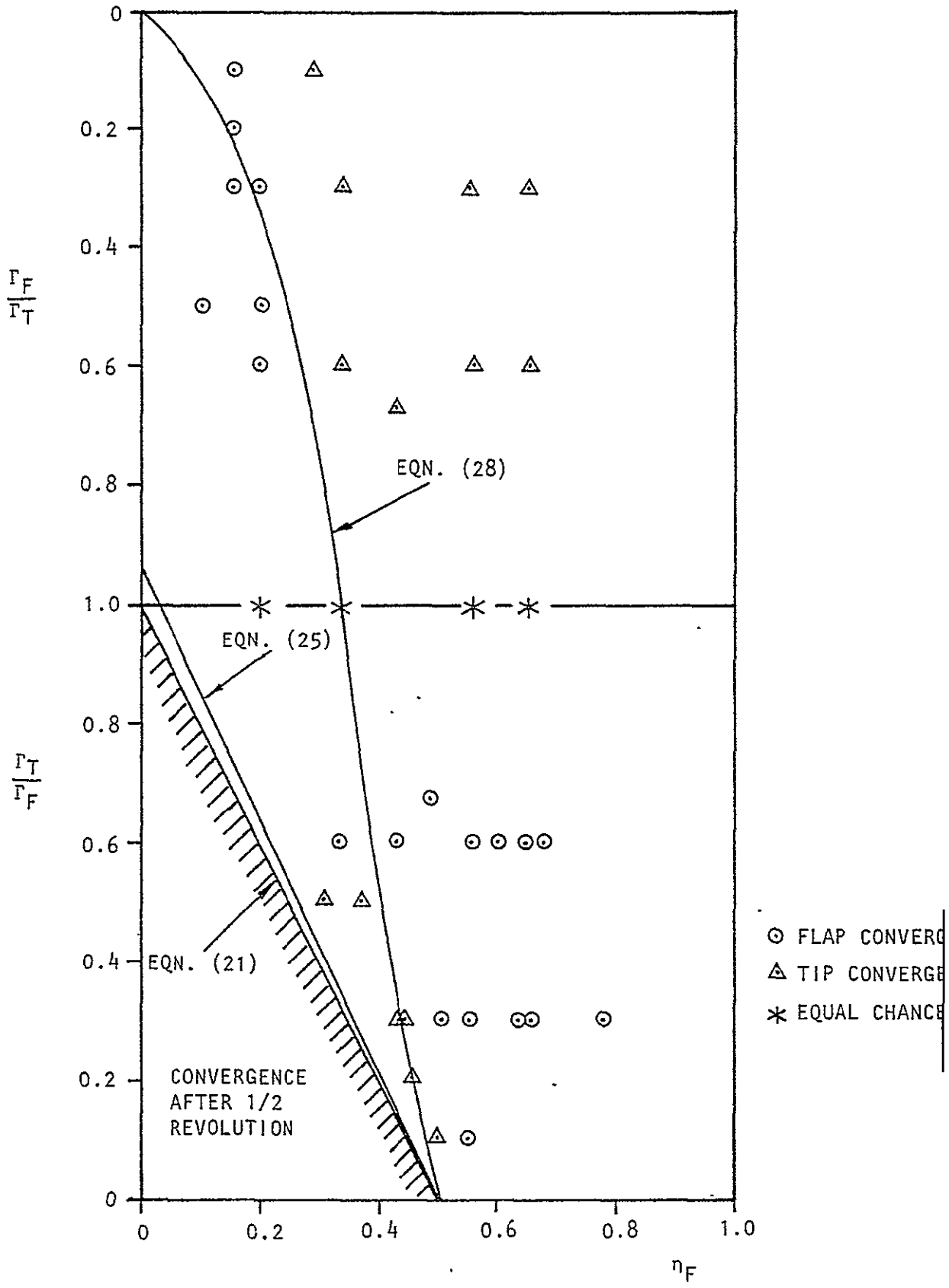

Figure 4.6 Twin-Pair Parametric Study: Identification of the Convergent Vortex

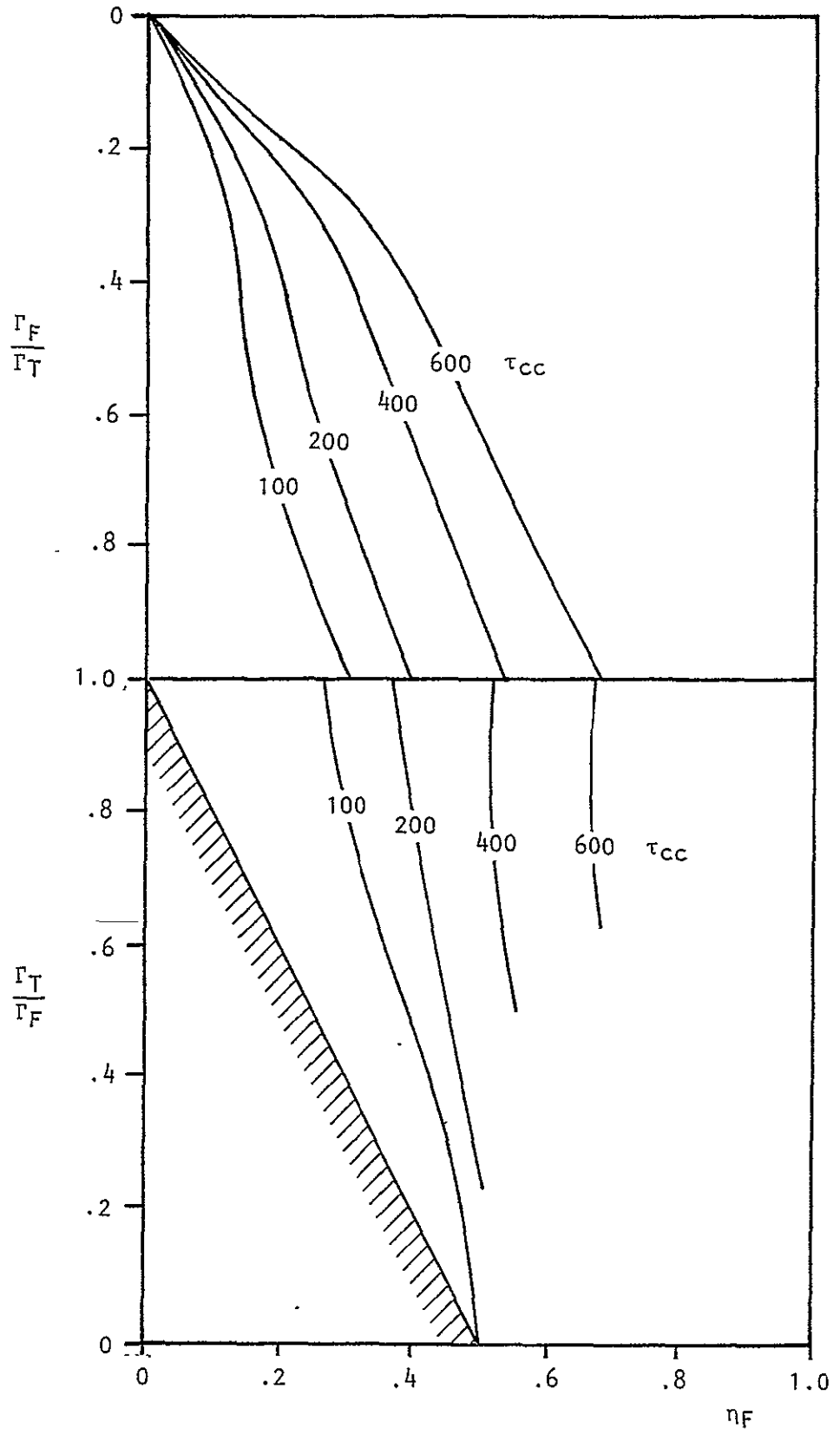

Figure 4.7a Twin Pair Parametric Study: Time-to-Converge
($C_L/AR = .1714$, $\lambda = 5.375$, $\delta/b = .098$)

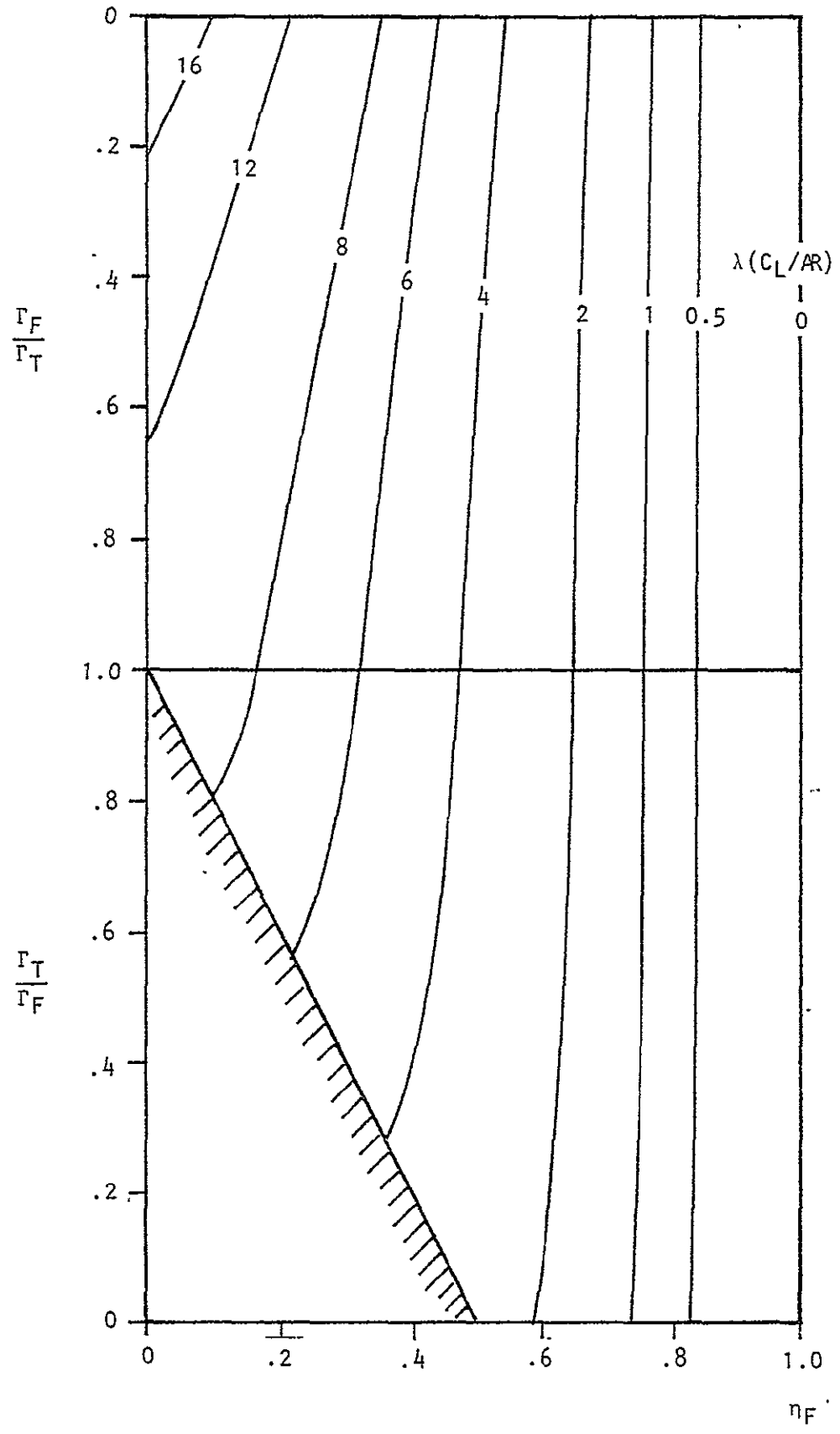

Figure 4.7b Twin Pair Parametric Study: Wavelength/Loading Parameter

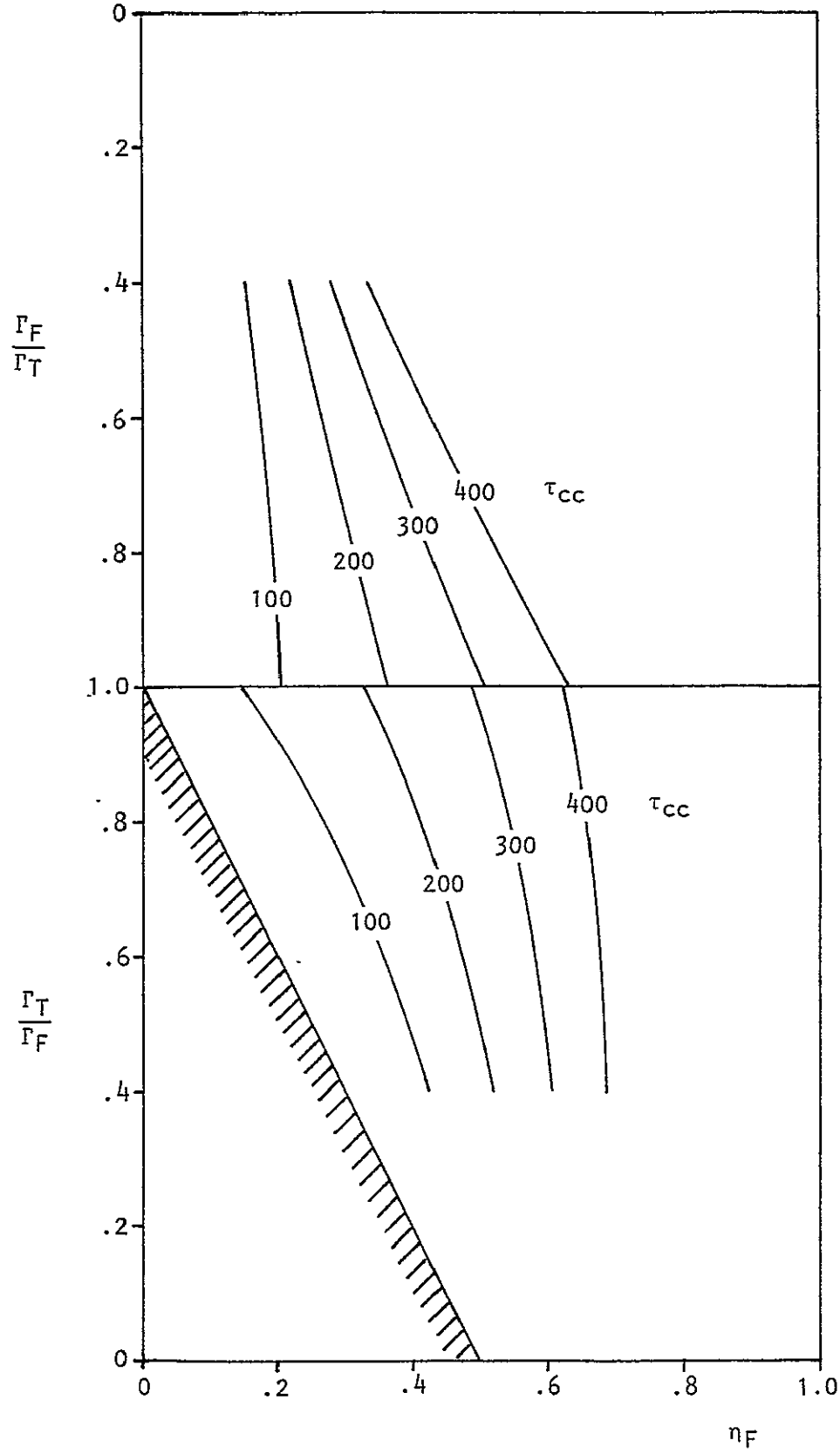

Figure 4.8 Twin Pair Parametric Study: Time-to-Converge
($C_L/AR = 0.25$, Correct λ, $\delta/b = 0.98$)

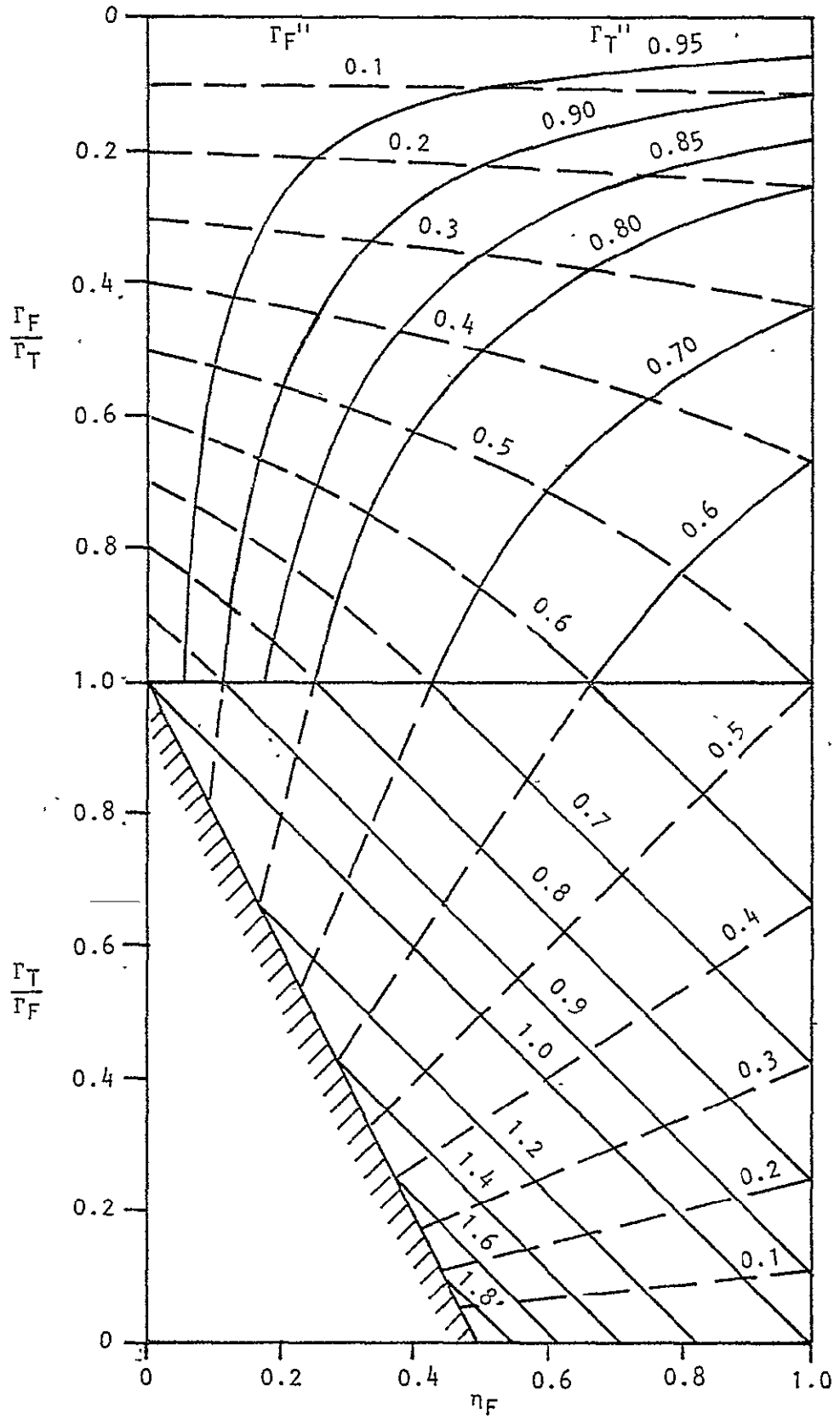

$$\Gamma_F'' = \frac{\Gamma_F}{U_\infty \; b/2} \left(\frac{AR}{C_L}\right) \qquad \Gamma_T'' = \frac{\Gamma_T}{U_\infty \; b/2} \left(\frac{AR}{C_L}\right)$$

NOTE: SOLID LINES DENOTE THE STRONGER VORTEX

Figure 4.9 Strength of the Vortex Remaining After Convergence

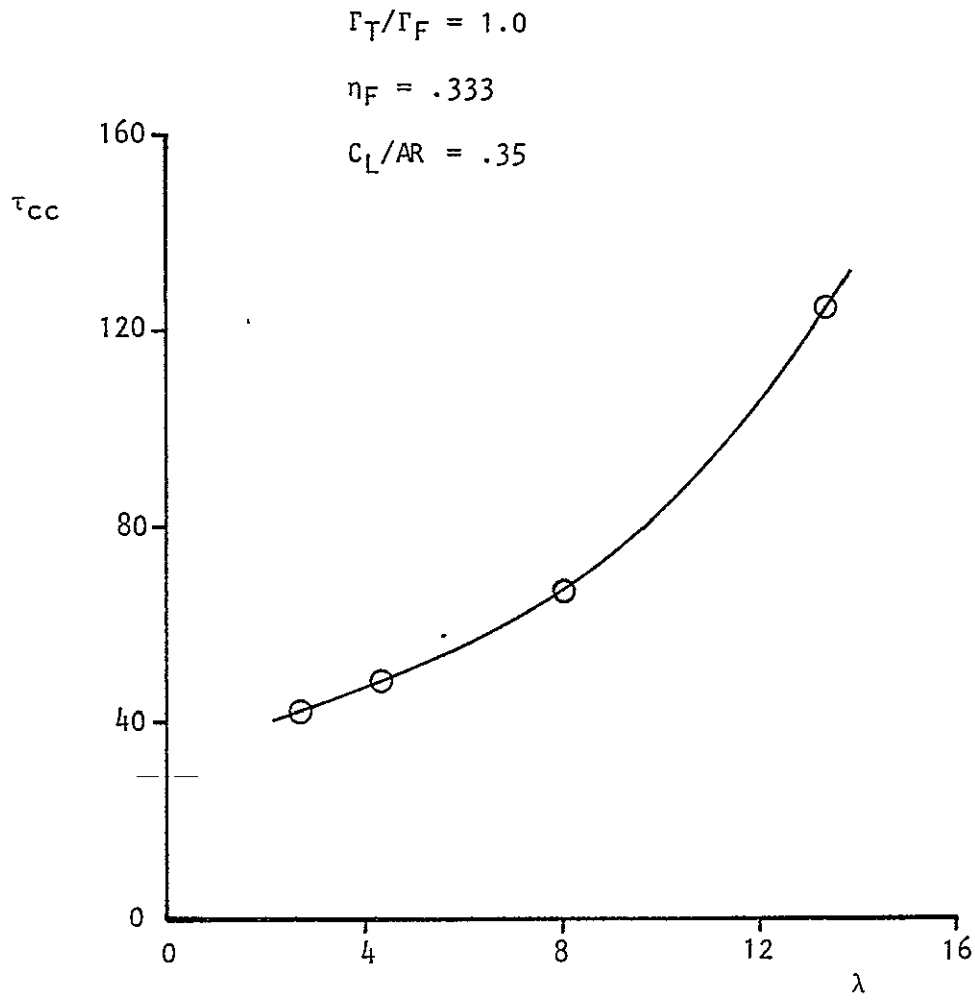

Figure 4.10 Effect of Spiral Wavelength on Time-to-Converge

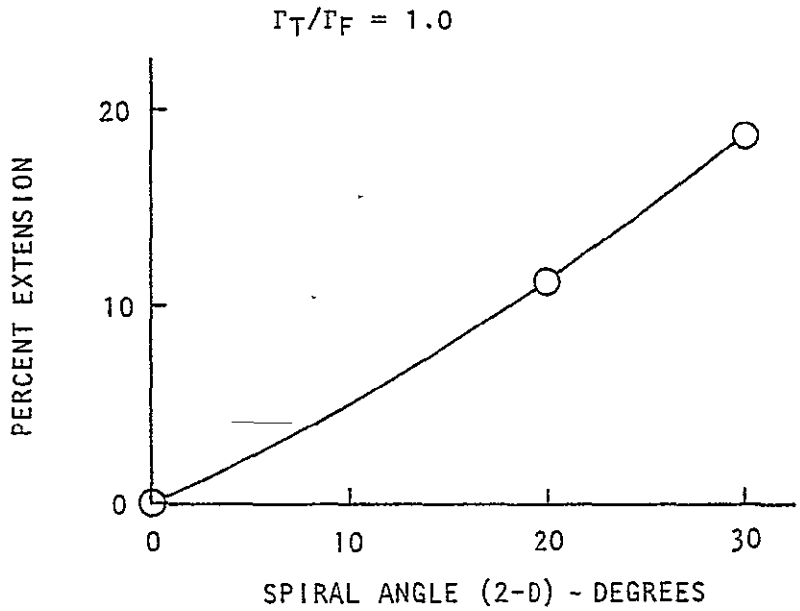

Figure 4.11 Three Dimensional Extension of Twin Spiral Waves

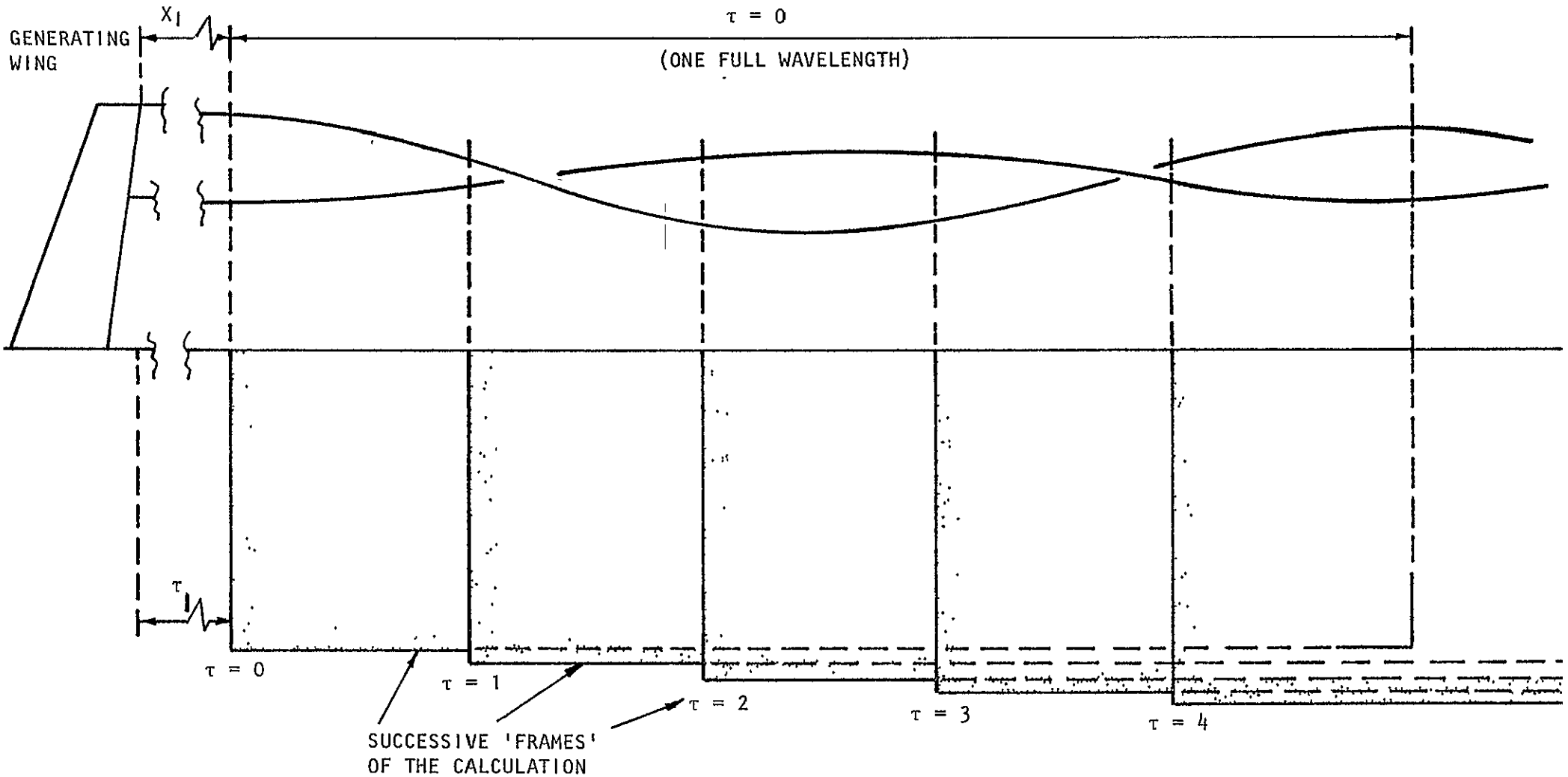

Figure 4.12 The Application of a Space-Fixed Calculation

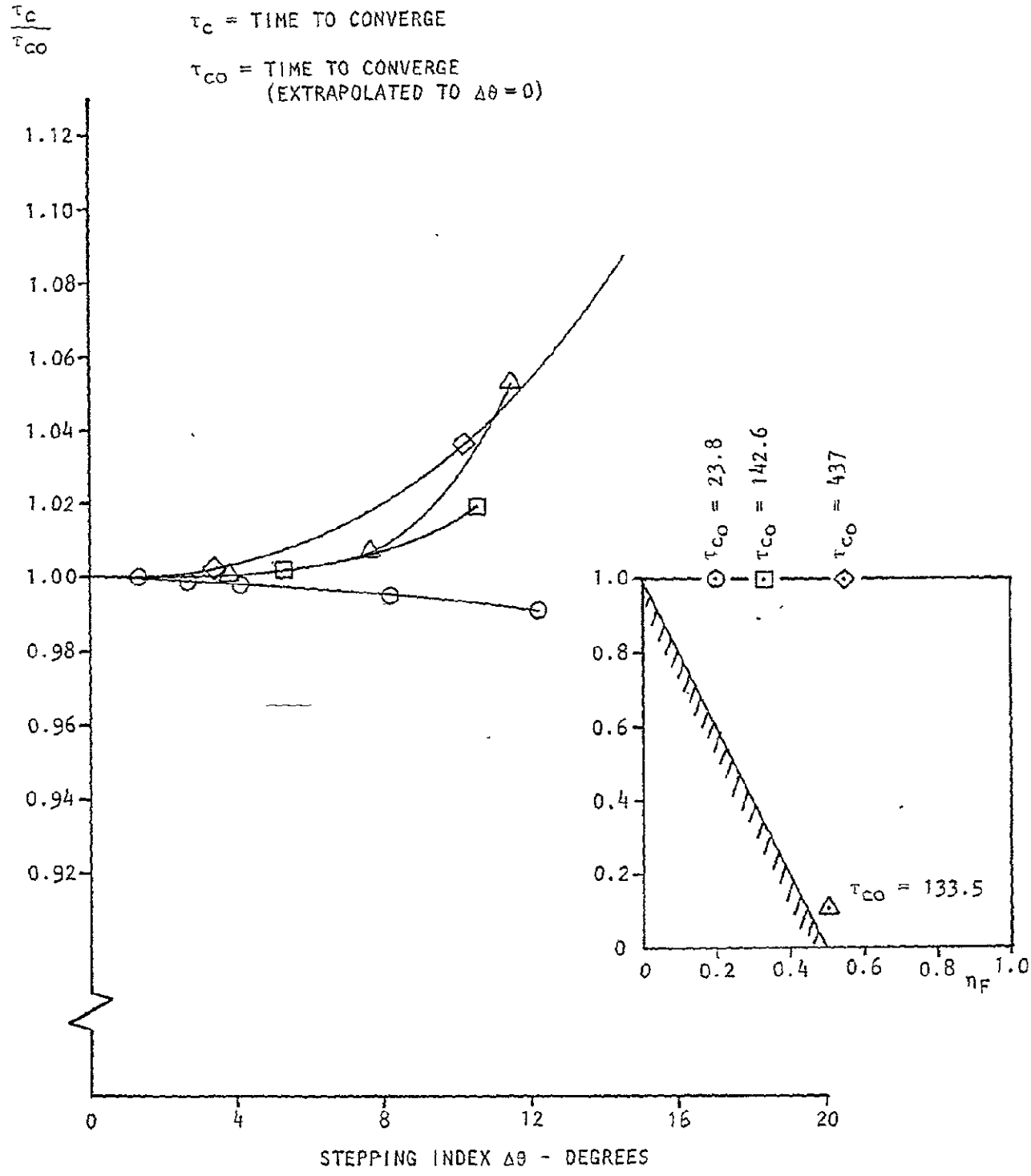

Figure 4.13 Effect of Integration Step-Size on Time-to-Converge

$C_L/AR = .1714$ $\lambda = 5.375$

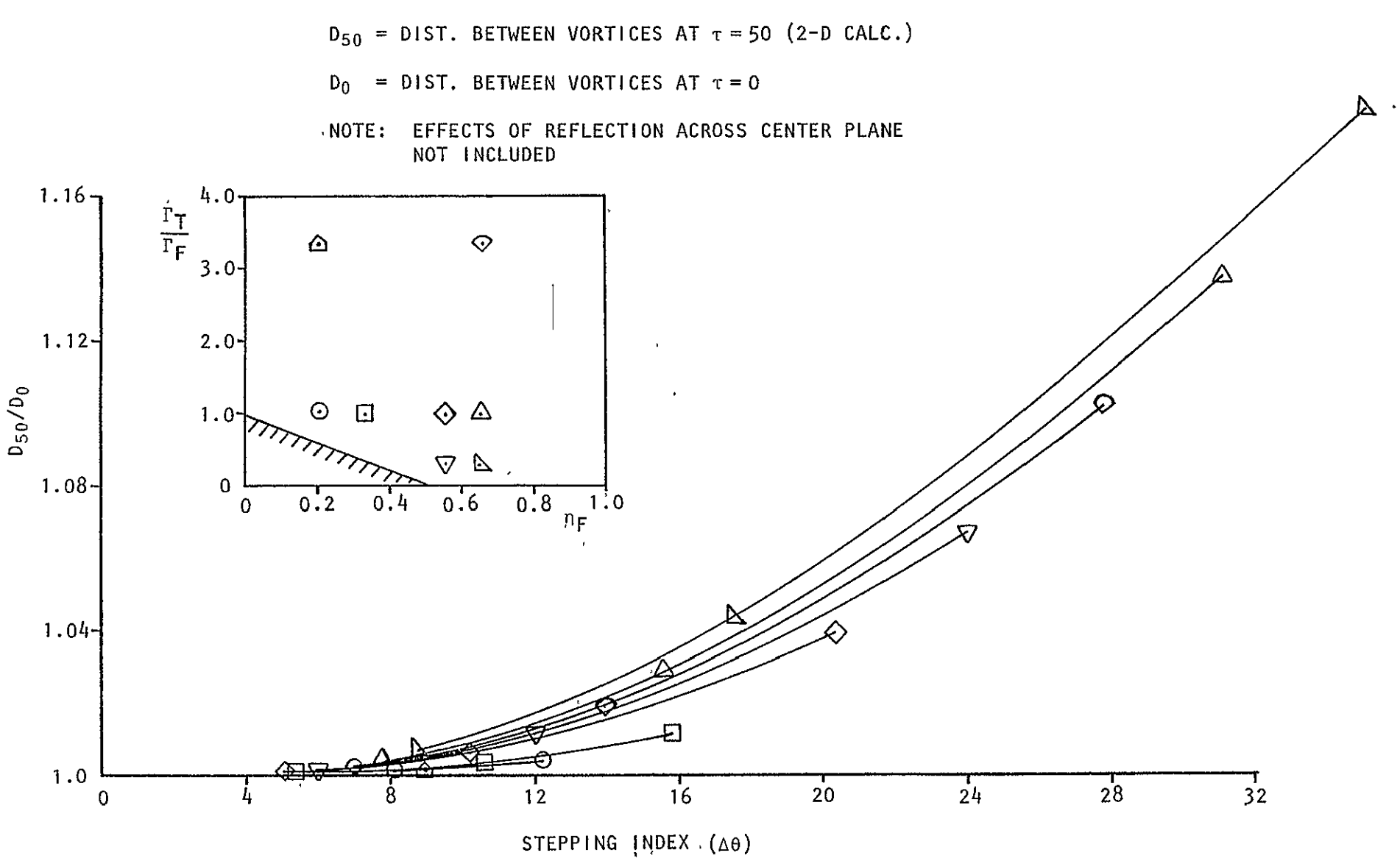

Figure 4.14 Effect of Integration Step-Size on Vortex Spacing

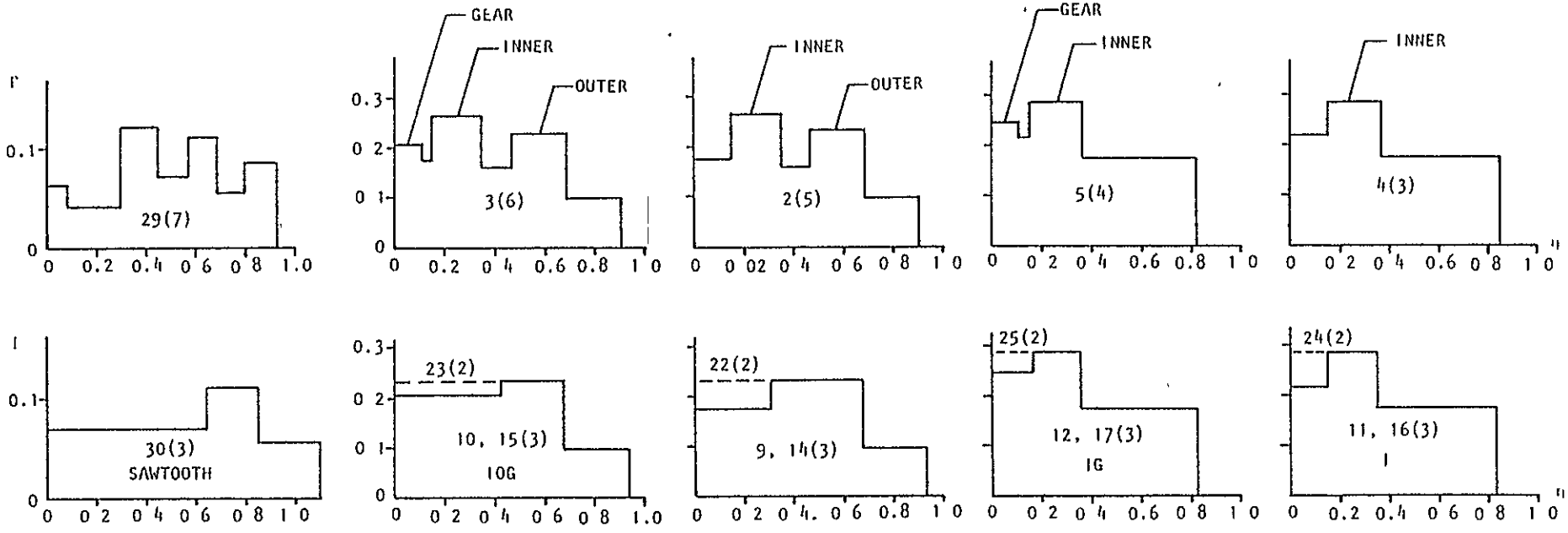

RUNS 2, 3, 4, 5, 29 2-D INITIALIZATION . RUNS 9, 10, 11, 12, 24, 3-D RELAXATION, A/C FIXED

RUNS 14, 15, 16, 17 3 PAIRS, SPACE FIXED RUNS 22, 23, 24, 25 2 PAIRS, SPACE FIXED

FIGURES IN PARENTHESES SHOW NUMBER OF PAIRS

FIGURES WITHOUT PARENTHESES SHOW RUN NUMBER

ORIGINAL PAGE IS OF POOR QUALITY

Figure 5.1 Span Load and Run Definition for Multiple-Pair Cases

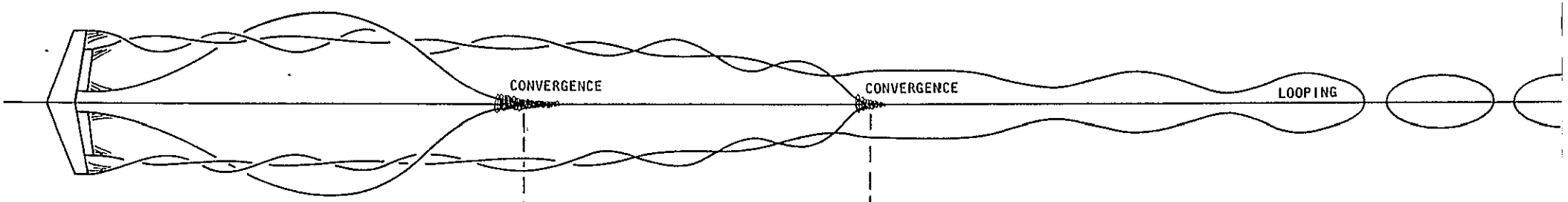

NEAR WAKE
(SECTION 5)

- o MULTIPLE PAIRS
- o VORTEX MERGING
- o VORTICES CONVECTED AWAY

COMPUTING

- o AIRCRAFT-FIXED RELAXATION

MIDDLE WAKE
(SECTION 4)

- o TWIN PAIR REMAINS
- o SPACING CHANGES DUE TO OTHER VORTICES
- o POSSIBLE DISTORTION OF SPIRAL FORM

COMPUTING

- o AIRCRAFT-FIXED, FROM NON-SPIRAL FORM
- o SPACE-FIXED FROM PARAMETRIC, IF NEAR-SPIRAL

FAR WAKE
(SECTION 3)

- o SINGLE ORGANIZED PAIR MAY REMAIN
- o LOOPING POSSIBLE
- o DECAY DEPENDS ON PREVIOUS DISTORTION

COMPUTING

- o SPACE-FIXED FOR "CROW" INSTABILITIES
- o VISCOUS ANALYSIS FOR BURST OR SLOW VISCOUS DECAY

NOTE. IN THE ABOVE SKETCH THE AXIAL DIMENSION IS FORESHORTENED AND THE NUMBER OF WAVES IS REDUCED.

ORIGINAL PAGE IS
OF POOR QUALITY

Figure 5.2 Calculation Regions for a Multiple-Pair Vortex Wake

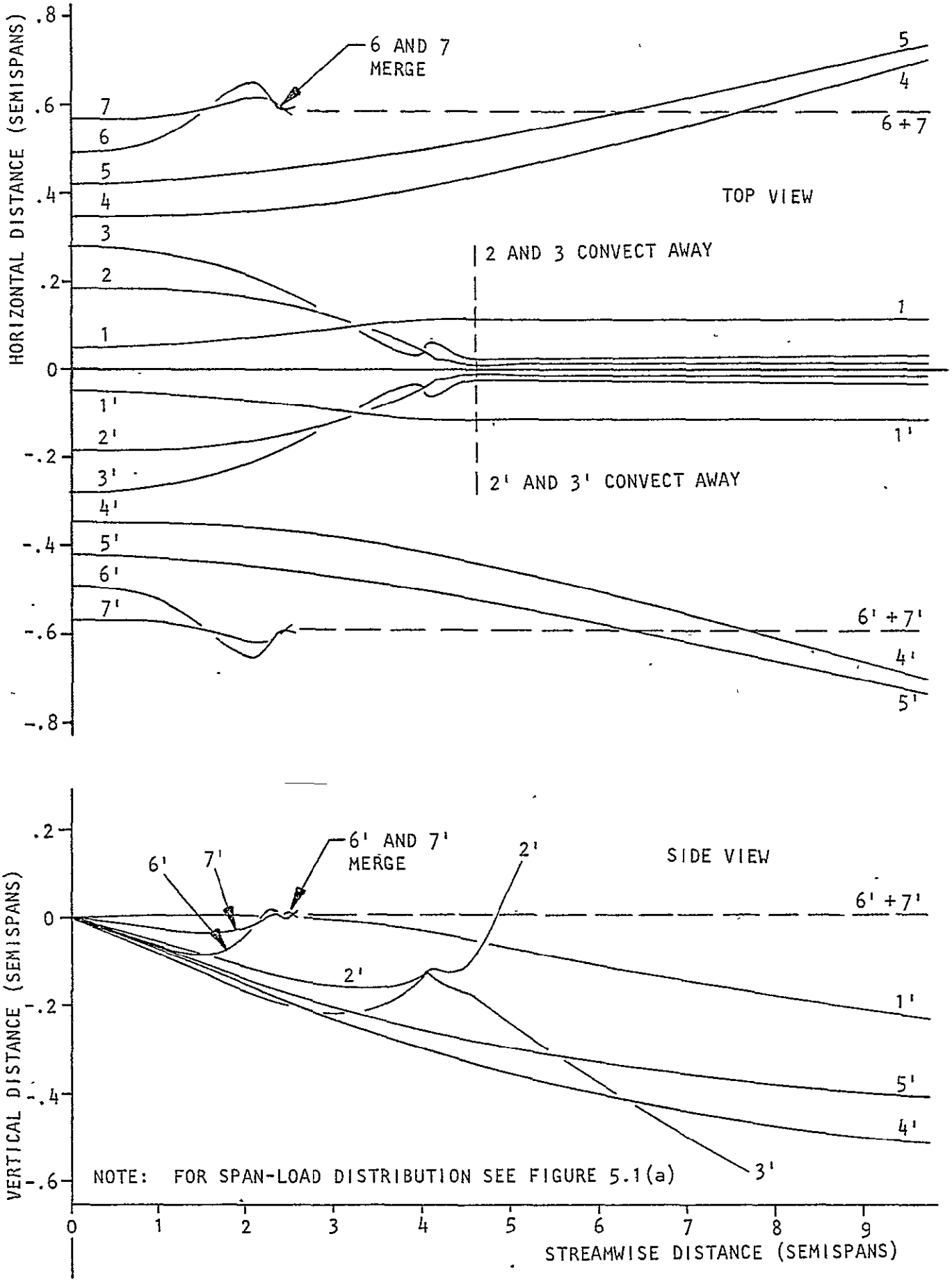

Figure 5.3 Simplification of the Near-Wake

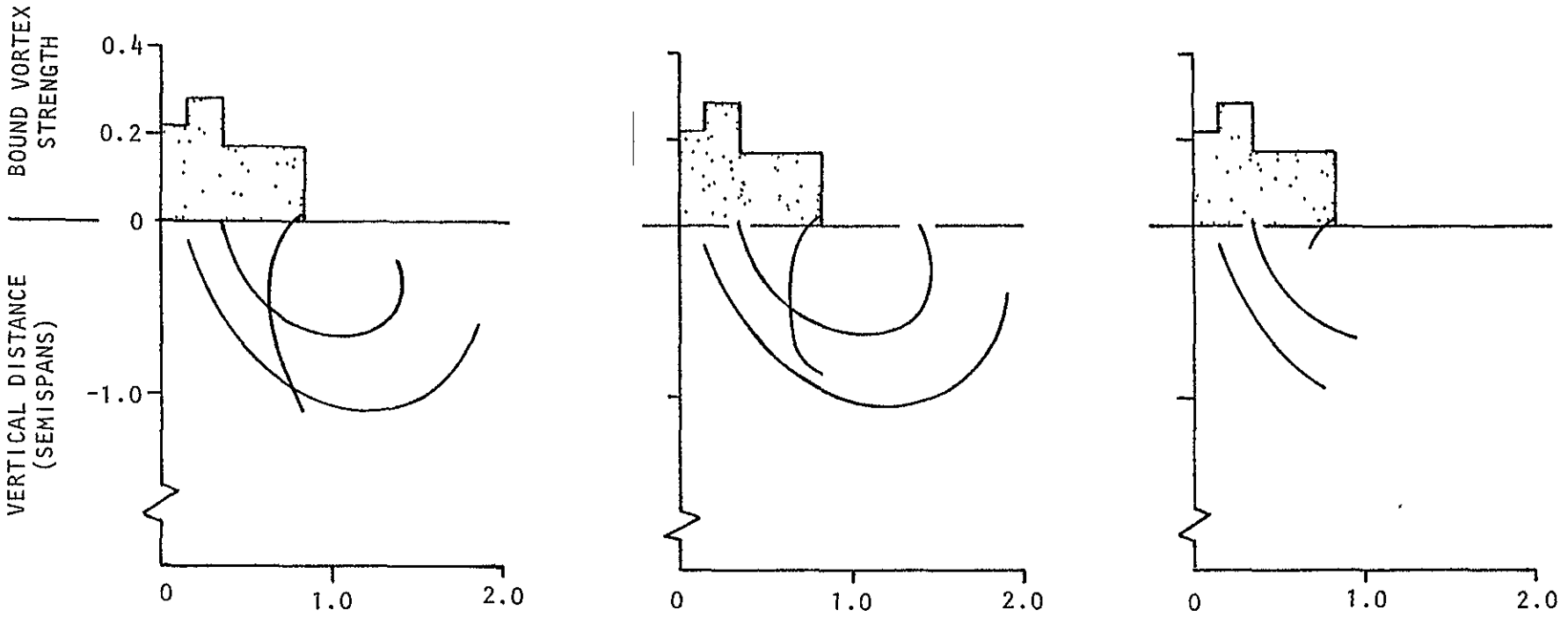

(a) "STANDARD" 2-D METHOD

(b) HACKETT AND EVANS METHOD (REF. 9)

(c) 3-D RELAXATION

Figure 5.4 Calculation of the Initial Wake — Aircraft Fixed

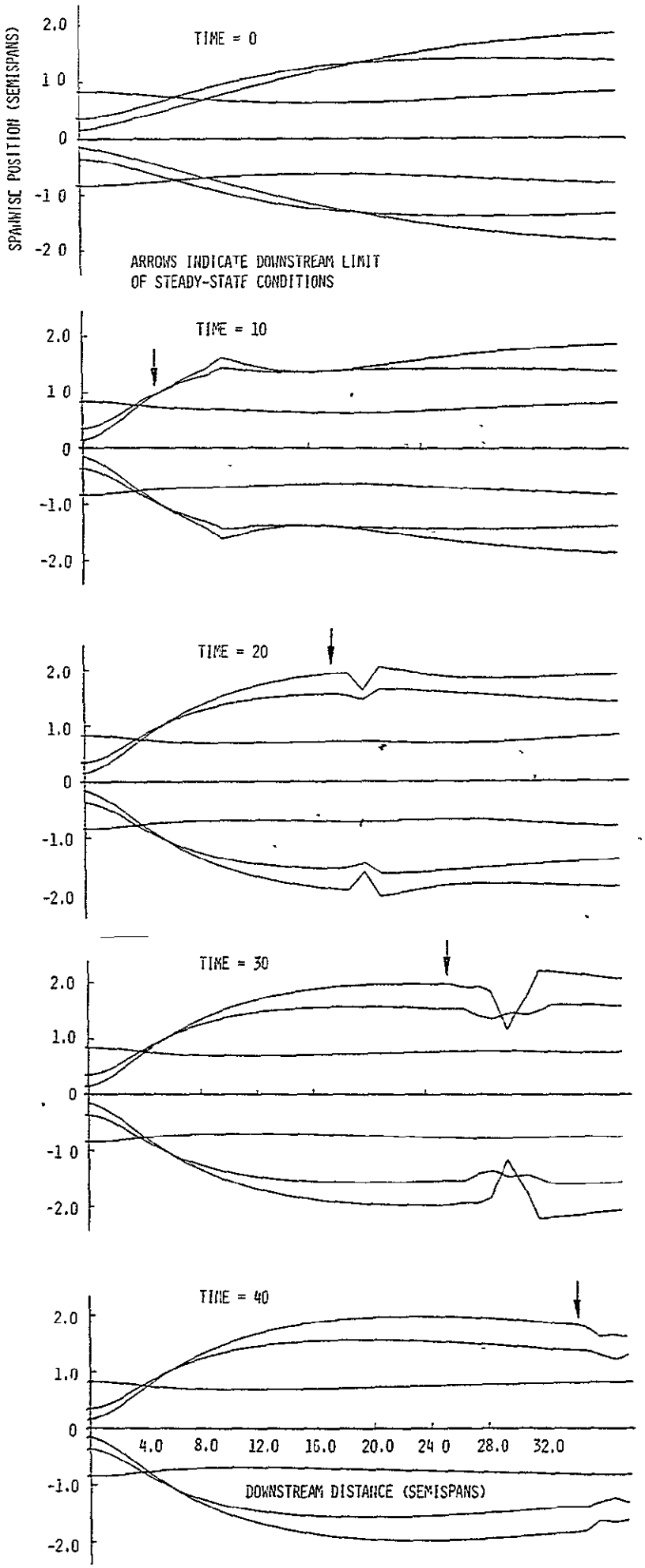

ORIGINAL PAGE IS
OF POOR QUALITY

Figure 5.5 Three-Dimensional Relaxation to a Steady-State — Aircraft Fixed

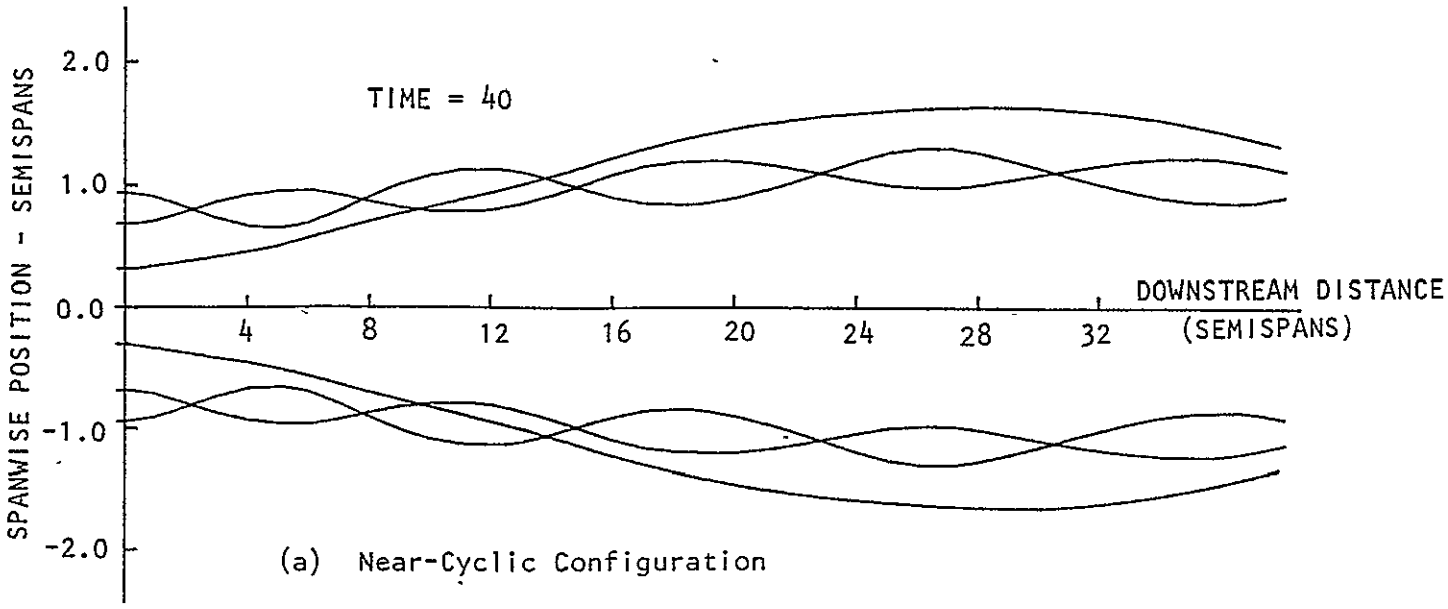

(a) Near-Cyclic Configuration

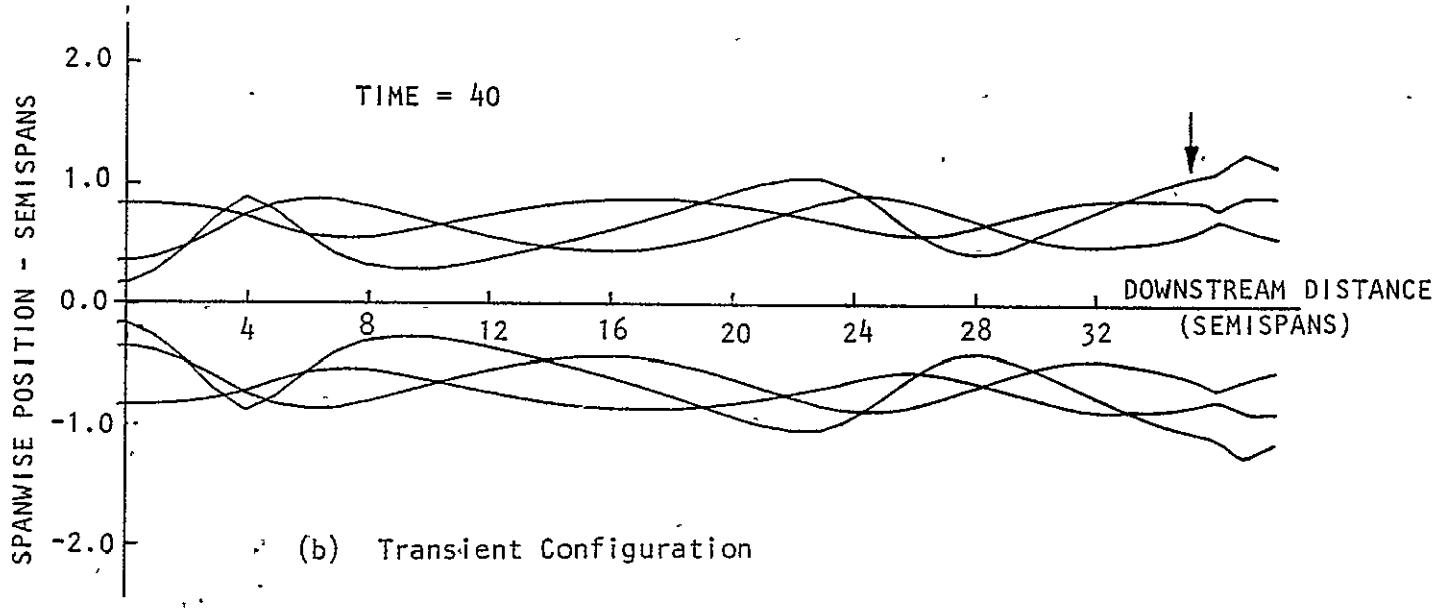

(b) Transient Configuration

Figure 5.6 Near-Cyclic and Transient Cases

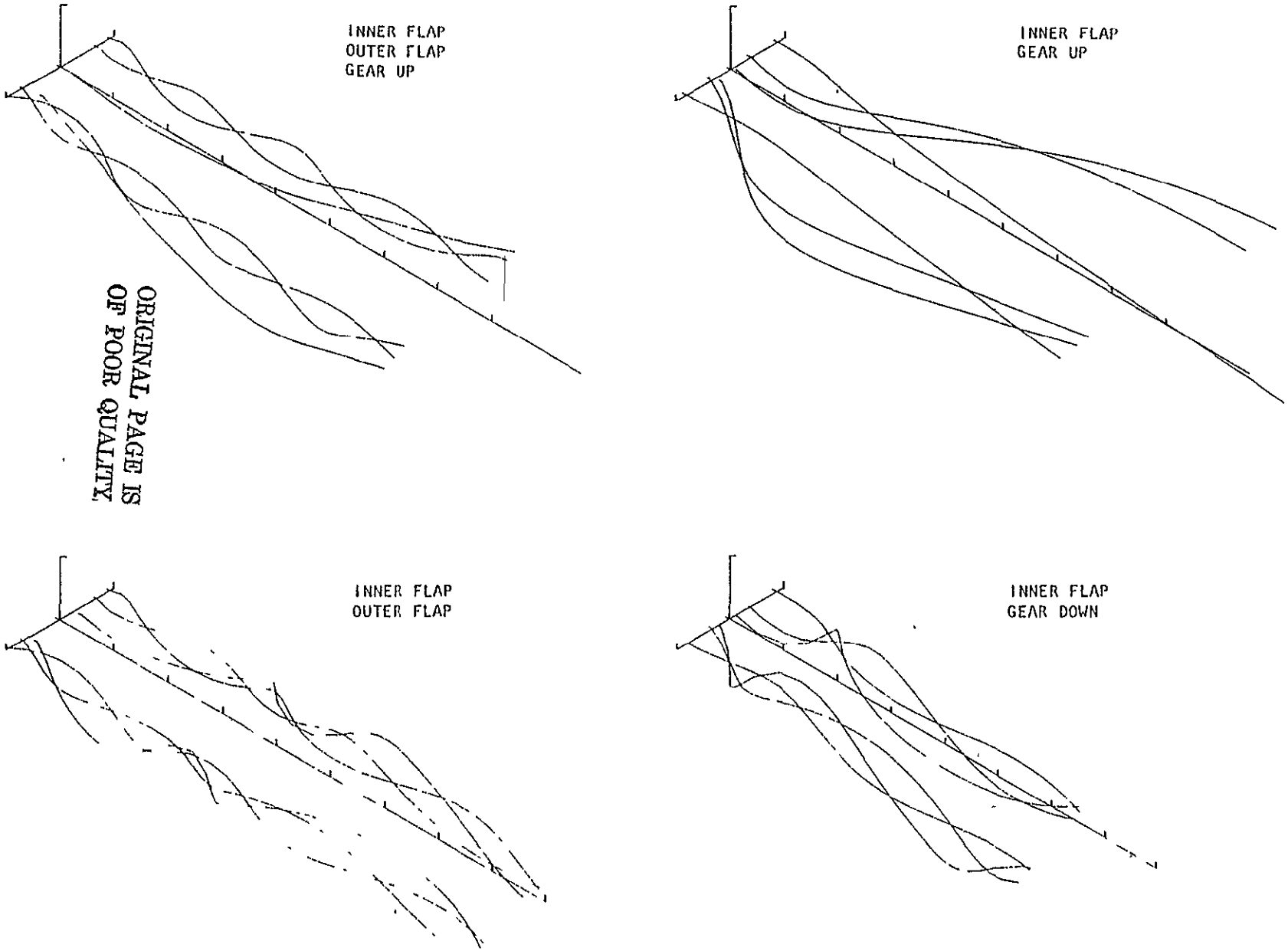

ORIGINAL PAGE IS
OF POOR QUALITY

Figure 5.7 Effect of the Outboard Flap and Landing Gear on the Near Wake of a Boeing 747 on Approach